

AD-A147 659

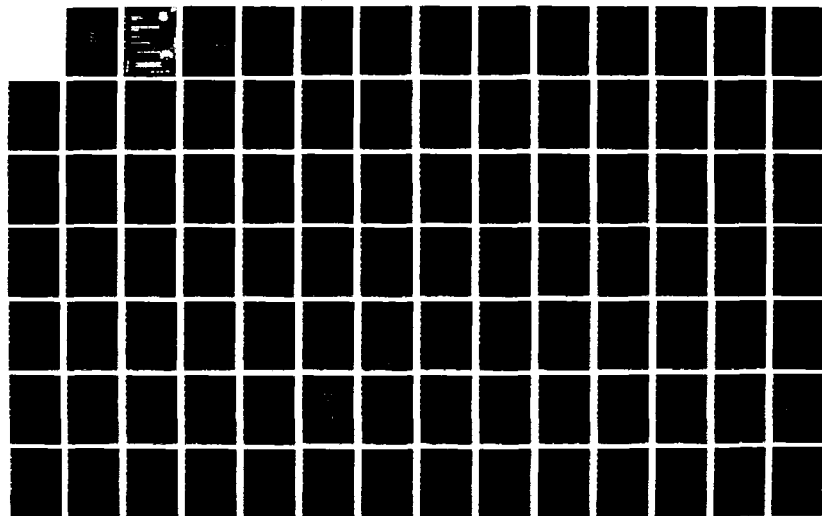
EMC (ELECTROMAGNETIC COMPATIBILITY) SPEC CRITERIA IN
VOLTERRA SYSTEMS(U) SIGNATRON INC LEXINGTON MA
L D TROMP ET AL. JUN 84 RADC-TR-84-147 F30602-82-C-0163

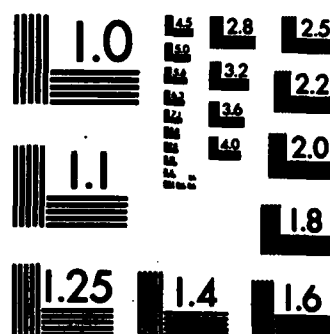
1/3

UNCLASSIFIED

F/G 20/14

NL





MICROCOPY RESOLUTION TEST CHART
NATIONAL BUREAU OF STANDARDS-1963-A

AD-A147 659

This report has been reviewed by the RADC Public Affairs Office (PA) and is releasable to the National Technical Information Service (NTIS). At NTIS it will be releasable to the general public, including foreign nations.

RADC-TR-84-147 has been reviewed and is approved for publication.

APPROVED:



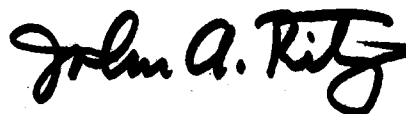
DANIEL J. KENNEALLY
Project Engineer

APPROVED:



W. S. TUTHILL, Colonel, USAF
Chief, Reliability & Compatibility Division

FOR THE COMMANDER:



JOHN A. RITZ
Acting Chief, Plans Office

If your address has changed or if you wish to be removed from the RADC mailing list, or if the addressee is no longer employed by your organization, please notify RADC (RBCT) Griffiss AFB NY 13441. This will assist us in maintaining a current mailing list.

Do not return copies of this report unless contractual obligations or notices on a specific document requires that it be returned.

UNCLASSIFIED
SECURITY CLASSIFICATION OF THIS PAGE

REPORT DOCUMENTATION PAGE				
1a. REPORT SECURITY CLASSIFICATION UNCLASSIFIED		1b. RESTRICTIVE MARKINGS N/A		
2a. SECURITY CLASSIFICATION AUTHORITY N/A		3. DISTRIBUTION/AVAILABILITY OF REPORT Approved for public release; distribution unlimited.		
2b. DECLASSIFICATION/DOWNGRADING SCHEDULE N/A				
4. PERFORMING ORGANIZATION REPORT NUMBER(S) N/A		5. MONITORING ORGANIZATION REPORT NUMBER(S) RADC-TR-84-147		
6a. NAME OF PERFORMING ORGANIZATION Signatron, Inc.	6b. OFFICE SYMBOL (If applicable)	7a. NAME OF MONITORING ORGANIZATION Rome Air Development Center (RBCT)		
6c. ADDRESS (City, State and ZIP Code) 12 Hartwell Avenue Lexington MA 02173		7b. ADDRESS (City, State and ZIP Code) Griffiss AFB NY 13441		
8a. NAME OF FUNDING/SPONSORING ORGANIZATION Rome Air Development Center	8b. OFFICE SYMBOL (If applicable) RBCT	9. PROCUREMENT INSTRUMENT IDENTIFICATION NUMBER F30602-82-C-0163		
8c. ADDRESS (City, State and ZIP Code) Griffiss AFB NY 13441		10. SOURCE OF FUNDING NOS.		
		PROGRAM ELEMENT NO. 62702F	PROJECT NO. 2338	TASK NO. 03
				WORK UNIT NO. 48
11. TITLE (Include Security Classification) EMC SPEC CRITERIA IN VOLTERRA SYSTEMS				
12. PERSONAL AUTHOR(S) Laurens D. Tromp, Michael Rudko				
13a. TYPE OF REPORT Final	13b. TIME COVERED FROM Feb 83 to May 84	14. DATE OF REPORT (Yr., Mo., Day) June 1984	15. PAGE COUNT 224	
16. SUPPLEMENTARY NOTATION N/A				
17. COSATI CODES			18. SUBJECT TERMS (Continue on reverse if necessary and identify by block number)	
FIELD	GROUP	SUB. GR.		
09	03		Electromagnetic Compatibility	
09	05		Nonlinear Volterra Transfer Functions	
			Metal-Insulator-Metal (MIM) Junction (See reverse)	
19. ABSTRACT (Continue on reverse if necessary and identify by block number) Identification of nonlinear transfer functions (NLTF) and their use in predicting electromagnetic compatibility (EMC) specification parameters such as intermodulation and harmonic distortion was studied. It was assumed that the nonlinear systems of interest can be modeled as lumped parameter circuits with zero-memory nonlinearities between circuit nodes. In this case, the NLTF poles are determined by the poles of the linear transfer function (LTF) of the circuit. Two different cases were considered. In the first case, a transient response measurement of the LTF output can be used to identify the linear system poles. The poles of the LTF then specify the poles of the NLTFs. In the second case, the received signal contains a strong direct path component which is independent of the nonlinear system which is to be identified. This situation arises in the identification of the "rusty bolt" (a Metal-Insulator-Metal junction). Under this condition, the "rusty bolt" linear response cannot be measured directly and it is then necessary to estimate the poles of both the LTF and NLTFs from sinusoidal steady state third-order nonlinear response measurements.				
20. DISTRIBUTION/AVAILABILITY OF ABSTRACT UNCLASSIFIED/UNLIMITED <input type="checkbox"/> SAME AS RPT. <input checked="" type="checkbox"/> DTIC USERS <input type="checkbox"/>			21. ABSTRACT SECURITY CLASSIFICATION UNCLASSIFIED	
22a. NAME OF RESPONSIBLE INDIVIDUAL Daniel J. Kenneally			22b. TELEPHONE NUMBER (Include Area Code) (315) 330-2519	22c. OFFICE SYMBOL RADC (RBCT)

DD FORM 1473, 83 APR

EDITION OF 1 JAN 73 IS OBSOLETE.

UNCLASSIFIED
SECURITY CLASSIFICATION OF THIS PAGE

UNCLASSIFIED

SECURITY CLASSIFICATION OF THIS PAGE

18. (Continued)

Rusty Bolt
System Identification

Accession For	
NTIS GRA&I	<input checked="" type="checkbox"/>
DTIC TAB	<input checked="" type="checkbox"/>
Unannounced	<input type="checkbox"/>
Justification	
By _____	
Distribution/	
Availability Codes	
Dist	Avail and/or Special
<input checked="" type="checkbox"/>	



UNCLASSIFIED

SECURITY CLASSIFICATION OF THIS PAGE

FOREWORD

This Final Technical Report describes the results obtained by SIGNATRON, Inc., of Lexington, MA on Air Force Contract F30602-82-C-0163 for Rome Air Development Center.

The objective of the study effort was to contribute to the technology required to characterize equipment EMC performance in forms which are relatable to C³I system level EMC analysis and design problems. The specific objective of this effort was to establish and develop criteria for the port specification of equipment level EMC performance in terms of nonlinear Volterra transfer functions with particular emphasis on the rusty bolt problem.

Dr. Leonard Ehrman was the Project Manager. Mr. Laurens D. Tromp was the Principal Analyst and Dr. Michael Rudko consulted to the project. In addition to SIGNATRON personnel, Dr. V.K. Jain also provided consulting service to the project. The authors would like to thank Dr. J.J. Bussgang for his suggestions and encouragement.

The support and assistance provided by the cognizant RADC personnel Mr. D. Kenneally, RADC Project Engineer and Mr. J. Spina, the Section Manager, are gratefully acknowledged.

EXECUTIVE SUMMARY

Air Force C³I systems may have to operate in an electromagnetically hostile environment. Collocated transmitters and receivers, on electronically dense platforms, are susceptible to performance degradation through nonlinear effects. The nonlinearities can occur in transmitters, receivers, or in the coupling paths ("rusty bolt" effect) between transmitters and receivers. Together the nonlinearities generate a spectrum of unwanted interference signals which degrade the desired signal spectral fidelity and EMC performance. The objective of this effort was to establish and develop criteria for the port specification of equipment level EMC performance in terms of nonlinear Volterra transfer functions with particular emphasis on the rusty bolt problem. The study concentrated on the identification (estimation) of nonlinear transfer functions (NLTF) and their use in predicting the EMC specification parameters such as gain compression and desensitization, harmonic distortion, cross modulation and intermodulation. It is assumed that the nonlinear systems of interest can be modeled as lumped parameter circuits with zero-memory nonlinearities between the circuit nodes. In this case the NLTF poles are determined by the poles of the linear part of the circuit. Two different cases are considered. In the first case, the linear transfer function (LTF) output can be measured and identified from a transient response. The poles of the LTF then specify the poles of the NLTFs. In the second case, the received signal contains a strong direct path component which is independent of the nonlinear system which is to be identified. This situation arises in the identification of the "rusty bolt" (a Metal-Insulator-Metal junction). Because of the strong direct component, the "rusty bolt" linear response cannot be measured directly. Under this condition, it is necessary to

estimate the poles of the LTF and NLTF's from sinusoidal steady state third order nonlinear response measurements.

The results of the study indicate the following:

1. Mean squared error between measured output and the output of the identified system is a more reliable predictor of the errors in the NLTF specification parameters than errors in pole locations.
2. Global mean squared error cannot be used to predict the error in the specification parameters in all cases, specially when the number of poles is misidentified. Instead, an error criterion which is segmented in frequency should be used.
3. For the rusty bolt lumped parameter circuit and an MIM i-v characteristic up to fifth order, the EMC specification parameters up to fifth order can be predicted with good quality provided that the number of poles are identified correctly and that the errors in the estimates of the linear transfer function poles and the antenna impedance are reasonable (say less than 30 percent).

The study has also produced the following list of recommendations for further research:

1. Design and implement algorithms for the two sinusoidal steady state poles and zeros identification techniques developed under this present contract and evaluate their performance in noise. The first technique uses magnitude measurements while the second technique uses phase measurements of a third order response to identify the poles and zeros.

2. Measure a MIM junction on a laboratory bench.
3. Identify and measure the nonlinear performance of the same MIM junction in an anechoic chamber. Predict the system nonlinear performance based on a lumped parameter circuit model and refine the model if necessary.
4. Upon successful identification of the rusty bolt and adequate prediction of the nonlinear system performance in step 3, perform identification on board an aircraft. A word of caution is in order. It should be noted that even if the results of step 3 indicate that a lumped parameter is adequate to represent a rusty bolt in anechoic chambers, the success of the experiment on board an aircraft is not guaranteed. The reason is that the aircraft rusty bolt will probably be of a distributed nature and the characteristics may be time varying. This would require the development of a distributed parameter (transmission line) and possibly time varying rusty bolt nonlinear model. Nevertheless, useful information can be obtained by performing the experiment.

TABLE OF CONTENTS

<u>SECTION</u>	<u>PAGE</u>
1 INTRODUCTION.....	1-1
2 THE IDENTIFICATION PROBLEM.....	2-1
2.1 INTRODUCTION.....	2-1
2.2 IDENTIFICATION TECHNIQUE SURVEY AND REVIEW.....	2-4
2.3 PROBE WAVEFORM INVESTIGATION.....	2-12
2.4 IDENTIFICATION ERROR ANALYSIS.....	2-13
3 NLTF SPECIFICATION PARAMETER INVESTIGATION.....	3-1
3.1 RELATIONSHIP OF SPECIFICATION PARAMETERS TO NLTF AND LTF.....	3-1
3.1.1 Nonlinear Systems Without Memory.....	3-2
3.1.1.1 Gain Compression and Desensitization.....	3-3
3.1.1.2 Crossmodulation.....	3-4
3.1.1.3 Intermodulation.....	3-5
3.1.2 Nonlinear Systems with Memory.....	3-6
3.1.2.1 Two-Tone Input Example.....	3-10
3.1.2.2 Specification Parameters.....	3-15
3.1.2.2.1 Gain Compression/Expansion..	3-15
3.1.2.2.2 Intermodulation, Harmonic Distortion and Desensitization.....	3-17
3.2 SENSITIVITY ANALYSIS.....	3-17
3.2.1 Two Pole Example.....	3-18
3.2.2 Three Pole Example.....	3-27
4 THE "RUSTY BOLT" PROBLEM.....	4-1
4.1 "RUSTY BOLT" MODELING.....	4-2
4.1.1 Volterra Transfer Functions of the Rusty Bolt.....	4-5
4.1.2 Linear Response and Transfer Functions....	4-5
4.1.3 Higher Order Output Voltage to Input Current Transfer Functions.....	4-8
4.1.4 Output Voltage to Input Voltage Transfer Functions.....	4-10

TABLE OF CONTENTS (Continued)

<u>SECTION</u>	<u>PAGE</u>
4.2 POWER CONSTRAINT ON THE "RUSTY BOLT" LINEAR RESPONSE MEASUREMENT.....	4-11
4.2.1 "Rusty Bolt" Linear Response Measurement..	4-11
4.2.2 Received Power Levels.....	4-14
5 RUSTY BOLT NLTF IDENTIFICATION.....	5-1
5.1 RUSTY BOLT IDENTIFICATION TECHNIQUES.....	5-1
5.1.1 Transient Probe Waveform Analysis for the Rusty Bolt.....	5-2
5.1.2 Sinusoidal Steady State Analysis for the Rusty Bolt.....	5-4
5.1.2.1 Third-Order Transfer Function Identification Using Sinusoidal Steady-State Measurements.....	5-5
5.1.2.2 Sinusoidal Steady State Identification Including the Effects of the Fifth Order NLTF.....	5-10
5.1.2.2.1 Two-Tone Input Example.....	5-12
5.1.2.3 Sinusoidal Steady State Poles and Zero Identification Using Phase Information.....	5-18
5.1.2.4 Identification of Rusty Bolt NLTF Specification Parameters Constants.....	5-18
5.1.2.4.1 Nonlinear Response Measurement.....	5-20
5.1.2.4.2 Determination of Gain Constants from Harmonic Measurements.....	5-22
5.2 SPECIFICATION PARAMETERS INVESTIGATION FOR THE RUSTY BOLT.....	5-25
5.2.1 Intermodulation and Harmonic Distortion Prediction Assuming a Third Order i-v Characteristic.....	5-25
5.2.1.1 Caution in Using Severely Misidentified Poles to Estimate Constants to Predict Nonlinear Performance.....	5-30

TABLE OF CONTENTS (Concluded)

<u>SECTION</u>	<u>PAGE</u>
5.2.2 Intermodulation and Harmonic Distortion Prediction Assuming a Fifth Order i-v MIM Characteristic.....	5-33
5.2.2.1 Determination of Combined Constant Associated with k_5	5-37
5.3 CONCLUSION.....	5-41
6 MEASUREMENT AND INSTRUMENTATION CRITERIA.....	6-1
6.1 TEST PROCEDURES AND REQUIREMENTS.....	6-2
6.1.1 Intermodulation and Harmonic Measurement..	6-
6.1.2 Rusty Bolt Experimental Criteria and Methodology.....	6-
6.1.2.1 Probe Waveform and NLTF Specifi- cation Measurement.....	6-6
6.1.2.2 System Dynamic Range and Trans- mitted Power.....	6-6
6.1.2.3 Rusty Bolt Identification and Model Validation.....	6-6
7 CONCLUSIONS AND RECOMMENDATIONS.....	7-1
APPENDIX A LINEAR IDENTIFICATION TECHNIQUES, AND A DFT-BASED 'RUSTY-BOLT' TESTING TECHNIQUE	
APPENDIX B THE ELECTRIC TUNNELING EFFECT AND PROPERTIES OF A METAL-INSULATOR-METAL (MIM) JUNCTION	
APPENDIX C VOLTERRA TRANSFER FUNCTIONS FOR A "RUSTY BOLT" EQUIVALENT CIRCUIT	

LIST OF FIGURES

FIGURE		PAGE
3-1	Relationship Between NMSE and SENR.....	3-21
3-2	True and Predicted Third Order Harmonic. Predicted based on a single identified pole at $\hat{s} = - .25$	3-23
3-3	True and Predicted Third Order Intermodulation Predicted based on a single non-optimized identified pole at $\hat{s} = - .25$	3-24
3-4	True and Predicted Third Order Harmonic. Predicted based on using optimized identified poles.....	3-25
3-5	True and Predicted Third Order Intermodulation. Predicted based on optimized identified pole.....	3-26
3-6	Frequency Responses of the True and Identified Systems for Three Pole Example.....	3-28
3-7	True and Predicted Third Harmonic. Predicted based on two identified poles at $\hat{s}_1 = -1$ and $\hat{s}_2 = -10$	3-30
3-8	True and Predicted Third Order Intermodulation. Predicted based on two identified poles at $\hat{s}_1 = -1$ and $\hat{s}_2 = -10$	3-31
4-1	Back-to-Back Diode Pair with an Antenna System which Represent a Symmetrical Nonlinearity.....	4-4
4-2	Simplified Circuit Model for the MIM Junction.....	4-4
4-3	Norton Equivalent Circuit for the MIM Junction.....	4-6
4-4	Circuit used in Determining the Linear Voltage $v_1(t)$	4-6
4-5	Example of "Rusty Bolt" Linear System Response Measurement.....	4-12
4-6	Sidelobe to Sidelobe "Rusty Bolt" Coupling.....	4-19
4-7	Mainbeam to Mainbeam "Rusty Bolt" Coupling.....	4-19
5-1	Fifth Order System Model.....	5-11
5-2	Third Order Intermodulation Magnitude as a Function of f_2	5-16
5-3	Intermodulation Magnitude at Frequency $2f_1-f_2$, $\left(\frac{k_3}{k_5}\right) = 20$ dB.....	5-17
5-4	Intermodulation Magnitude at Frequency $2f_1-f_2$, $\left(\frac{k_3}{k_5}\right) = 10$ dB.....	5-19

LIST OF FIGURES (Concluded)

<u>FIGURE</u>		<u>PAGE</u>
5-5	True and Estimated Third Order Harmonic using Volterra Voltage to Voltage Transfer Function, Estimate Based on Two Poles.....	5-28
5-6	True and Estimated Third Order Harmonic using Volterra Voltage to Voltage Transfer Function, Estimate Based on Two Poles.....	5-29
5-7	True and Estimated Third Order Harmonic using Volterra Voltage to Voltage Transfer Function, Estimate Based on a Single Pole.....	5-31
5-8	True and Estimated Third Order Intermodulation using Volterra Voltage to Voltage, Estimate Based on a Single Pole.....	5-32
5-9	True and Estimated Fifth Order Harmonic using Volterra Voltage to Voltage Transfer Functions.....	5-38
6-1	Harmonic Generation Measurement.....	6-4
6-2	Intermodulation Generation Measurement.....	6-4

LIST OF TABLES

<u>TABLE</u>		<u>PAGE</u>
3-1	First and Second Order Nonlinear Responses.....	3-12
3-2	Third Order Nonlinear Responses.....	3-13
3-3	Optimized Identification of the System	
	$H_1(s) = \frac{9}{(s+1)(s+10)}$	3-19
3-4	Non-Optimized Identification of the System	
	$H_1(s) = \frac{9}{(s+1)(s+10)}$	3-20
5-1	Estimated Constants as a Function of Fundamental Measurement Frequency.....	5-34
5-2	Comparison of Estimated Constants using a Highly Ill-Conditioned System of Equations and Harmonic Measurements with the Assumption $k_5=0$	5-39

SECTION 1

INTRODUCTION

Air Force C³I systems may have to operate in an electromagnetically hostile environment. Collocated transmitters and receivers, on electromagnetically dense platforms, are susceptible to performance degradation through nonlinear effects. The objective of this program was to specify equipment level EMC performance in terms of nonlinear transfer functions (NLTFs) and to evaluate the quality of the specification parameters. The NLTFs are defined by Volterra theory. The specification parameters, such as harmonic distortion, intermodulation and crossmodulation can be specified by the NLTFs.

The approach taken in this program is to identify the NLTFs, use the NLTFs to predict the specification parameters and analyze the resulting errors in the EMC performance criteria. It is assumed that the nonlinear systems of interest can be modeled as lumped parameter circuits with zero-memory nonlinearities between the circuit nodes. In this case the NLTF function poles are determined by the poles of the linear part of the circuit.

Two different situations are treated in this report. In the first, the linear transfer function output can be measured. That is, the measured signal is the output of the nonlinear system excited by a known input plus noise. In this case, a linear system identification technique, such as the pencil-of-functions method [Jain (1980)], can be used to identify the poles of the linear system based on the transient response. These poles then specify the poles of the NLTFs.

In the second, the received signal is composed of the nonlinear system output, additive noise and a strong direct path component which is independent of the system. This case arises

in the identification of a "rusty bolt" (a Metal-Insulator-Metal or Metal-Oxide-Metal) function. Because of the relative strength of the direct path transmission between the input and the output, the linear system response cannot be measured. It is then necessary to estimate the poles of the linear and nonlinear transfer functions based on the sinusoidal steady state measurements of the third-order transfer functions.

The report is organized as follows. First, the general case where the linear system output can be measured is considered in Sections 2 and 3.

In Section 2, the problem of lumped parameter nonlinear system identification is defined. The Volterra series representation of such systems is given and the fact that the linear system transfer function poles determine the nonlinear transfer function poles is presented. The NLTF identification problem then reduces to the identification of the linear transfer function poles and of the residues of the NLTFs. A survey of linear system identification techniques based on the analysis of the transient response is presented. Criteria to be used in specifying the probe waveform and typical probe waveforms are described. The identification of the linear system poles requires two steps. The characteristic polynomial of the system function must be estimated and then be factored in order to determine the poles. The errors that can be made include the misidentification of the number of poles or, equivalently, of the degree of the characteristic polynomial, errors in the coefficients of the characteristic polynomial and errors resulting from the factoring operation. It is shown that relatively large errors in pole locations may result even if the number of poles is determined correctly and the errors in the coefficients are small.

In Section 3, the EMC specification parameters are first related to the NLTFs of the system. The specification parameters of interest include gain compression and desensitization, cross modulation, intermodulation and harmonic distortion. A sensitivity analysis of the effects of linear system function errors on the NLTFs and the specification parameters is performed.

Based on several examples, it is concluded that mean squared error between the measured output and the output of the identified system is a more reliable predictor of the errors in the NLTF specification parameters than are errors in pole locations. It is, however, found that the global mean squared error between the outputs cannot be used to predict the error in the specification parameters in all cases, especially when the number of poles is misidentified. Instead an error criterion which is segmented in frequency should be used.

Sections 4, 5 and 6 deal with the second type of NLTF identification where the linear system function cannot be directly identified. Air Force C³I platforms, such as the E-3A (AWACS) and E-4B, contain a large number of colocated transmitters and receivers. There is a recognized interference problem in these dense electronic platforms due to harmonic and intermodulation interference caused by the nonlinearity of metal-insulator-metal (MIM) or metal-oxide-metal (MOM) functions in the structure. These functions are colloquially referred to as "rusty bolts". The nonlinear characteristics cause harmonic, cross modulation and intermodulation products which couple to a re-radiating structure. The nonlinear products which fall into the passband of nearby receivers degrade system performance.

In Section 4, a lumped parameter circuit model of the "rusty bolt" and the nonlinear transfer functions that are to be used in the analysis are derived. It is shown that, in this case also, the NLTFs depend only on a linear transfer function and on

the coefficients of the nonlinear current-voltage MIM characteristic. It is demonstrated, however, that in a typical measurement situation on board an aircraft, the power level of the output of the "rusty bolt" linear transfer function can be expected to be some 40 dB below that of the free space direct path signal between the transmitting and receiving antennas. Identification of the rusty bolt linear system poles based on such a relatively weak rusty bolt output signal would not be feasible in practice. Therefore, the rusty bolt can only be identified from direct measurements of the nonlinear response.

Section 5 addresses the problem of rusty bolt NLTF identification. Rusty bolt identification based on transient and steady state nonlinear response measurements is first considered. It is concluded that identification based on the sinusoidal steady state response is better suited for the rusty bolt problem because of the difficulty of separating the nonlinear transient response from the linear transient response or the direct path component. Sinusoidal steady state probing allows the separation of the different order responses and can be used to measure the frequency response of the third order nonlinear transfer function. Based on the rusty bolt circuit model and on the third order NLTF frequency response, the poles of the linear transfer function can be identified. The remaining unknowns, the rusty bolt NLTF specification parameter constants, can then be determined from harmonic measurements.

Once the identification is completed the nonlinear specification parameters of the rusty bolt such as intermodulation and harmonic distortion can be predicted. Section 5.2 examines the errors that can be encountered in the identified parameters and in the predicted EMC specification parameters.

The measurement and instrumentation criteria to be used in the sinusoidal steady state identification of the rusty bolt are presented in Section 6.

Finally the conclusions which can be drawn from this study and recommendations for future work are described in Section 7.

SECTION 2

THE IDENTIFICATION PROBLEM

2.1 INTRODUCTION

A nonlinear system which exhibits no jumps or hysteresis can be represented by a Volterra series. The system's output $y(t)$ due to an excitation $x(t)$ is given by

$$\begin{aligned} y(t) &= \sum_{n=1}^{\infty} \int_{-\infty}^{\infty} \cdots \int_{-\infty}^{\infty} h_n(u_1, \dots, u_n) \prod_{i=1}^n x(t-u_i) du_i \\ &= \sum_{n=1}^{\infty} y_n(t) \end{aligned} \tag{2.1}$$

where $y_n(t)$ is the n th-order system output. The system is then characterized, i.e., its input-output relation is completely specified, when the n th-order impulse responses $h_n(u_1, \dots, u_n)$, $n=1, 2, \dots$ are identified.

If the system's nonlinearity is mild, the output is given by the first few, normally the first three, terms of the series:

$$y(t) \approx \sum_{n=1}^3 y_n(t) . \tag{2.2}$$

In order to characterize an n th order system, it is necessary to determine $h_n(u_1, \dots, u_n)$, $n=1, 2, \dots$ or, equivalently, the higher-order transfer functions which are the n -dimensional Laplace transforms of $h_n(u_1, \dots, u_n)$; for the mild case, $n=3$, and:

$$H_1(s) = L_1[h_1(u)]$$

$$H_2(s_1, s_2) = L_2[h_2(u_1, u_2)] \quad (2.3)$$

$$H_3(s_1, s_2, s_3) = L_3[h_3(u_1, u_2, u_3)] ,$$

where L_n denotes the n -dimensional Laplace transformation.

This problem is, in general, extremely complex since it involves the determination of multidimensional functions. It has however been shown that, in the case where the nonlinear system is a lumped parameter circuit with zero-memory nonlinearities between circuit nodes, the equivalent higher order transfer function poles can be obtained from the poles of the linear transfer function [Graham and Ehrman (1973); Ewen (1975)]. More precisely, let the transfer function of the linear part of the system be given by

$$\begin{aligned} H_1(s) &= \frac{\prod_{i=1}^M (s+q_i)}{\prod_{i=1}^N (s+p_i)} , \quad M < N \\ &= \sum_{i=1}^N \frac{R_i}{s+p_i} \end{aligned} \quad (2.4)$$

where, $-q_1, -q_2, \dots, -q_M$; $-p_1, -p_2, \dots, -p_N$; R_1, R_2, \dots, R_N , are, respectively, the zeros, poles and residues of the transfer function and it has been assumed for notational simplicity that the poles are distinct. Then, the 2nd and 3rd-order transfer functions are given, respectively, by [Ewen, (1975)]

$$H_2(s_1, s_2) = \sum_{k_1=1}^L \sum_{k_2=1}^N A_{k_1 k_2} \frac{s_1 + s_2 + 2a_{k_2}}{(s_1 + s_2 + a_{k_1} + a_{k_2})(s_2 + a_{k_2})(s_1 + a_{k_2})}$$

$$H_3(s_1, s_2, s_3) = \frac{1}{3} \sum_{k_1=1}^J \sum_{k_2=1}^L \sum_{k_3=1}^N \frac{C_{k_1 k_2 k_3}}{(s_1 + s_2 + s_3 + (a_{k_1} + a_{k_2} + a_{k_3}))}$$

(2.5)

$$\begin{aligned} & \left[\frac{1}{(s_1 + a_{k_3})(s_1 + s_3 + (a_{k_2} + a_{k_3}))} + \frac{1}{(s_2 + a_{k_3})(s_1 + s_2 + (a_{k_2} + a_{k_3}))} \right. \\ & + \frac{1}{(s_1 + a_{k_3})(s_1 + s_2 + (a_{k_2} + a_{k_3}))} + \frac{1}{(s_3 + a_{k_3})(s_2 + s_3 + (a_{k_2} + a_{k_3}))} \\ & \left. + \frac{1}{(s_2 + a_{k_3})(s_2 + s_3 + (a_{k_2} + a_{k_3}))} + \frac{1}{(s_3 + a_{k_3})(s_1 + s_3 + (a_{k_2} + a_{k_3}))} \right] \end{aligned}$$

where, the quantities $J, L, N, a_{k_1}, a_{k_2}$ are uniquely determined by the poles of the linear transfer function $H_1(s)$. The complete identification of the nonlinear transfer functions of the system requires, therefore, the identification of the linear transfer function and the determination of the constants $A_{k_1 k_2}$ and $C_{k_1 k_2 k_3}$ for the permissible values of k_1, k_2 , and k_3 .

The poles of the linear transfer function thus play a crucial role in the identification of the linear and nonlinear parts of the system. They not only specify the denominator of $H_1(s)$, but also linear combinations of these poles determine the poles of $H_2(s_1, s_2)$ and $H_3(s_1, s_2, s_3)$.

In this section we will present a survey and review of linear system identification techniques, discuss the factors to be used to specify the probe waveforms and analyze the effect of errors in pole locations on the quality of the linear system frequency response identification. Since the identification of the nonlinear transfer functions is also based on the identified linear system poles, the general conclusions will also apply to the accuracy of nonlinear identification. This problem is discussed more fully in Section 3 where NLTF specification parameters such as harmonic distortion and intermodulation are related to the linear and nonlinear transfer functions and the effects on identification errors of these parameters are analyzed.

2.2 IDENTIFICATION TECHNIQUE SURVEY AND REVIEW

An important class of identification techniques for lumped parameter, linear, time invariant, systems is based on the estimation of the characteristic polynomial of the system function. The characteristic polynomial is then factored to obtain the poles. Methods based on this procedure will be presented in this section. Two other techniques which may be used, the equation error and quasi-linearization methods, are presented in Appendix A by V.K. Jain. Note that these methods are based on the analysis of the transient response of the system. A method which uses steady state measurements is described in Section 5.

These transient analysis methods are related to the Prony method [Prony (1895)] of modeling data by a linear combination of exponentials. The relationship between Prony's method and spectral estimation is described by Kay and Marple [1981]. Applications of Prony's method and various implementations and refinements of the technique are presented by Bucker (1977), Chuang and Moffatt (1976), Jackson and Soong (1978), Jackson et al (1978), McDonough (1963), Mittra and Pearson (1978), Prado and

Moroney (1978) and Scqahubert (1979). Note that, as described below, the pencil of functions method [Jain, 1974, Jain, 1980] may be viewed as a variation and an improvement of Prony's technique.

The system to be identified is excited by a known probe waveform $x(t)$ and the output $y(t)$ is measured. Since the identification is performed by computer analysis, sampled versions of the system input and output are used. The sampled measured output $y(n)$ contains noise and can therefore be expressed as

$$y(n) = \hat{y}(n) + e(n) \quad (2.6)$$

where $\hat{y}(n)$ is the model output of the system to be identified and $e(n)$ is the additive noise component. The system function of the model is given in the z -domain by

$$\frac{\hat{Y}(z)}{X(z)} = \frac{P(z)}{Q(z)} = \frac{P(z)}{\prod_{i=1}^p (z - z_i)} \quad (2.7)$$

where $X(z)$ and $\hat{Y}(z)$ are, respectively, the z -transform of the sequence of input samples $x(n)$ and of $\hat{y}(n)$. The natural log of z_1, \dots, z_p divided by the sampling time interval are the poles. In the discussion that follows we will, for convenience, refer to the z_i 's as the poles. Suppose that the input is such that $X(z)$ is a rational function of z :

$$X(z) = \frac{R(z)}{S(z)} = \frac{R(z)}{\prod_{i=p+1}^{p+q} (z - z_i)} \quad (2.8)$$

where z_{p+1}, \dots, z_{p+q} are the poles of the input $X(z)$. It follows from (2.7) and (2.8) that

$$\hat{Y}(z) = \frac{P(z) R(z)}{\prod_{i=1}^{p+q} (z - z_i)} = \frac{P(z) R(z)}{\psi(z)} \quad (2.9)$$

where $\psi(z)$ is the characteristic polynomial of $\hat{Y}(z)$, and is equal to

$$\begin{aligned} \psi(z) &= Q(z) S(z) = \prod_{i=1}^{p+q} (z - z_i) \\ &= \sum_{i=0}^{p+q} a_i z^{p+q-i}, \quad a_0 = 1. \end{aligned} \quad (2.10)$$

Note that the system model's poles z_1, \dots, z_p and the input poles z_{p+1}, \dots, z_{p+q} are the roots of the characteristic polynomial of $\hat{Y}(z)$. That is,

$$\psi(z_i) = 0, \quad i = 1, 2, \dots, p+q. \quad (2.11)$$

It is therefore desired to estimate the characteristic polynomial $\psi(z)$ or, equivalently, the coefficients of the characteristic polynomial a_1, \dots, a_{p+q} based on the measurements $y(n)$, $n = 0, 1, \dots, N-1$. The system poles can then be obtained by factoring $\psi(z)$.

The coefficients of the characteristic polynomial are chosen as those which minimize the mean square difference E between the model output $\hat{y}(n)$ and the measured output $y(n)$ where, using (2.6), E is defined as

$$\begin{aligned} E &= \frac{1}{N} \sum_{i=0}^{N-1} e^2(n) \\ &= \frac{1}{N} \sum_{i=0}^{N-1} [y(n) - \hat{y}(n)]^2 . \end{aligned} \quad (2.12)$$

It can be readily shown [Kay and Marple, 1981] that the optimum coefficients are the solution of the matrix equation

$$[Y]^T [Y] \underline{A} = \begin{bmatrix} E \\ 0 \\ \vdots \\ 0 \end{bmatrix} \quad (2.13)$$

where, $[Y]$ is equal to

$$[Y] = \begin{bmatrix} y(p+q) & \dots & y(0) \\ \vdots & & \\ y(N-1) & \dots & y(N-p-q-1) \end{bmatrix} \quad (2.14)$$

A is the vector of coefficients

$$\underline{A}^T = (1, a_1, \dots, a_{p+q}) \quad . \quad (2.15)$$

and E is the mean-squared error.

Note that $[Y]^T[Y]$ is the covariance matrix of the measured sequence $y(n)$. It is also the Gram matrix [Jain, 1974] of the set of vectors

$$\{y_0^T \dots y_{p+q}^T\} \quad (2.16)$$

where,

$$y_0^T = (y(0), \dots, y(N-p-q-1))$$

$$y_1^T = (y(1), \dots, y(N-p-q))$$

$$\vdots$$

$$y_{p+q}^T = (y(p+q), \dots, y(N-1)) \quad .$$

The vector of coefficients is then the solution to the matrix equation in (2.13). Using (2.12), the coefficients define the characteristic polynomial

$$\psi(z) = \sum_{i=0}^{p+q} a_i z^{p+q-i} \quad (2.17)$$

and the poles are obtained as the roots of $\psi(z)$.

Three classes of identification techniques can then be defined based on the method used to solve the matrix equation (2.13)

$$[C] \underline{A} = [Y]^T [Y] \underline{A} = \begin{bmatrix} E \\ 0 \\ \cdot \\ \cdot \\ 0 \end{bmatrix}. \quad (2.18)$$

The first solution for the coefficients is obtained by inverting $[C]$. This is the method generally used when performing spectral estimation [Morf (1974), Morf et al (1976, 1977, 1978), Friedlander et al (1979)].

The second estimates the vector of coefficients as the eigenvector corresponding to the smallest eigenvalue of $[C]$. This method was used by Van Blaricum (1978) and Van Blaricum and Mitra (1978, 1980). The third, the pencil-of-functions method developed by Jain (1974, 1980), estimates the coefficients as the diagonal cofactors of $[C]$. Note that the pencil-of-functions method is derived for the case where the error, in the case of idealized measurements, between the model output $\hat{y}(n)$ and the measured output $y(n)$ is zero. It is related, therefore, to the solution of (2.18) with $E=0$.

In the above formulation of the identification problem, the input poles would be identified together with the system poles. The system poles only can be identified by augmenting the set of vectors in (2.16) and thus [C] with vectors obtained from the input poles which are known (Rudko and Bussgang (1982), Jain (1980)). The solution of (2.18) for the coefficients requires that the number of poles be known. The number can be estimated based on the rank of [C] [Jain (1974, 1980), Chow (1972)].

It should be noted that the pencil-of-functions method developed by Jain (1974, 1980) permits several refinements and improvements of the basic technique presented above. In particular, instead of using shifted versions of the vector y_0 to form the set of vectors in (2.16) it uses the outputs of a cascade of filters. As long as the input is passed through the same filters as the output, no extra poles need be identified. Jain has also developed a noise correction technique which improves the performance of the pencil-of-functions method in the presence of noise (Jain, 1980).

As mentioned above, the identification of the linear system poles requires the factoring of the characteristic polynomial (2.17). It should be noted [Dudley, 1979] that small errors in the polynomial coefficients can produce large errors in the pole locations. This is discussed further in Section 2.4.

Once the poles have been found, the system zeros or residues must be determined in order to complete the identification procedure. The system zeros may be found by using the pencil of functions technique [Jain, 1980]. The residues can be identified by minimizing the mean-squared error between the measured output $y(n)$ and the model output $\hat{y}(n)$. Suppose that the poles z_1, \dots, z_p of the model have been identified and that the poles of the input z_{p+1}, \dots, z_{p+q} are known. Then, using (2.12) and (2.13)

$$\hat{Y}(z) = \frac{P(z) R(z)}{\psi(z)} = \frac{P(z) R(z)}{\prod_{i=1}^{p+q} (z - z_i)} . \quad (2.19)$$

Performing a partial fraction expansion of $\hat{Y}(z)$ and taking the inverse z-transform it follows that

$$\hat{y}(n) = \sum_{i=1}^{p+q} b_i z_i^n \quad (2.20)$$

where b_1, b_2, \dots, b_n are the residues of $Y(z)$. The residues are determined by minimizing

$$E = \sum_{i=0}^{N-1} [y(n) - \hat{y}(n)]^2 . \quad (2.21)$$

The solution (Kay and Marple, 1981) requires a matrix inversion:

$$\underline{B} = [\underline{\phi}^T \underline{\phi}]^{-1} \underline{\phi}^T \underline{Y} \quad (2.22)$$

where

$$\underline{\Phi} = \begin{bmatrix} z_1^1 & z_2^1 & z_{p+q}^1 \\ \vdots & & \\ z_1^{N-1} & z_2^{N-1} & z_{p+q}^{N-1} \end{bmatrix}$$

$$\underline{B} = [b_1 b_2 \dots b_{p+q}]^T$$

$$\underline{Y} = [y(0) \dots y(N-1)]^T .$$

The performance of this technique in the case where the measured output contains noise is analyzed in Section 2.4

2.3 PROBE WAVEFORM INVESTIGATION

The general problem of the synthesis of optimal inputs for system identification is difficult and the general formulation [Mehra, 1974; Mehra, 1976; and Mehra and Lainiotis, 1976] is cumbersome to implement. Consequently, probe waveforms are chosen on a more heuristic basis. In the choice of the excitation the following factors need to be considered:

1. The excitation must be easy to implement in practice.
2. It must excite the system poles. Since the response due to the system is the sum of decaying real or complex exponentials, the identification is based on the transient system response. This transient response must be excited by the input.

3. It must be adjustable so that, as a first step, it will essentially only excite the linear part of the system.
4. It must result in an easily analyzable and identifiable output.

Based on such general measurements [Jain, (1980)] has implemented several classes of inputs which resulted in the successful identification of the system poles using the pencil-of-functions technique. These inputs included triangular waves, oscillatory pulses modulated either by a decaying exponential or by a negative slope ramp, square pulses and exponentials. The choice of input does not appear to be critical as long as the factors above are satisfied and the bandwidth of the input is larger than the bandwidth of the system (or portion of the frequency response range of frequencies) under test.

2.4 IDENTIFICATION ERROR ANALYSIS

As discussed in Section 2.2, system identification based on transient analysis requires the following steps:

- The calculations of the covariance matrix $[C]$ (Equation (2.18))
- The determination of the number of poles,
- The estimation of the coefficients of the characteristics polynomial (Equations (2.10) and (2.17)),
- The factorization of the characteristic polynomial in order to determine the poles,

- The estimation of the zeros or residues of the system function.

If, as is true in practice, the identification is based on noisy measurements each one of these steps may produce erroneous results. The elements of the covariance matrix will contain noise components. As a result an incorrect number of poles may be determined. In such cases, the coefficients of the characteristic polynomial and, consequently, the identified poles will, in most cases, be far from the true values. If the number of poles is determined correctly, the error in the identified pole locations can still be large even if the coefficient errors are small. Consider an example presented by Dudley [1979]. Suppose that the system has three poles and that the characteristic polynomial is given by

$$\psi(z) = \sum_{i=0}^3 a_i z^i \quad (2.23)$$

where,

$$a_0 = -1.662, a_1 = 5.036, a_2 = -5.349, a_3 = 2.0 \quad .$$

The poles, which are the roots of the polynomial in (2.23), can be calculated to be

$$z_1 = -0.08780, z_2 = -0.04866 + j 0.3947 ,$$

$$z_3 = -0.04866 - j 0.3947 \quad .$$

If the coefficients are estimated to be

$$\hat{a}_0 = -1.669, \hat{a}_1 = 5.036, a_2 = -5.348, a_3 = 2.001 ,$$

the identified pole locations become

$$\hat{z}_1 = -0.06692, \hat{z}_2 = -0.05725 + j 0.4030,$$

$$\hat{z}_3 = -0.05725 - j 0.4030 .$$

The largest relative error in the polynomial coefficients is

$$\left| \frac{\hat{a}_0 - a_0}{a_0} \right| \times 100 = 0.42\% .$$

However the largest errors in pole locations z_1 and z_2 are

$$\left| \frac{\hat{z}_1 - z_1}{z_1} \right| \times 100 = 24\%$$

and

$$\frac{R_e\{z_2\} - R_e\{\hat{z}_2\}}{R_e\{z_2\}} \times 100 = 18\% .$$

It can therefore be observed that the errors in coefficients have been strongly magnified. Note the error amplification described above is of primary importance only if the desired result is the locations of the system poles. In the context of present study, however, it is desired to estimate parameters such as harmonic distortion and intermodulation which are related to the frequency response of the system. As will be shown in Sections 3 and 5, the frequency response may be accurate even though the pole locations may have large errors associated with them. This can be justified by the fact that the frequency response is determined by the characteristic polynomial (and thus its coefficients) and not by the locations of individual poles.

Finally, the linear identification is completed by calculating the residues or zeros of the system function. The zeros may be identified using the pencil of functions method. The values obtained are essentially independent of the identified poles [Jain (1980)]. The residues are identified by minimizing the mean-square error between the system output $y(n)$ and the approximate output (2.20)

$$\sum_{\ell=1}^N b_{\ell} \hat{z}_{\ell}^n \quad (2.24)$$

where, $\hat{z}_1, \dots, \hat{z}_N$ are the poles which have been previously identified. Since the identified poles are used in the determination of the residues, the residues can in some cases compensate for errors in the poles.

It should be noted that the final step of nonlinear transfer function identification based on transient measurement requires the determination of the residues or zeros of the nonlinear transfer functions. This can be accomplished using the same technique as for the identification of the linear system residues or zeros.

In the next section, we will discuss the nonlinear transfer function (NLTF) specification parameters. We will also present results that apply to the general identification and EMC specification parameter prediction problem.

SECTION 3

NLTF SPECIFICATION PARAMETER INVESTIGATION

Air Force C³I systems can suffer degradation due to intra-system nonlinear mechanisms that are usually associated with the co-location of multiple transmitters and receivers on electronically dense platforms. The nonlinearities can occur in transmitters, coupling paths and in receivers. Together the nonlinearities generate a spectrum of unwanted interference signals which degrade the desired signal spectral fidelity and EMC performance. The EMC specification parameters such as harmonic distortion, gain compression, intermodulation, cross-modulation and spurious response can be expressed in terms of nonlinear transfer functions (NLTF). The NLTF (Volterra transfer functions) in turn can be expressed as functions of the linear transfer function (LTF). In this section, we will investigate the features of the NLTF and the specification parameters for the general problem. The "rusty bolt" path nonlinearity which is a special case of the class of nonlinear systems where the lumped parameter circuit contains zero-memory nonlinearities between circuit nodes is discussed in Sections 4 and 5. We will begin with a discussion of nonlinear systems.

3.1 RELATIONSHIP OF SPECIFICATION PARAMETERS TO NLTF AND LTF

Traditionally, the EMC community has primarily used power series to analyze nonlinear systems. In the following discussion, presented for background purposes [Graham and Ehrman (1973), Weiner and Spina (1980)], we will use power series to illustrate the EMC specification parameters. We will then introduce in the next subsection the Volterra series, the Volterra NLTF's, and the relationship between the EMC specification parameters and the NLTF.

3.1.1 Nonlinear Systems Without Memory

In almost all cases of interest in communications system analysis, the input to the system is the sum of a desired and one or more interfering signals. These signals interact in the nonlinearities to produce various types of responses. The most common of these responses are given names so that they can be easily referred to, e.g., intermodulation, crossmodulation, compression, and desensitization. In this section we will categorize and give examples of these effects. The thrust of this discussion comes from Graham and Ehrman (1973). To begin, consider a nonlinear system represented by the power series:

$$y(t) = \sum_{n=1}^{\infty} a_n x(t)^n . \quad (3.1)$$

The system has no memory since the output at time t depends only on the input at the same instant. Let the input, $x(t)$, be the sum of $S_1(t)$, a desired signal, and $I_2(t)$ and $I_3(t)$, two interferences. The output, $y(t)$ is then:

$$\begin{aligned} y(t) = & a_1 [S_1(t) + I_2(t) + I_3(t)] \\ & + a_2 [S_1(t) + I_2(t) + I_3(t)]^2 \\ & + a_3 [S_1(t) + I_2(t) + I_3(t)]^3 \\ & . \\ & . \\ & . \end{aligned} \quad (3.2)$$

3.1.1.1 Gain Compression and Desensitization

Now let us specialize Equation (3.2) to certain cases. First let

$$\begin{aligned} S_1(t) &= S_1 \cos \omega_1 t, \\ I_2(t) &= I_2 \cos \omega_2 t, \\ I_3(t) &= 0. \end{aligned} \tag{3.3}$$

That is, $S_1(t)$ and $I_2(t)$ are unmodulated tones. Then:

$$\begin{aligned} y(t) = & a_1 S_1 \left[1 + \frac{3a_3}{4a_1} S_1^2 + \frac{3a_3}{2a_1} I_2^2 \right] \cos \omega_1 t \\ & + \text{terms at other frequencies.} \end{aligned} \tag{3.4}$$

Equation (3.4) demonstrates that the output at the signal frequency is made up of three terms. The first term, of amplitude $a_1 S_1$, is the desired linear response. The second term, of amplitude $3/4 a_3 S_1^3$, is the third order compression term. If the sign of a_3 is opposite that of a_1 , the desired signal output will be smaller than that predicted by linear theory by the amount $3/4 a_3 S_1^3$. The third term, of amplitude $3/2 a_3 I_2^2 S_1$, is the third order desensitization term. If the sign of a_3 is opposite that of a_1 the output will be smaller than that predicted by linear theory.

3.1.1.2 Crossmodulation

Assume:

$$S_1(t) = S_1 \cos \omega_1 t,$$

$$I_2(t) = I_2 [1 + m(t)] \cos \omega_2 t; m < 1, \quad (3.5)$$

$$I_3(t) = 0.$$

That is, $S_1(t)$ is an unmodulated tone, and $I_2(t)$ is an amplitude modulated signal. Then:

$$y(t) \approx a_1 S_1 \left[1 + \frac{3a_3}{4a_1} S_1^2 + \frac{3a_3}{2a_1} I_2^2 + \frac{3a_3}{a_1} I_2^2 m(t) \right] \cos \omega_1 t$$

$$+ \text{terms at other frequencies.} \quad (3.6)$$

Equation (3.6) includes the desensitization and compression terms of Equation (3.4) plus a new term, $(3a_3/a_1)I_2^2 m(t)$. The new term represents crossmodulation, that is, a transfer of the modulation $m(t)$ from the interference to the desired signal.

3.1.1.3 Intermodulation

Assume:

$$S_1(t) = S_1 \cos \omega_1 t,$$

$$I_2(t) = I_2 \cos \omega_2 t, \quad (3.7)$$

$$I_3(t) = I_3 \cos \omega_3 t.$$

That is, the desired signal and the two interferences are unmodulated tones. Then

$$\begin{aligned} y(t) = & a_1 S_1 \left[1 + \frac{3a_3}{4a_1} S_1^2 + \frac{3a_3}{2a_1} (I_2^2 + I_3^2) \right] \cos \omega_1 t \\ & + a_2 I_2 I_3 [\cos (\omega_2 + \omega_3)t + \cos (\omega_2 - \omega_3)t] \\ & + \frac{3}{4} a_3 [I_2^2 I_3 \cos(2\omega_2 \pm \omega_3)t + I_2 I_3^2 \cos(2\omega_3 \pm \omega_2)t] \\ & + \text{terms at other frequencies.} \end{aligned} \quad (3.8)$$

The terms in Equation (3.8) at frequencies $\omega_2 \pm \omega_3$ are second order intermodulation terms. The terms at $2\omega_2 \pm \omega_3$ and $2\omega_3 \pm \omega_2$ are third order intermodulation terms. If any of the frequency combinations fall in the system passband, they will be processed by the remainder of the system following the nonlinearity in the same manner as the desired signal. Third order intermodulation

can be a serious problem if ω_2 and ω_3 are near the system pass-band. Second order distortion is usually a less serious problem in a receiver, since either one or both of the interference frequencies must be far removed from the system passband for $\omega_2 \pm \omega_3$ to equal ω_1 .

The examples given in this section have, for introductory purposes, been in terms of real signals and a zero-memory power-series nonlinearity. In the next subsection we will introduce the Volterra series. It will also be shown that the specification parameters such as intermodulation, harmonic distortion, etc., are related to the Volterra transfer functions.

3.1.2 Nonlinear Systems With Memory

The analysis in the previous section assumed that the nonlinear system was memoryless. In many cases this is not so and a valid analysis should take this into account.

Suppose that the nonlinear system can be described by a Volterra series. Then, the system is described by the time domain input-output relationship.

$$y(t) = \sum_{n=1}^{\infty} y_n(t) \quad (3.9)$$

where

$$y_n(t) = \int_{-\infty}^{\infty} \dots \int_{-\infty}^{\infty} h_n(u_1, \dots, u_n) \prod_{i=1}^n x(t - u_i) du_i$$

or by the input-spectrum/output-spectrum relationship

$$Y(f) = \int_{-\infty}^{\infty} \int_{-\infty}^{\infty} \dots \int_{-\infty}^{\infty} H_n(f_1, \dots, f_n) X(f_1), \dots, X(f_n) \delta(f - f_1 - \dots - f_n) df_1 \dots df_n. \quad (3.10)$$

One of the most important multiple signal input waveforms for a nonlinear system characterized by a Volterra series is the sum of several unmodulated tones. If we express $M/2$ tones as the sums of M exponentials of complex amplitude A_m and frequency f_m , we have

$$x(t) = \frac{1}{2} \sum_{m=1}^M A_m e^{j2\pi f_m t}. \quad (3.11)$$

Since $x(t)$ must always be real, f_m will include identical positive and negative frequencies, and A_m for a negative frequency will be the complex conjugate of A_m for the positive frequency. A real signal is the sum of a positive frequency complex signal and its negative frequency complex conjugate. Alternatively, a real signal is twice the real part of either the positive frequency complex signal or its negative frequency complex conjugate. The frequency spectrum of this $x(t)$ is

$$X(f) = \frac{1}{2} \sum_m A_m \delta(f - f_m) \quad (3.12)$$

where $\delta(f - f_m)$ is a unit impulse at $f = f_m$ in the frequency domain.

Since, using (3.9), the system response $y(t)$ may be written in the form

$$y(t) = \sum_n y_n(t), \quad (3.13)$$

where the various $y_n(t)$ are the individual terms in the Volterra series of the system output. Our objective is to determine the various order responses $y_n(t)$ in terms of the nonlinear transfer functions of the system. For example,

$$y_1(t) = \frac{1}{2} \sum_{m=1}^M A_m H_1(f_m) e^{j2\pi f_m t}, \quad (3.14)$$

by inspection from Equation (3.11), where $H_1(f_m)$ is the linear transfer function of the system at frequency f_m . The n -th order output can occur at many frequency combinations, depending on the number of complex inputs, M , and the order, n . A general expression for the output frequency, denoted by f_Σ , is

$$f_\Sigma = m_1 f_1 + m_2 f_2 \dots + m_M f_M, \quad (3.15)$$

where $m_1, m_2 \dots m_M$ are integers ranging from 0 to n , and

$$\sum_{i=1}^M m_i = n. \quad (3.16)$$

Define the vector \underline{m} as

$$\underline{m} = [m_1, m_2, \dots, m_M]. \quad (3.17)$$

For $x(t)$ given by Equation (3.11), the n th order output is then given by

$$y_n(t) = \frac{1}{2} \sum_{\underline{m}} B_n(\underline{m}) H_n e^{j2\pi f_{\Sigma} t}, \quad (3.18)$$

where the \underline{m} under the sum indicates that the sum includes all the distinct sets $\{m_i\}$ such that $m_i < m_{i+1}$ and Equation (3.16) is satisfied and

$$B_n(\underline{m}) = \frac{n! A_1^{m_1} A_2^{m_2} \dots A_M^{m_M}}{2^{n-1} m_1! m_2! \dots m_M!}, \quad (3.19)$$

and

$$H_n = H_n(\underbrace{f_1, \dots, f_1}_{m_1 \text{ times}}, \underbrace{f_2, \dots, f_2}_{m_2 \text{ times}}, \dots, \underbrace{f_M, \dots, f_M}_{m_M \text{ times}}). \quad (3.20)$$

There are

$$\frac{(M + n - 1)!}{n!(M - 1)!} \quad (3.21)$$

distinguishable combinations of m_i satisfying Equation (3.16) so that there will be $\binom{M+n-1}{n}$ terms to sum in Equation (3.18) for each n^{th} order nonlinear response. For example, if there are $M=4$ complex exponentials in $x(t)$ and we are interested in the $n=2$, or second order response, we can expect to sum

$$\frac{(4 + 2 - 1)!}{2!(4 - 1)!} = \frac{5!}{2!3!} = 10 \quad (3.22)$$

terms. For $n=3$, the third order term, there will be 20 such components.

The essential point to note here is that the complex amplitude of each of the spectral components in Equation (3.18) is given by the product $B_n(\underline{m}) H_n$ where B_n , given by Equation (3.19), is dependent on the input signal amplitudes A_m and is independent of frequency. The frequency dependence of the component is entirely given by H_n , the n th order nonlinear transfer function. It should now be evident that the key step in characterizing the output terms of a nonlinear system with memory resides in determining the magnitude and phase of the multi-dimensional transfer functions H_n .

When the nonlinear system has no memory it can be satisfactorily characterized by a power series $H_n=a_n$, the coefficients of the power series. It follows then that the preceding discussion also applies to a power series nonlinearity. In that case the n th order response components of the power series can be obtained by simply replacing H_n by a_n in (3.18).

3.1.2.1 Two-Tone Input Example

Multi-tone testing of quasi-linear (almost linear) systems is widely employed to characterize the nonlinear distortion. The

most important case is two-tone testing. In this section we shall utilize the general results of the previous section and show by an example how to obtain the output terms of a nonlinear system excited by two sinusoids. We have

$$x(t) = \frac{1}{2} \left[A_1 e^{j2\pi f_1 t} + A_2 e^{j2\pi f_2 t} + A_1^* e^{-j2\pi f_1 t} + A_2^* e^{-j2\pi f_2 t} \right], \quad (3.23)$$

where we now identify $M=4$, $A_3 = A_1^*$, $A_4 = A_2^*$; and $f_3 = -f_1$, $f_4 = -f_2$ by comparing terms in Equation (3.23) with Equation (3.11). Since $M=4$, m_1, m_2, m_3, m_4 must satisfy

$$m_1 + m_2 + m_3 + m_4 = n. \quad (3.24)$$

for non-negative integer values of m_i for each nonlinear order n . Using (3.21), four combinations of m_i for $n=1$, ten for $n=2$, and twenty for $n=3$ will satisfy (3.24).

The first and second order output components are listed in Table 3-1 [Busgang, Ehrman and Graham (1974)]. The frequency combinations of m_i associated with each response are noted. Note that both negative and positive frequency terms are present and that the complex amplitude of each negative frequency is the complex conjugate of each positive frequency term. The type of nonlinear response is also indicated in the last column of the table. No DC terms are generated by any odd order n . Also note that for every positive frequency term there is a corresponding negative frequency component with a complex conjugate amplitude. The physical output of such a system is one half the sum of both the positive and negative frequency components and will always be a real function. Of course, one can take the real part of the positive frequency terms and get the same result.

TABLE 3-1

FIRST AND SECOND ORDER NONLINEAR RESPONSES

COMBINATION NO.	COMBINATION				FREQUENCY OF RESPONSE	AMPLITUDE OF RESPONSE	TYPE OF RESPONSE
	m_1	m_2	m_3	m_4			
<u>$n = 1$</u>							
1	1	0	0	0	f_1	$A_1 H_1 (f_1)$	Linear
2	0	1	0	0	f_2	$A_2 H_1 (f_2)$	
3	0	0	1	0	$-f_1$	$A_1^* H_1 (-f_1)$	
4	0	0	0	1	$-f_2$	$A_2^* H_1 (-f_2)$	
<u>$n = 2$</u>							
1	1	1	0	0	f_1+f_2	$A_1 A_2 H_2 (f_1, f_2)$	Second Order Intermodulation
2	0	1	1	0	f_2-f_1	$A_2 A_1^* H_2(f_2, -f_1)$	
3	0	0	1	1	$-f_1-f_2$	$A_1^* H_2(-f_1, -f_2)$	
4	1	0	0	1	f_1-f_2	$A_1 A_2^* H_2(f_1, -f_2)$	
5	1	0	1	0	$f_1-f_1 = 0$	$ A_1 ^2 H_2 (f_1, -f_1)$	Second Harmonic
6	0	1	0	1	$f_2-f_2 = 0$	$ A_2 ^2 H_2(f_2, -f_2)$	
7	2	0	0	0	$2f_1$	$1/2 A_1^2 H_2(f_1, f_1)$	
8	0	2	0	0	$2f_2$	$1/2 A_2^2 H_2(f_2, f_2)$	
9	0	0	2	0	$-2f_1$	$1/2 A_1^{*2} H_2(-f_1, -f_1)$	
10	0	0	0	2	$-2f_2$	$1/2 A_2^{*2} H_2(-f_2, -f_2)$	

Each of the $n=1$ terms is a linear response. Four of the $n=2$ components are second harmonics and the remainder are second order intermodulation terms. Two of these are at DC.

The third order output components are listed in Table 3-2. Again the frequency, complex amplitude, and particular combination of m_i associated with the response is noted. We have also identified in the last column the type of response. Note the presence of terms causing third order gain compression and desensitization of the linear term at the input frequencies f_1 and f_2 . There is also a set of third order intermodulation products as well as a set of third harmonics.

These results can be extended to higher order nonlinearities.

Finally, let us write out explicitly the terms at a particular output frequency as a further illustration of the interpretation of Tables 3-1 and 3-2. At frequency f_2 , we have six responses, three at positive and three at negative frequencies. The positive frequency terms are the linear response (1,2) and the two third order components (3,1) and (3,10). The first number in the parenthesis denotes the order of the response (n) and the second number in the parenthesis indicates the combination number listed in Tables 3-1 and 3-2. Hence, at frequency f_2 ,

$$\begin{aligned}
 y(t) = & \frac{1}{2} [A_2 H_1(f_2) \\
 & + \frac{3}{2} |A_1|^2 A_2 H_3(f_1, f_2, -f_1) \\
 & + \frac{3}{4} |A_2|^2 A_2 H_3(f_2, f_2, -f_2)] e^{j2\pi f_2 t} \\
 & + \text{c.c. terms.}
 \end{aligned}
 \tag{3.25}$$

TABLE 3-2
THIRD ORDER NONLINEAR RESPONSES

COMBINATION NO.	COMBINATION				FREQUENCY OF RESPONSE	AMPLITUDE OF RESPONSE	TYPE OF RESPONSE
	m_1	m_2	m_3	m_4			
1	1	1	1	0	$f_1 + f_2 - f_1 = f_2$	$3/2 A_1 ^2 H_3(f_1, f_2, -f_1)$	Third Order Desensitization
2	0	1	1	1	$f_2 - f_1 - f_2 = -f_1$	$3/2 A_1^* A_2 ^2 H_3(f_2, -f_1, -f_2)$	
3	1	0	1	1	$f_1 - f_1 - f_2 = -f_2$	$3/2 A_1 ^2 A_2^* H_3(f_1, -f_1, -f_2)$	
4	1	1	0	1	$f_1 + f_2 - f_2 = f_1$	$3/2 A_1 A_2 ^2 H_3(f_1, f_2, -f_2)$	Third Order Intermodulation
5	2	1	0	0	$2f_1 + f_2$	$3/4 A_1^2 A_2 H_3(f_1, f_1, f_2)$	
6	0	2	1	0	$2f_2 - f_1$	$3/4 A_1^* A_2^2 H_3(f_2, f_2, -f_1)$	
7	0	0	2	1	$-2f_1 - f_1$	$3/4 A_1^* A_2^2 H_3(-f_1, -f_1, -f_2)$	
8	1	0	0	2	$f_1 - 2f_2$	$3/4 A_1 A_2^* H_3(f_1, -f_2, -f_2)$	
9	2	0	1	0	$2f_1 - f_1 = f_1$	$3/4 A_1 A_1 ^2 H_3(f_1, f_1, -f_1)$	Third Order Compression
10	0	2	0	1	$2f_2 - f_2 = f_2$	$3/4 A_2 A_2 ^2 H_3(f_2, f_2, -f_2)$	
11	1	0	2	0	$f_1 - 2f_1 = -f_1$	$3/4 A_1 ^2 A_1^* H_3(f_1, -f_1, -f_1)$	
12	0	1	0	2	$f_2 - 2f_2 = -f_2$	$3/4 A_2 ^2 A_2^* H_3(f_2, -f_2, -f_2)$	
13	2	0	0	1	$2f_1 - f_2$	$3/4 A_1^2 A_2^* H_3(f_1, f_1, -f_2)$	Third Order Intermodulation
14	1	2	0	0	$f_1 + 2f_2$	$3/4 A_1 A_2^2 H_3(f_1, f_2, f_2)$	
15	0	1	2	0	$f_2 - 2f_1$	$3/4 A_2 A_1^* H_3(f_2, -f_1, -f_1)$	
16	0	0	1	2	$-f_1 - 2f_2$	$3/4 A_1^* A_2^2 H_3(-f_1, -f_2, -f_2)$	
17	3	0	0	0	$3f_1$	$1/4 A_1^3 H_3(f_1, f_1, f_1)$	Third Harmonic
18	0	3	0	0	$3f_2$	$1/4 A_2^3 H_3(f_2, f_2, f_2)$	
19	0	0	3	0	$-3f_1$	$1/4 A_1^* H_3(-f_1, -f_1, -f_1)$	
20	0	0	0	3	$-3f_2$	$1/4 A_2^* H_3(-f_2, -f_2, -f_2)$	

where, the notation "c.c. terms" indicates the complex conjugates necessary for a real output signal. Alternatively, $y(t)$ is given by

$$y(t) = \text{Re}\left\{ \left[A_2 H_1(f_2) + \frac{3}{2} |A_1|^2 A_2 H_3(f_1, f_2, -f_1) + \frac{3}{4} |A_2|^2 A_2 H_3(f_2, f_2, -f_2) \right] e^{j2\pi f_2 t} \right\} . \quad (3.26)$$

The first term is the small signal linear response, the second term is the desensitization at frequency f_2 caused by the signal at f_1 , and the third term is the source of the compression of the f_2 term generated by the amplitude A_2 .

3.1.2.2 Specification Parameters

3.1.2.2.1 Gain Compression/Expansion

It is possible to predict gain compression or expansion using small signal theory involving third order nonlinear transfer functions. According to the small signal nonlinear theory outlined in Section 3.1.1, the complex amplitude of the output signal of a system excited by a single tone of amplitude A at frequency f is

$$A H_1(f) + \frac{3}{4} A |A|^2 H_3(f, f, -f) + \dots \text{(higher order terms)}. \quad (3.27)$$

The observed gain is the ratio of output amplitude to input amplitude at the input frequency. From Equation (3.27) the magnitude of this ratio is

$$|H_1(f)| \left[\left[1 + \frac{3}{4} |A|^2 \operatorname{Re} \left\{ \frac{H_3(f, f, -f)}{H_1(f)} \right\} \right]^2 + \left[\frac{3}{4} |A|^2 \operatorname{Im} \left\{ \frac{H_3(f, f, -f)}{H_1(f)} \right\} \right]^2 \right]^{1/2} . \quad (3.28)$$

Gain compression or expansion appears as the factor multiplying H_1 in Equation (3.28). In many cases H_3 is real and it will be possible to drop the last term of the second factor so that the gain "compression" factor becomes

$$\left[1 + \frac{3}{4} |A|^2 \operatorname{Re} \left\{ \frac{H_3(f, f, -f)}{H_1(f)} \right\} \right] . \quad (3.29a)$$

The initial effect observed as the signal level is increased will be expansion if the sign of $\operatorname{Re}\{H_3/H_1\}$ is positive and compression if the sign is negative. The cases in which the approximation involved in (3.29a) are most inaccurate are those where $H_3(f, f, -f)$ and $H_1(f)$ are nearly in quadrature. Equation (3.29a) permits calculation of predicted compression/expansion for small signal levels where nonlinearities of order higher than three can be neglected.

The gain compression/expansion factor in dB, x , is

$$x = 20 \log_{10} \left[1 + \frac{3}{4} |A|^2 \operatorname{Re} \left\{ \frac{H_3}{H_1} \right\} \right] , \quad (3.29b)$$

where the arguments of H_3 are $f, f, -f$ and of H_1 is f .

3.1.2.2.2 Intermodulation, Harmonic Distortion and Desensitization

Tables 3-1 and 3-2 specify the second and third order intermodulation at the output of the system when the input is the sum of two tones. The Tables also specify the second and third harmonics and third-order desensitization. Expressions for the specification parameters shown in Tables 3-1 and 3-2 involving non-linear transfer functions higher than third order can similarly be derived.

3.2 SENSITIVITY ANALYSIS

In Section 3.1 we related the EMC specification parameters to the NLTFs. As discussed in Section 2.1 the NLTFs themselves are a function of the LTF. It is therefore possible to analyze the effects of LTF identification errors on the NLTFs and on the specification parameters.

A common method for measuring the quality of the identification technique is the normalized mean squared error (NMSE). If $h(t)$ is the system impulse response and $H(f)$ its Fourier transform then the NMSE is defined as

$$\text{NMSE} = \int_{-\infty}^{\infty} |h(t) - \hat{h}(t)|^2 dt / \int_{-\infty}^{\infty} |h(t)|^2 dt \quad (3.30a)$$

or

$$\text{NMSE} = \int_{-\infty}^{\infty} |H(f) - \hat{H}(f)|^2 df / \int_{-\infty}^{\infty} |H(f)|^2 df \quad (3.30b)$$

where $\hat{h}(t)$ and $\hat{H}(f)$ are, respectively, estimates of the system impulse and frequency responses.

In order to evaluate the effects of errors in pole locations on the quality of the linear identification as measured by the NMSE and on the nonlinear specification parameters consider the following example.

3.2.1 Two Pole Example

Suppose that the linear transfer function is given by

$$H_1(s) = \frac{9}{(s+1)(s+10)} = \frac{1}{s+1} + \frac{-1}{s+10} \quad (3.31)$$

Tables 3-3 and 3-4 show the results of identifying the system using a technique based on the pencil of functions method [Rudko and Busgang (1982)] for different values of signal energy to noise energy ratio (SENR). Two separate identifications were performed. In the first, referred to as the optimized identification, the iterative identification technique developed by Rudko and Busgang (1982) was used. In the second, referred to as the non-optimum identification, the sampling rate and the number of samples used were not optimized and both poles were identified at once. The purpose of the second identification was to permit the evaluation of the effect of larger errors in poles on the linear NMSE and on the nonlinear specification parameters. In practice, if no a priori information is available as to the locations of the poles the performance of the identification may be close to that of the non-optimum case. The residues were calculated as described in Section 2.2 by minimizing the mean squared difference between the true and the model outputs. Figure 3-1 shows the relationship between the NMSE and the signal to noise ratio for both cases. Note the improvement in performance in the optimized case. Also, examining Tables 3-3 and 3-4, the NMSE

Table 3-3
Optimized Identification of the System $H_1(s) = \frac{9}{(s+1)(s+10)}$

<div> <div>TRUE POLES</div> <div> $s_1 = -1$ $s_2 = -10$ </div> <div>TRUE RESIDUES</div> <div> $R_1 = 1.0$ $R_2 = -1.0$ </div> </div>				
SENR (dB)	No. of I.D. Poles	Identified Poles	Identified Residues	N.M.S.E.
10	2	-3.53 -7	3.59 -3.66	.23
20	2	-1.57 -9.85	1.36 -1.39	4.62×10^{-2}
30	2	-10.15 -1.11	-1.07 1.07	2.83×10^{-3}
40	2	-10.07 -1.03	-1.02 1.02	2.36×10^{-3}
50	2	-10.02 -1.01	-1.01 1.01	2.64×10^{-5}
60	2	-10.01 -1.01	-1 1	2.46×10^{-6}

Table 3-4
Non-Optimized Identification of the System $H_1(s) = \frac{9}{(s+1)(s+10)}$

<div> <div>TRUE POLES</div> <div> $s_1 = -1$ $s_2 = -10$ </div> <div>TRUE RESIDUES</div> <div> $R_1 = 1.0$ $R_2 = -1.0$ </div> </div>				
SENR (dB)	No. of I.D. Poles	Identified Poles	Identified Residues	N.M.S.E.
10	1	-0.25	.34	.33
20	1	-0.29	.48	.28
30	1	-0.30	.39	.27
40	2	-7.92 -1.37	-1.25 1.26	1.59×10^{-2}
50	2	-9.41 -1.37	-1.01 1.02	7.86×10^{-5}
60	2	-9.83 -1.01	-1.01 1.01	1.49×10^{-5}

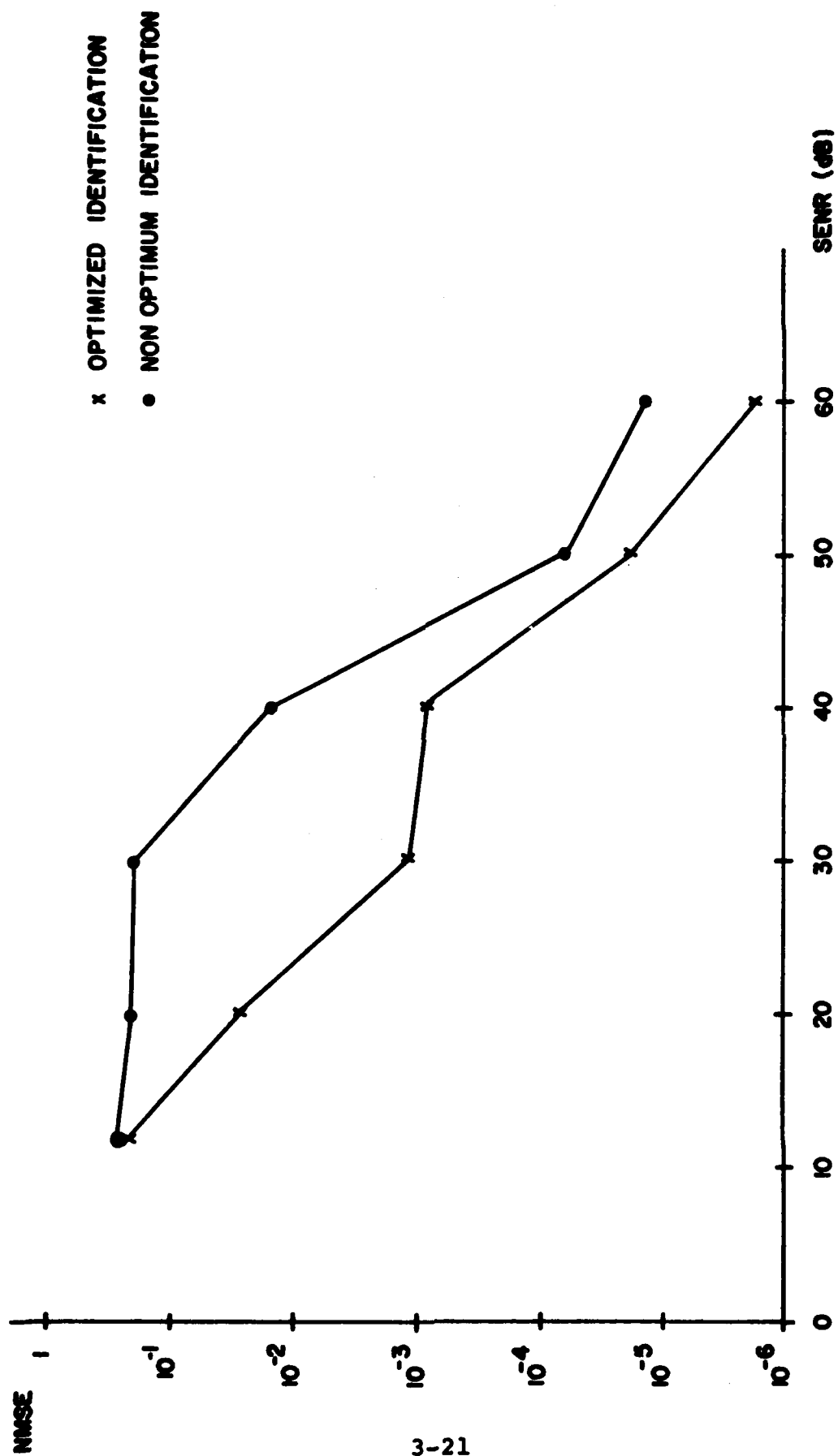


Figure 3-1 Relationship between NMSE and SENR

appears to be proportional to the errors in pole locations although the percentage errors are different. As will be pointed out below this is not always the case.

To evaluate the effects of linear identification errors on the nonlinear specification parameters the third order transfer function was assumed to be given by

$$H_3(s_1, s_2, s_3) = -k_3 H_1(s) H_1(s_2) H_1(s_3) H_1(s_1 + s_2 + s_3). \quad (3.32)$$

This form permits the direct evaluation of the third harmonic and intermodulation specification parameters based on the identified linear transfer functions.

The magnitudes of the true and predicted third order harmonic and intermodulation for the non-optimum identified pole at a SENR = 10 dB are shown in Figures 3-2 and 3-3. The error between the true and predicted third harmonic specification parameter varies from 0 to 55 dB for the frequency range shown. The error in predicting the third order intermodulation varies from 0 to 32 dB. The error in predicting the EMC specification parameters is large because the linear transfer function is severely misidentified. The number of poles in the linear transfer function is misidentified and the identified pole is 75 percent in error. The NMSE for this case is 33.4 percent. The precise relationship between NMSE and the predicted EMC specification performance is not clear in this case. In general, however, if the NMSE is large, the prediction of the nonlinear performance will be poor.

True and predicted third order harmonic and intermodulation EMC specification parameters for optimized pole identifications are shown in Figures 3-4 and 3-5. Harmonic and intermodulation

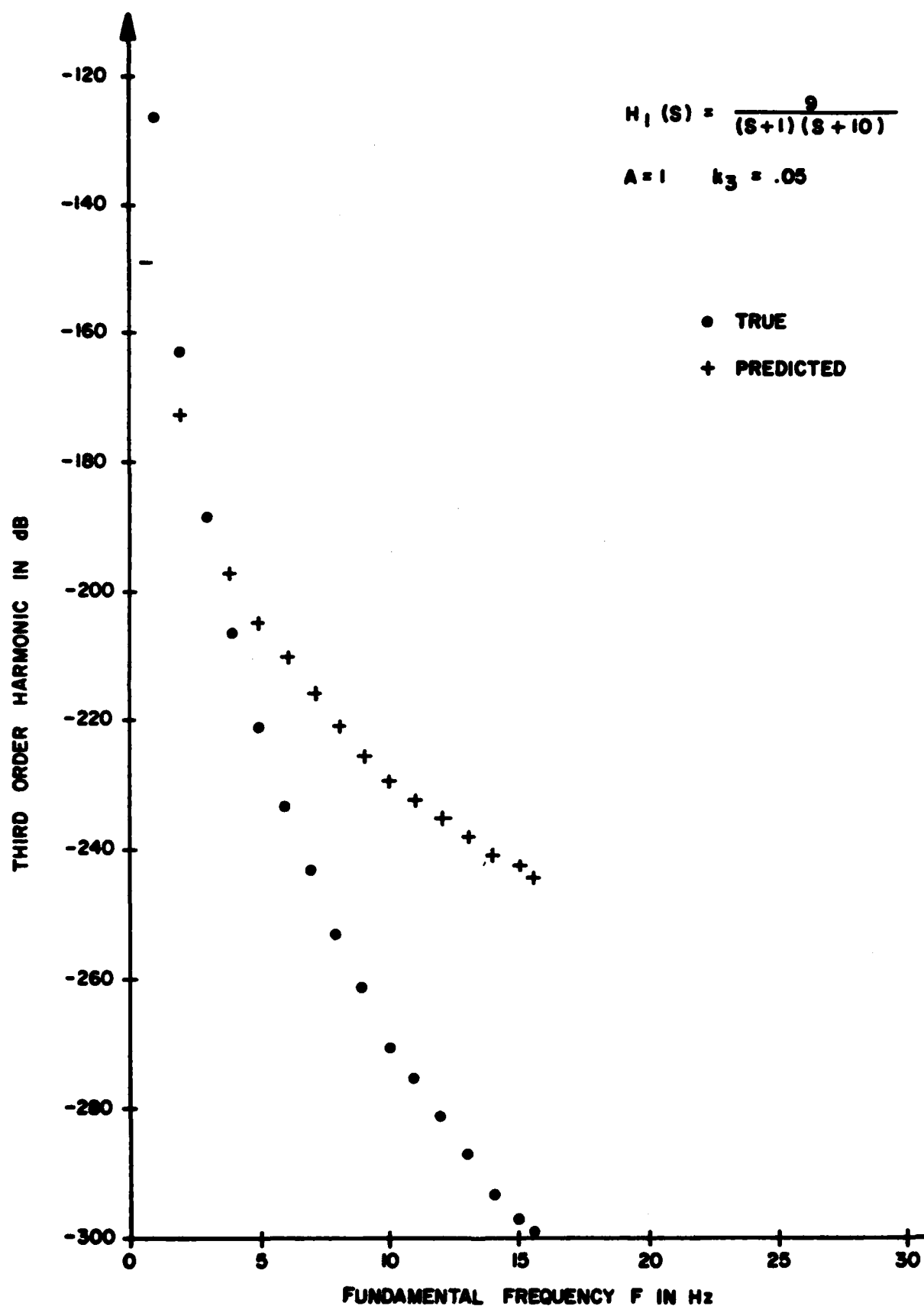


Figure 3-2 True and Predicted Third Order Harmonic. Predicted Based on a Single Identified Pole at $\hat{s} = -.25$.

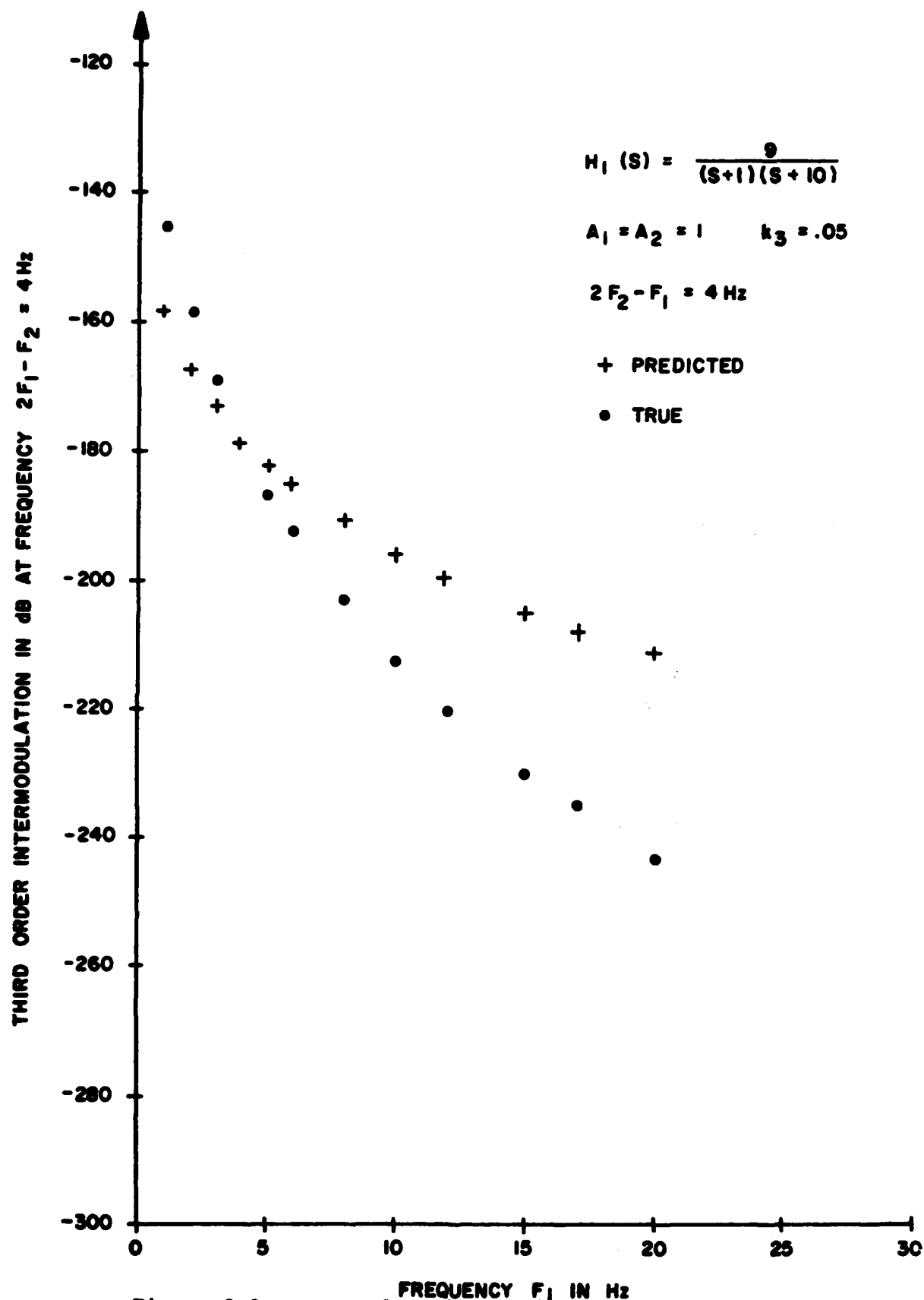


Figure 3-3 True and Predicted Third Order Intermodulation.
 Predicted Based on a Single Nonoptimized Identified
 Pole at $-.25$. 3-24

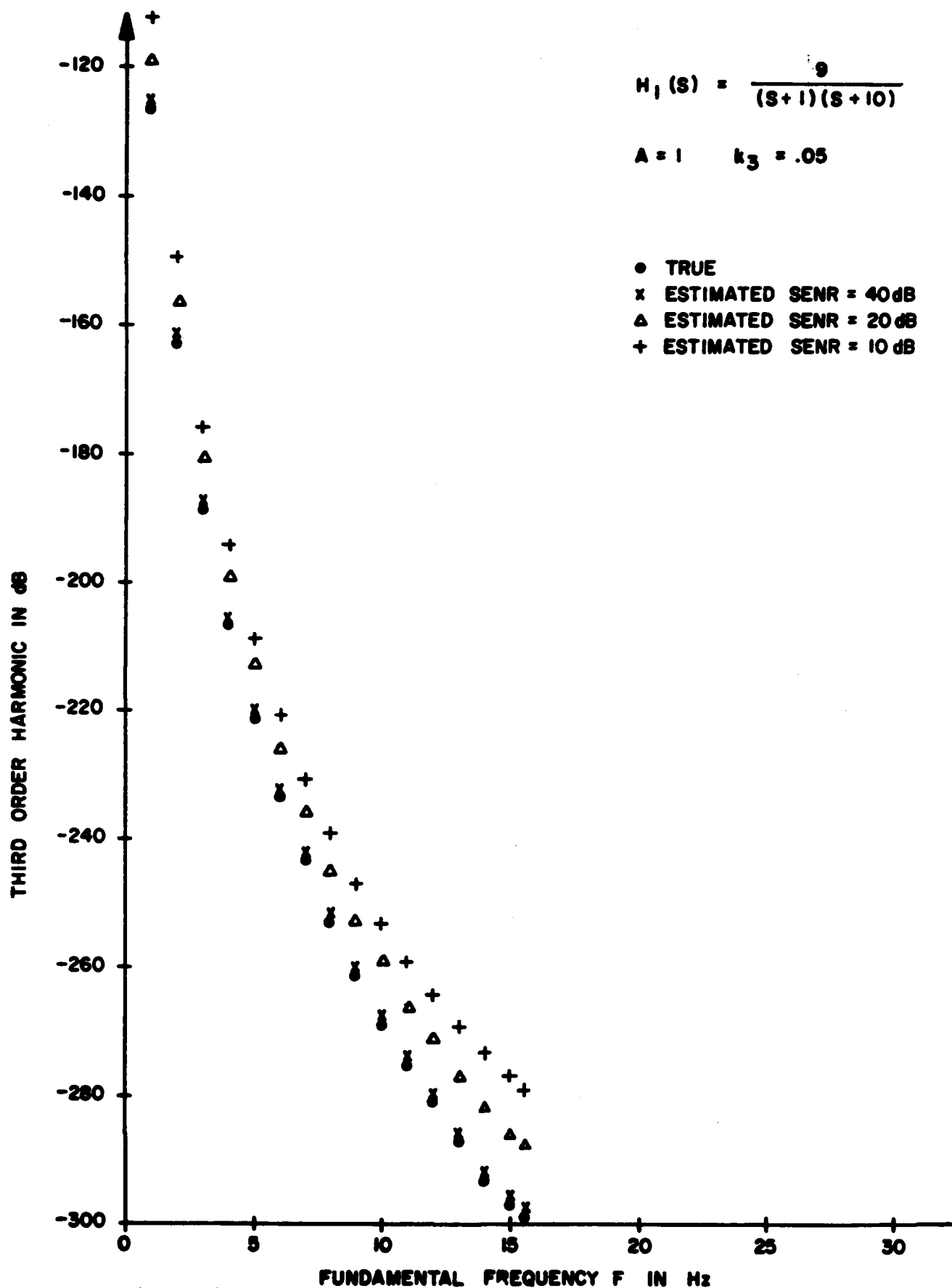


Figure 3-4 True and Predicted Third Order Harmonic. Predicted Based on Using Optimized Identified Poles.

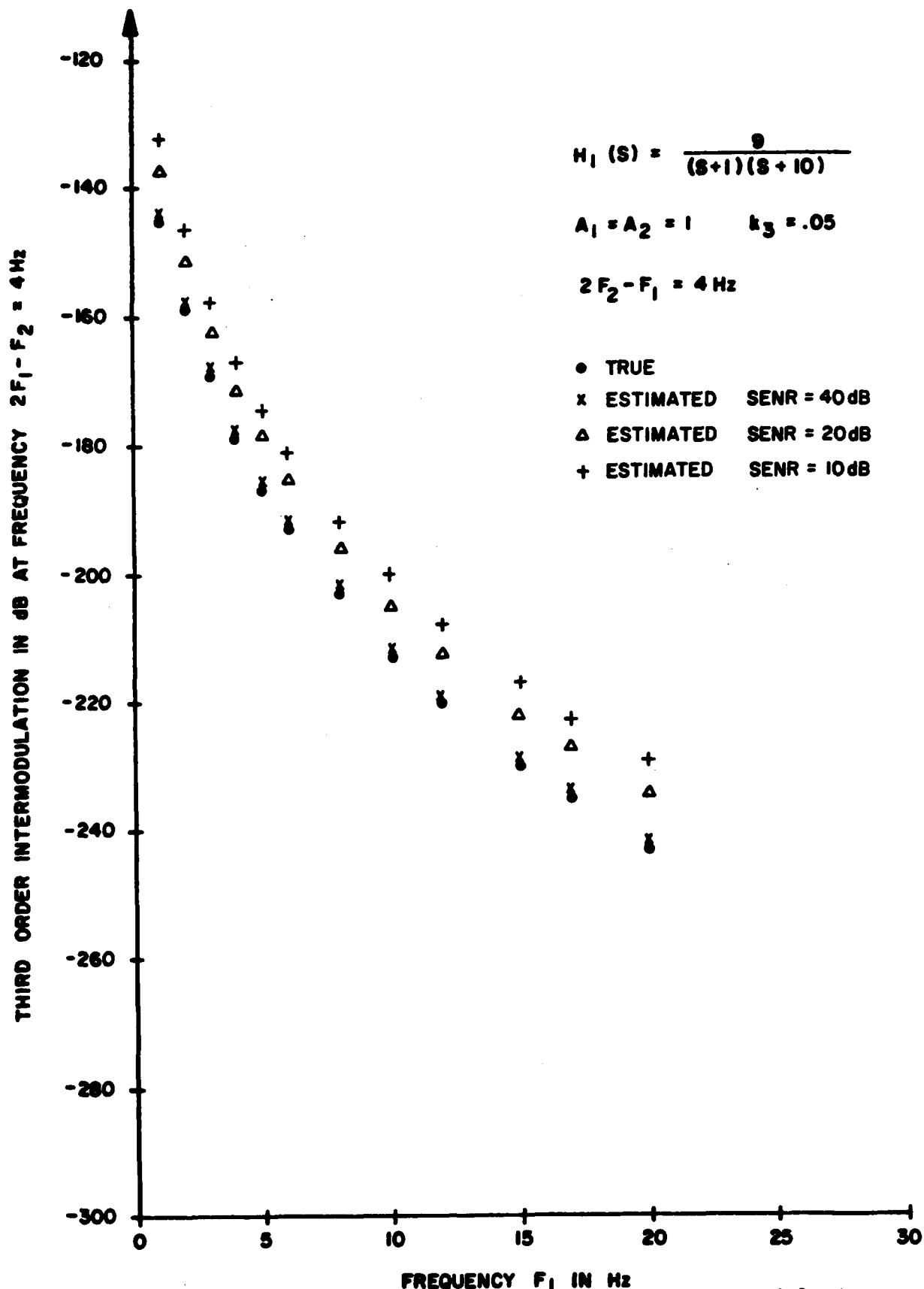


Figure 3-5 True and Predicted Third Order Intermodulation.
 Predicted Based on Optimized Identified Poles.

results with poles identified with SENR of 10, 20 and 40 dB are shown in the two figures. Clearly as the SENR increases, the poles are identified with greater accuracy and consequently the predicted nonlinear performance improves. The error in predicted nonlinear performance for the case where the poles are identified with a SENR = 40 dB is about a constant .7 dB across the whole frequency band shown in Figures 3-4 and 3-5. The NMSE for this case is about .24 percent. The error in predicting nonlinear performance for the case when the poles are identified with a SENR = 30 dB is about 2.5 dB and the error when the SENR = 50 dB is about 0.2 dB. These two cases are not shown in the figures. The NMSE for the SENR = 30 dB case is 0.29 percent and for the SENR = 50 dB case it is 2.6×10^{-3} percent. If we compare the error in predicting the nonlinear performance for the cases where the poles are identified with SENR's of 30, 40 and 50 dB with the NMSE of each case, we see that the errors are somewhat proportional to each other, but the constant of proportionality varies. For the cases discussed, small NMSE implied small error in the prediction of the nonlinear performance. However this is not always the case as we see in the next example.

3.2.2 Three Pole Example

In the preceding examples the errors in the nonlinear specification parameters were somewhat proportional to the NMSE and the errors in pole locations. This is however, not true in all cases. Consider the following example.

$$H(s) = \frac{891}{(s+1)(s+10)(s+100)} = \frac{1}{s+1} + \frac{-1.1}{s+10} + \frac{.1}{s+100} \quad (3.33)$$

Suppose also that only the two lower frequency poles are identified and that the identified system function is equal to

$$\hat{H}(s) = \frac{-0.1(s-89)}{(s+1)(s+10)} = \frac{1.0}{s+1} + \frac{-1.1}{s+10} \quad (3.34)$$

The Bode plots of the frequency responses of the true and identified systems are shown in Figure 3-6. Note that the true and identified frequency responses coincide for $\omega < 89$ and are different only for $\omega > 89$ where the two curves have different slopes.

The NMSE was calculated in this case as

$$NMSE = \frac{\int_{f_1}^{f_2} |H(f) - \hat{H}(f)|^2 df}{\int_{f_1}^{f_2} |H(f)|^2 df}, \quad 0 < f_1 < f_2 < \infty \quad (3.35)$$

for $f_1 = 0$, $f_2 = 100$ Hz or $0 < \omega < (2\pi)(100) = 628$ rad/sec. It was found to be very small, namely

$$NMSE = 1.22 \times 10^{-4} \text{ or } 0.012\%.$$

The identified system function was then used to predict the intermodulation and the harmonic distortion of a third-order nonlinear system whose third-order transfer function is equal to

$$H_3(f_1, f_2, f_3) = -k_3 H_1(f_1) H_1(f_2) H_1(f_3) H_1(f_1 + f_2 + f_3) \quad (3.36)$$

and where it was supposed that the coefficient k_3 was identified correctly. The true and predicted third-order harmonic and intermodulation are shown in Figures 3-7 and 3-8, respectively.

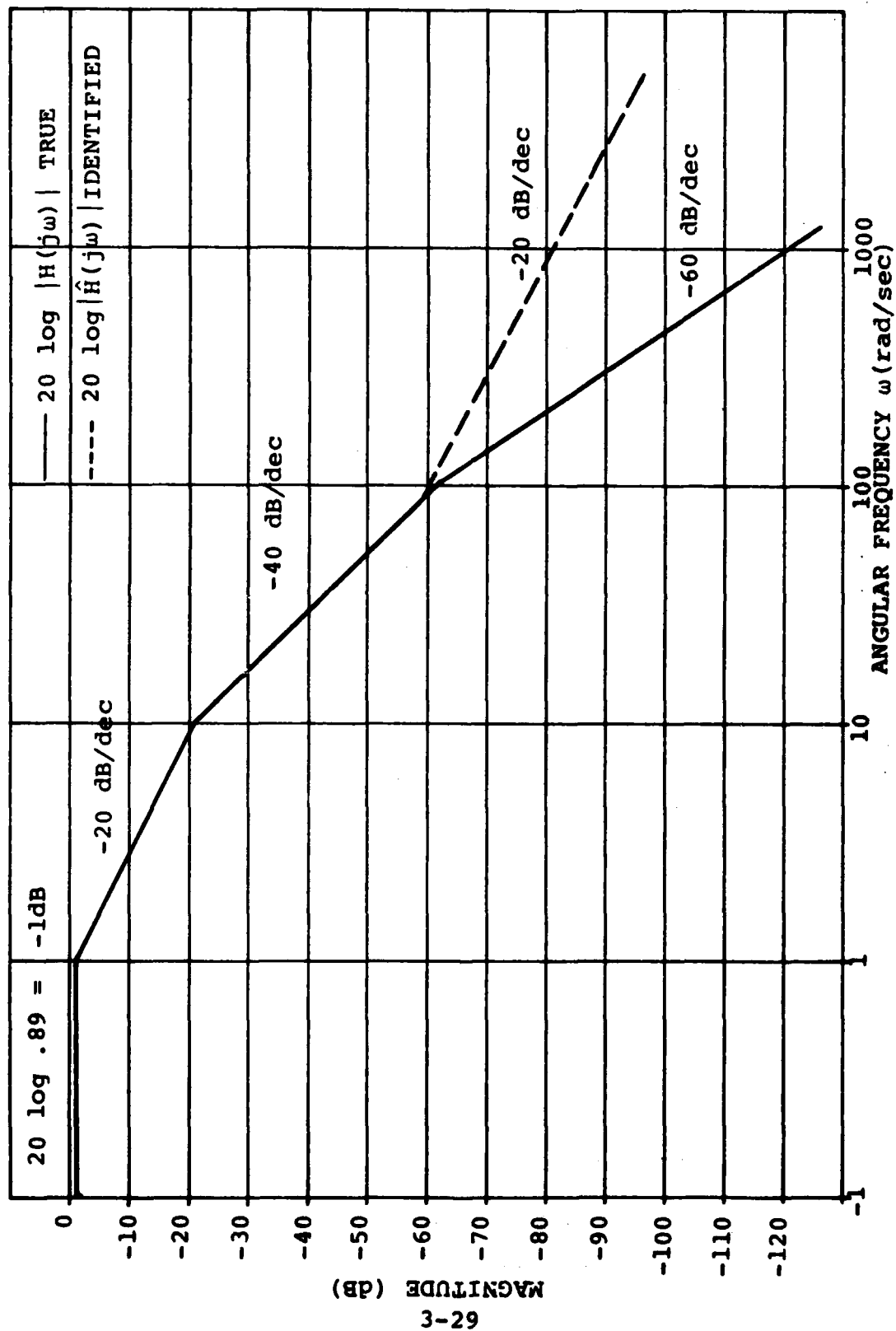


Figure 3-6 Frequency Responses of the True and Identified Systems

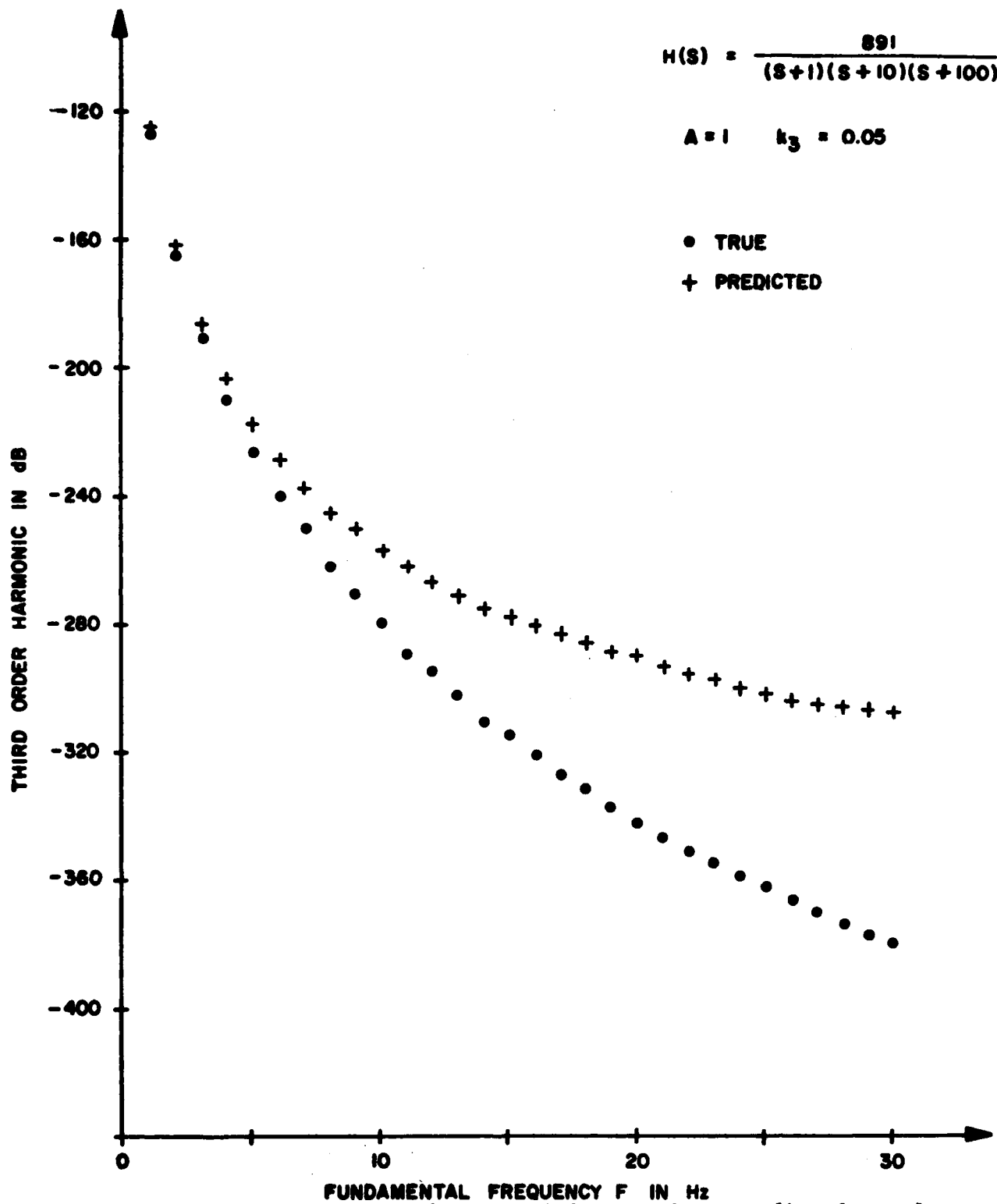


Figure 3-7 True and Predicted Third Harmonic. Predicted Based on Two Identified Poles at $s_1 = -1$ and $s_2 = -10$.

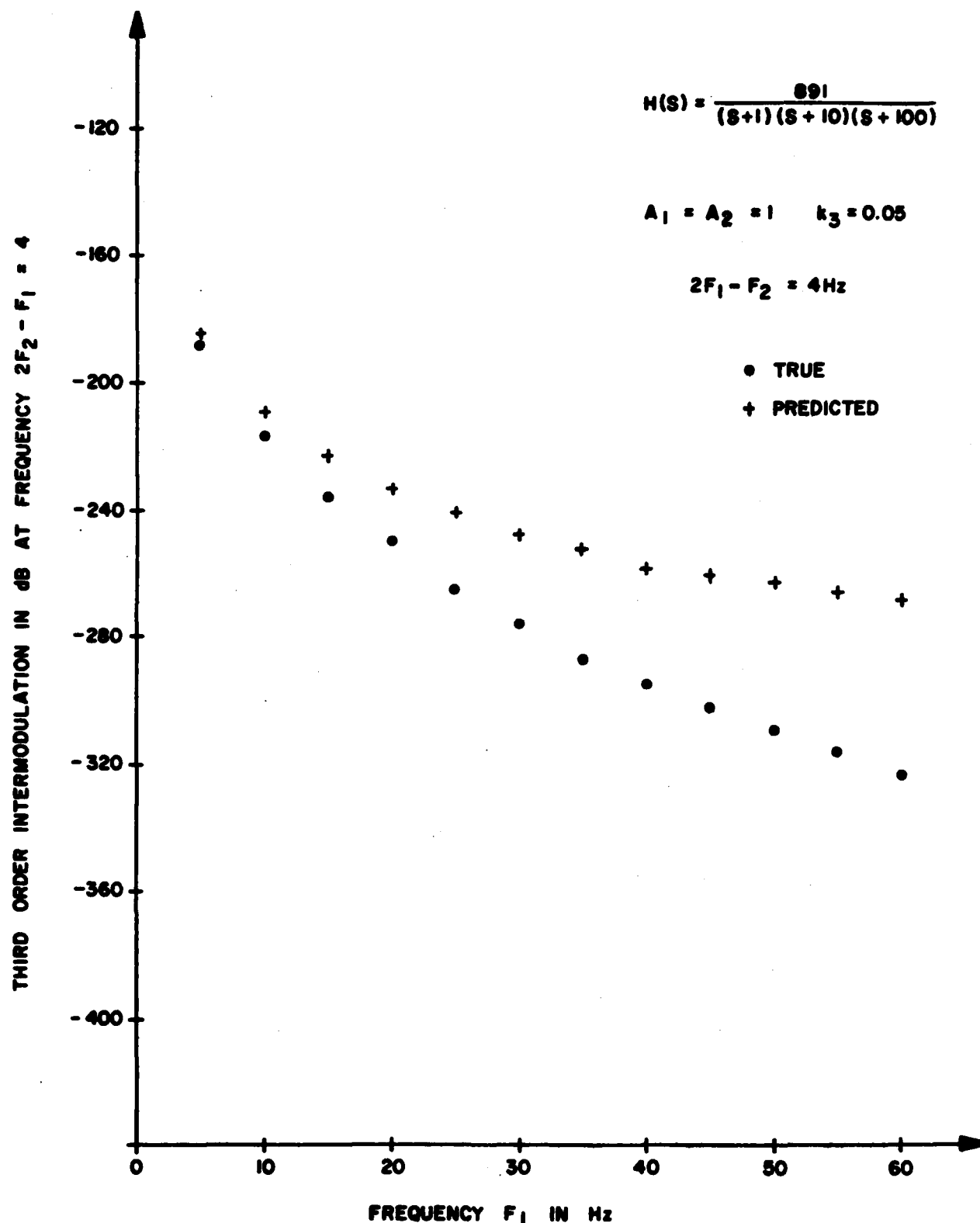


Figure 3-8 True and Predicted Third Order Intermodulation.
 Predicted Based on Two Identified Poles at
 $\hat{s}_1 = -1$ and $\hat{s}_2 = -10$.

Observe that the errors in the nonlinear specification parameters are much larger than the linear system NMSE. In fact, for certain frequencies they are as large as 20% whereas the NMSE was 0.012%. Therefore in this case, the linear system NMSE cannot be used to predict the accuracy of the estimated nonlinear specification parameters. Several additional conclusions and observations can be drawn from this example.

The NMSE is insensitive to errors in frequency response in the skirts (outside the passband) of the filters. In general, it is insensitive to errors in regions where the amplitude of the frequency response is low.

This conclusion can be further confirmed by calculating the NMSE over a frequency range which includes only the skirts of the filter. The NMSE was calculated using Equation (3.35) for the identified system whose frequency response is shown in Figure 3-6 between $f_1 = 10$ Hz and $f_2 = 100$ Hz or equivalently for $62.8 < \omega < 628$. The resulting NMSE was found to be 0.168 or 16.8%. This value is indicative of the percentage errors in the predicted nonlinear specification shown in Figures 3-7 and 3-8.

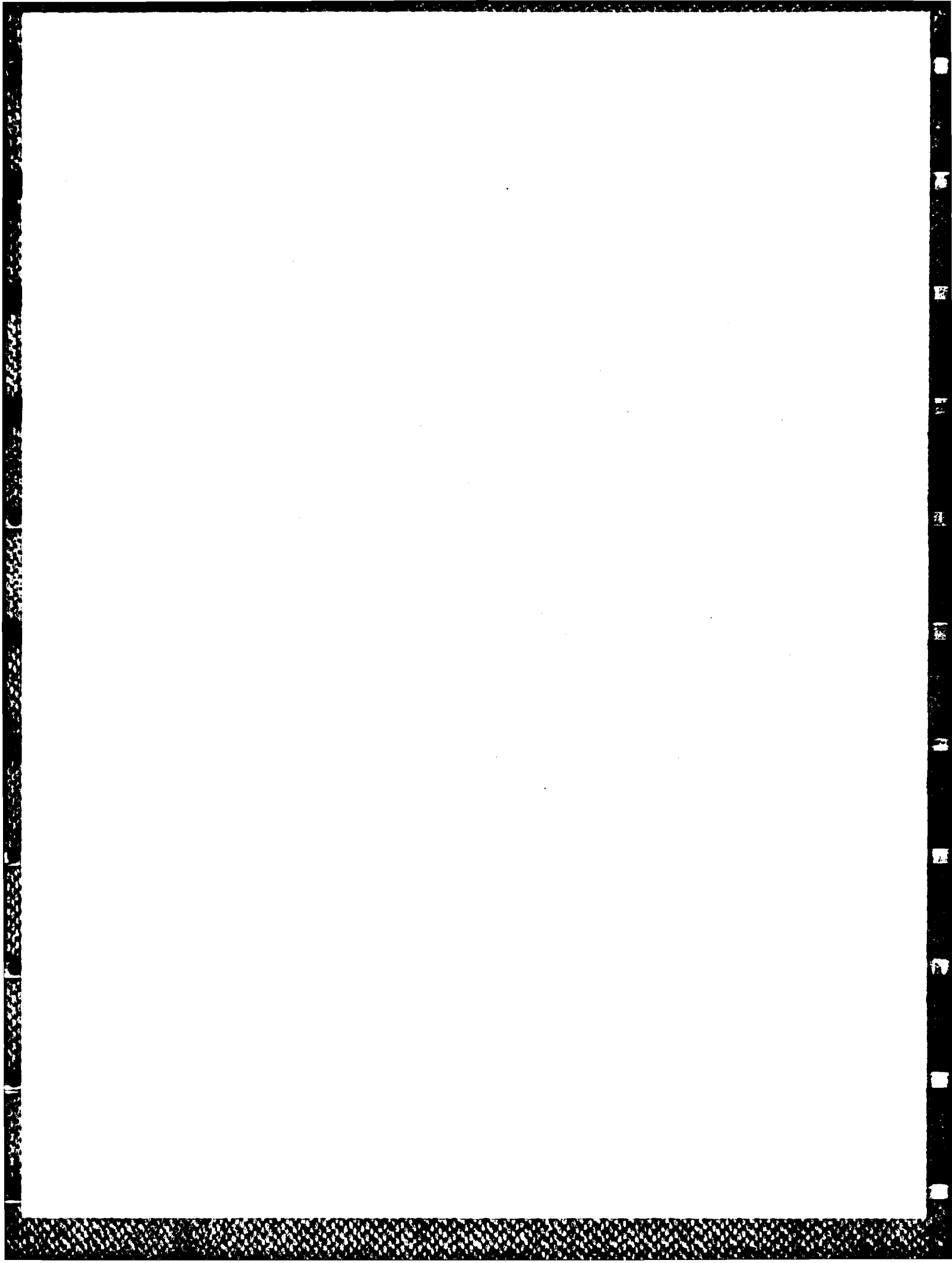
The above also points to the rather obvious fact that the identified frequency response outside the passband is important in the estimation of the nonlinear specification parameters.

Finally, we can conclude that the linear system NMSE cannot reliably predict the accuracy of the estimated nonlinear specification parameters.

From this example, it appears that a segmented NMSE calculated over separate frequency bands such as the passband and the skirts of the filter provides a better prediction of the accuracy of the nonlinear specification parameters than does a global NMSE calculated over the entire frequency range of interest. The specification of the exact procedure to be used would need to be included in a further study.

It is however clear that a NMSE segmented in frequency, that is calculated over several frequency bands, rather than the error in pole location should be used as a specification criterion. In practice the errors in pole locations cannot be used for two reasons. First, the true pole locations are not known in practice. Second, the error in pole locations is difficult to specify if the number of poles is misidentified.

In this section, it was shown that direct linear identification can be used to identify (estimate) the nonlinear transfer functions (NLTF's) and from this EMC specification parameters performance such as harmonic and intermodulation distortion can be predicted. The "rusty bolt" is a nonlinearity which occurs in the coupling path between colocated transmitters and receivers. This nonlinearity can cause severe degradation to the operation of Air Force C³I systems. The identification of the linear transfer function of the rusty bolt is complicated by a highly dominant direct path transmission signal. The identification techniques discussed in Section 2 and the procedure used to predict nonlinear performance in this Section 3 cannot readily be used. The rusty bolt problem needs special consideration and attention. The rusty bolt problem and identification is discussed in Sections 4 and 5.



SECTION 4

THE 'RUSTY BOLT' PROBLEM

Nonlinearities in transmitters, receivers, or in the coupling paths ("rusty bolt" effect) between transmitters and receivers can cause severe degradation to the operation of Air Force C³I systems.

The Air Force C³I platforms, such as the E-3A (AWACS) and E-4B, contain a large number of collocated transmitters and receivers. There is a recognized interference problem in these dense electronic platforms due to harmonic and intermodulation interference caused by the nonlinearity of metal-insulator-metal (MIM) or metal-oxide-metal (MOM) junctions in the structure. Although the surfaces involved can be distributed in nature, the junction is colloquially called the "rusty bolt". When these structures are irradiated with high density electromagnetic signals (RF fields) from transmitters, RF currents are induced into the junctions and a voltage is generated across the nonlinear element in the structure. The MOM and MIM junctions have nonlinear current-voltage characteristics (i.e., nonlinear impedance) which are primarily due to electron tunneling effects. We will discuss the physics and properties of the MIM junction ("rusty bolt") in Appendix B. The nonlinear characteristics cause harmonic, cross modulation and intermodulation (IM) products which couple to a re-radiating structure. The nonlinear products which fall into passbands of nearby receivers degrade system performance.

The IM interference problem can be particularly severe in airborne collocated systems because of the relatively small platforms. Power level differences between transmit and receive signals can exceed 170 dB. Highly sensitive wideband receivers are particularly susceptible to intermodulation (IM) distortion

because the IM power level can reach or exceed the level of the receiver noise power. The following example will illustrate the problem. Suppose that we have an airborne receiver with a sensitivity of about -110 dBm, a local transmitter power level of 50 Watts and a requirement that IM products be 15 dB below signal level. This would require IM levels about 172 dB below transmitter power level. These low levels of IM power requirements clearly indicate that passive nonlinearities in the coupling paths between collocated emitters and receivers on airborne platforms can be a primary factor in limiting system performance.

One of the objectives of this contract is to investigate the identification or estimation of nonlinear transfer functions and their use in the development of EMC performance specifications for the Air Force C³I systems. Of interest is the development of a simple circuit model of the "rusty bolt" (MIM junction) and the nonlinear transfer functions that are to be used in the analysis. In this section, we obtain an equivalent circuit for the MIM junction and the nonlinear Volterra transfer functions up to the fifth order. The Volterra functions are derived in Appendix C. The Volterra functions discussed in this section can be manipulated to an equivalent symmetrical form.

4.1 "RUSTY BOLT" MODELING

It is important to find a good compromise between accuracy and simplicity in modeling nonlinearities such as the rusty bolt (MIM junction). The i-v characteristics of MIM junctions have been investigated by many authors, [Simmons (1963), Forlani and Minnaja (1961) and Bond et al., (1979)]. In Appendix B we discuss the electric tunneling effect for a metal-insulator-metal (MIM) junction.

Some authors think of the MIM junction as a pair of back-to-back diodes with an antenna system as shown in Figure 4-1. The i - v relationship of the back-to-back diode pair is then approximated as

$$i_d = k_1 v_d + k_3 v_d^3 \quad (4.1)$$

neglecting nonlinear capacitive effects [Uslenghi, 1980]. Values are given to the constants k_1 and k_3 to match the computed and measured results. Other authors define some ideal nonlinear element, usually memoryless, without any reference to any real existing device.

A commonly accepted and more sophisticated lumped parameter equivalent circuit for a MIM junction was used by Long and Schwartz (1974). It is shown in Figure 4-2. An antenna and a shunting capacitance apply an a.c. voltage across a nonlinear resistor. The antenna is represented by its Thevenin equivalent impedance Z_a . The junction is modeled by a junction resistance r_d in series with a parallel combination of a junction capacitance impedance Z_c and a circuit element with nonlinear current characteristic $i_r(v)$. The capacitance is considered to be linear. This is not unreasonable since measurements by Bond, et al. (1979) on AL-AL₂O₃-AL junctions showed no measurable change of junction capacitance as function of applied bias voltage. Bond, et al., concluded that the dielectric constant of AL₂O₃ is not a function of voltage and will conduct UHF signals in a linear manner. An oxide layer is a common insulator for the many rusty bolt path nonlinearities onboard Air Force airplanes.

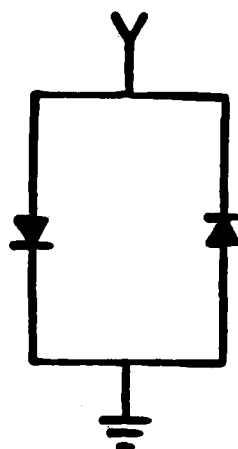


Figure 4-1 Back-to-Back Diode Pair with an Antenna System which Represent a Symmetrical Nonlinearity

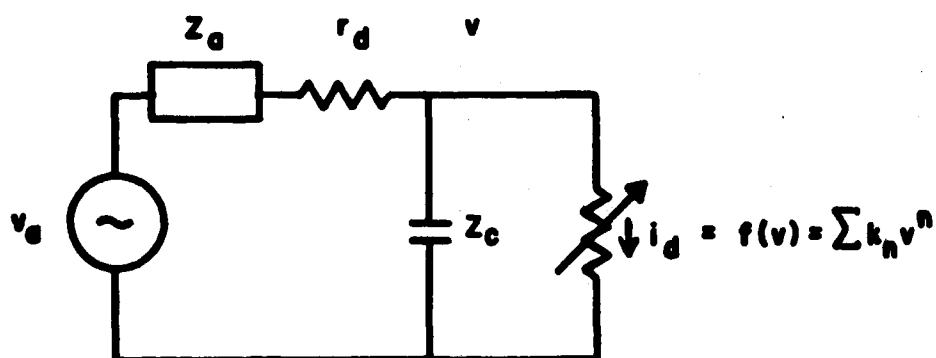


Figure 4-2 Simplified Circuit Model for the MIM Junction

There is evidence that typical MIM junctions have almost symmetrical i - v transfer characteristics. In other words electrical conduction is about equal in either direction. This implies that when a power series approximation is used, the symmetrical characteristics will contain only odd-order terms.

4.1.1 Volterra Transfer Functions of the Rusty Bolt

A Norton equivalent circuit for the MIM junction is shown in Figure 4-3. The antenna impedance Z_a and the junction resistance r_d have been combined into an equivalent impedance Z_e . The driving current source $i_a(t)$ is the convolution of the antenna driving voltage $v_a(t)$ and the equivalent admittance (inverse of the impedance Z_e). The nonlinear exponential current-voltage characteristic of the MIM junction discussed in Appendix B can be expanded into a power series

$$i_d = \sum_n k_n v^n \quad (4.2)$$

where the series coefficients k_n are a function of the dielectric material, work function of the metal, the electron charge and mass, Planck's constant, dielectric thickness and junction geometry. The current through the nonlinear resistor, i_d , can be interpreted as a set of voltage controlled current sources connected in parallel across the junction capacitor.

4.1.2 Linear Response and Transfer Functions

We will now obtain the linear impulse response of the equivalent circuit for the MIM junction by considering $i_a(t)$ as an input current source and $v(t)$ as the output. Ultimately, we will be interested in the linear and nonlinear transfer functions between the input and output voltages.

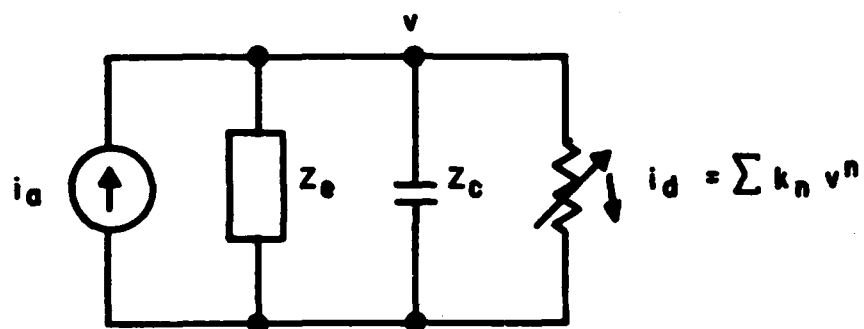


Figure 4-3 Norton Equivalent Circuit for the MIM Junction

$$I(s) = \frac{V_d(s)}{Z_e(s)}$$

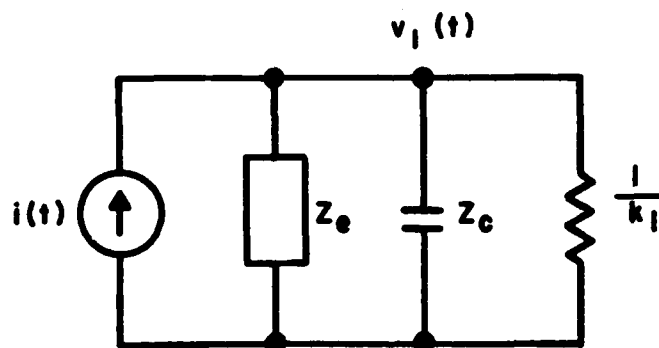


Figure 4-4 Circuit Used in Determining the Linear Voltage $v_1(t)$

In general, the voltage response $v(t)$ can be expressed as

$$v(t) = \sum_{k=1}^{\infty} v_k(t) \quad (4.3)$$

where $v_k(t)$ denotes the k 'th order portion of the response. To determine the linear portion of the response, the nonlinear voltage controlled current sources can be ignored. The circuit to be analyzed is shown in Figure 4-4.

The linear voltage, $v_1(t)$ is given by

$$v_1(t) = \int_{-\infty}^{\infty} h_1(\tau) i_a(t-\tau) d\tau . \quad (4.4)$$

The Laplace transform of $v_1(t)$ is equal to

$$V_1(s) = H_1(s) I_a(s) . \quad (4.5)$$

The transfer function $H_1(s)$ can be obtained from the node equation

$$\frac{V_1(s)}{Z_e(s)} + \frac{V_1(s)}{Z_c(s)} + k_1 V_1(s) = I_a(s) , \quad (4.6)$$

which yields

$$H_1(s) = \frac{V_1(s)}{I_a(s)} = \frac{Z_e(s)Z_C(s)}{Z_e(s)+Z_C(s)+k_1 Z_e(s)Z_C(s)} \quad (4.7)$$

The voltage to voltage transfer function is then given by

$$H_{v1}(s) = \frac{V_1(s)}{V_a(s)} = \frac{H_1(s)}{Z_e(s)} = \frac{Z_C(s)}{Z_e(s)+Z_C(s)+k_1 Z_e(s)Z_C(s)} \quad (4.8)$$

4.1.3 Higher Order Output Voltage to Input Current Transfer Functions

The nonlinear output voltage to input current transfer functions of the circuit shown in Figure 4-3 are given below. These NLTFs and the corresponding higher order responses are derived in Appendix C. All the Volterra functions discussed in this section and derived in Appendix C can be manipulated to an equivalent symmetrical form.

Second Order Transfer Function

$$H_2(s_1, s_2) = -k_2 H_1(s_1+s_2) H_1(s_1) H(s_2) \quad (4.9)$$

Third Order Transfer Function

$$H_3(s_1, s_2, s_3) = H_1(s_1) H_1(s_2) H_1(s_3) H_1(s_1+s_2+s_3) [2k_2^2 H_1(s_2+s_3) - k_3] \quad (4.10)$$

Fourth Order Transfer Function

$$\begin{aligned} H_4(s_1, s_2, s_3, s_4) &= H_1(s_1 + s_2 + s_3 + s_4) \{-k_2 H_2(s_1, s_2) H_2(s_3, s_4) \\ &- 2k_2 H_1(s_1) H_3(s_2, s_3, s_4) - k_3 H_1(s_1) H_1(s_2) H_2(s_3, s_4) - k_4 \prod_{i=1}^4 H(s_i)\} \end{aligned} \quad (4.11)$$

Fifth Order Transfer Function

$$\begin{aligned} H_5(s_1, s_2, s_3, s_4, s_5) &= H_1(s_1 + s_2 + s_3 + s_4 + s_5) \{-2k_2 H_2(s_1, s_2) H_3(s_3, s_4, s_5) \\ &- 2k_2 H_1(s_1) H_4(s_2, s_3, s_4, s_5) \\ &- 3k_3 [H_1(s_1) H_2(s_2, s_3) H_2(s_4, s_5) + H_1(s_1) H_1(s_2) H_3(s_3, s_4, s_5)] \\ &- 4k_4 H_1(s_1) H_1(s_2) H_1(s_3) H_2(s_4, s_5) - k_5 \prod_{i=1}^5 H(s_i)\} . \end{aligned} \quad (4.12)$$

The above equations show that the output voltage to input current nonlinear Volterra transfer functions for the lumped parameter "rusty bolt" circuit depend only on the nonlinear coefficients (constant k's) and the linear transfer function $H_1(s)$. From this we see that the linear transfer function plays a crucial role in the identification of the nonlinear transfer function.

4.1.4 Output Voltage to Input Voltage Transfer Functions

In the previous subsection, we discussed Volterra transfer functions by considering the input to the "rusty bolt" lumped parameter circuit to be a current source and the output to be the voltage generated across the parallel combination of the capacitor and the nonlinear resistor. In this subsection we give non-linear Volterra transfer functions for the "rusty bolt" lumped parameter circuit, when the input is the antenna voltage source and the output is the voltage generated across the parallel combination of the capacitor and the nonlinear resistor. We refer to these functions as the voltage to voltage Volterra transfer functions.

The linear (first order) voltage to voltage transfer function for the lumped parameter circuit was given in Section 4.1.2 (Equation (4.8)). The derivation of the higher orders voltage to voltage transfer functions is presented in Appendix C. The resulting second and third order voltage to voltage Volterra transfer functions are given below.

Second Order Transfer Function

$$H_{v2}(s_1, s_2) = -k_2 H_{v1}(s_1) H_{v1}(s_2) H_{v1}(s_1 + s_2) Z_e(s_1 + s_2) \quad (4.13)$$

Third Order Transfer Function

$$H_{v3}(s_1, s_2, s_3) = [-2k_2 H_{v2}(s_2, s_3) - k_3 H_{v1}(s_2) H_{v1}(s_3)] H_{v1}(s_1) H_{v1}(s_1 + s_2 + s_3) Z_e(s_1 + s_2 + s_3) \quad (4.14)$$

where $Z_e(s)$ is the sum of the antenna impedance and the MIM junction resistance. As we can see from Equations (4.13) and (4.14), the voltage to voltage Volterra transfer functions take the same form as the expressions for the voltage to current transfer functions. The only difference is the impedance factor which multiplies all the terms and is evaluated at the sum frequency.

The voltage to voltage Volterra transfer functions for the lumped parameter circuit depend only on the nonlinear coefficients, the linear transfer function and the equivalent antenna impedance.

4.2 POWER CONSTRAINT ON THE "RUSTY BOLT" LINEAR RESPONSE MEASUREMENT

In the previous section on "Rusty Bolt" modeling, it was shown that the nonlinear Volterra transfer function of the simple circuit depends only on the linear transfer function and the coefficients of the nonlinear i-v MIM characteristic and in the case of the voltage to voltage nonlinear transfer function also on the circuit antenna impedance. Therefore, knowledge of the linear transfer function plays a crucial role in the identification of the nonlinear transfer functions. In this section, we discuss the practical limitations in measuring the linear response.

4.2.1 "Rusty Bolt" Linear Response Measurement

The measurement of the rusty bolt linear response is modeled in the system shown in Figure 4-5. We assume that the measurement is performed onboard an aircraft and that only a single transmitter will be active. We have modelled the MIM junctions which are distributed throughout the aircraft as a lumped system which we call the rusty bolt. The rusty bolt is irradiated by the transmitter and reradiates energy which is

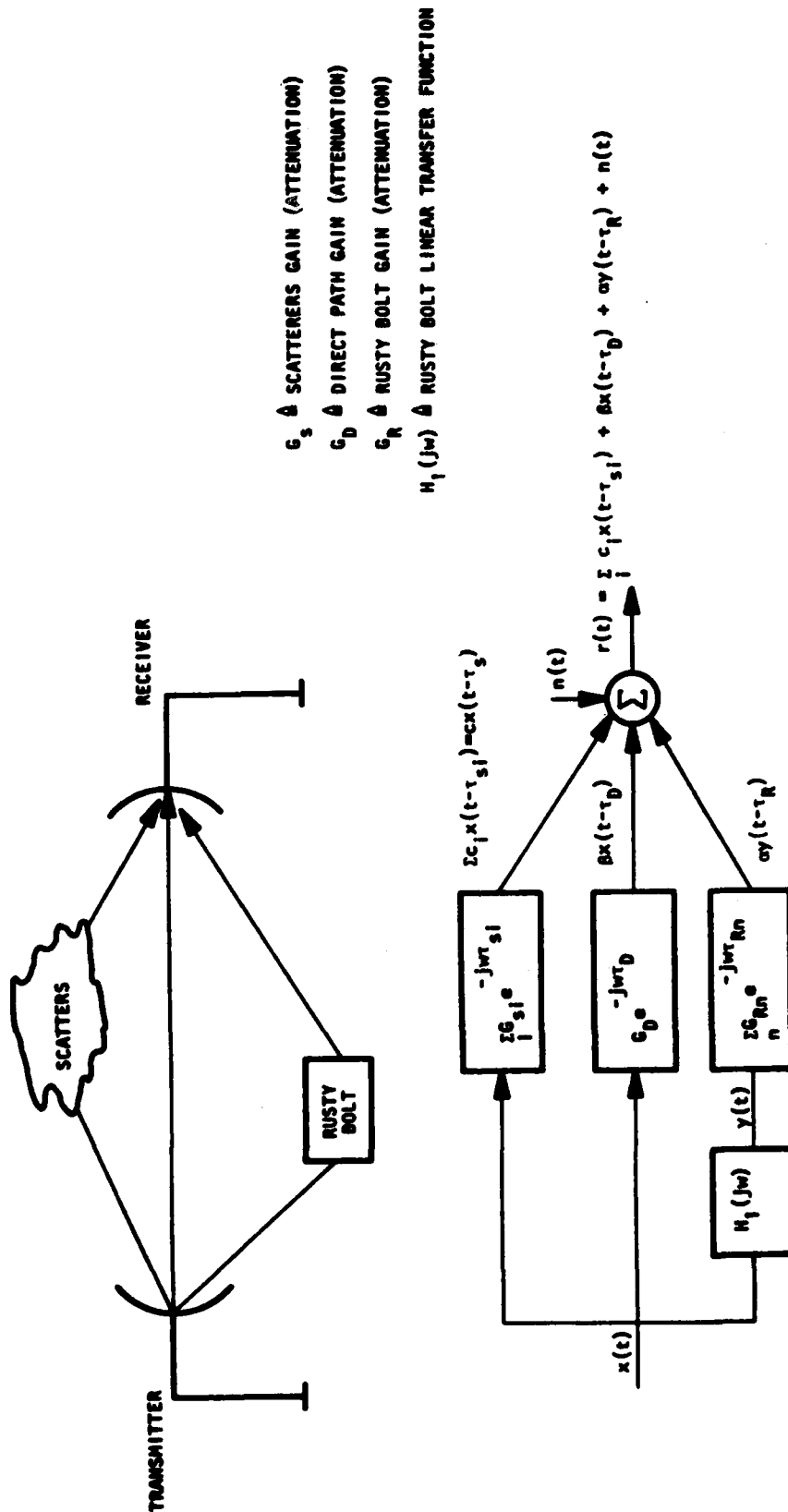


Figure 4-5 EXAMPLE OF "RUSTY BOLT" LINEAR SYSTEM RESPONSE MEASUREMENT

received by a receiver that is tuned, for the purpose of this measurement, to the transmitter frequency. In addition to the rusty bolt, there will be a contribution due to free space transmission (which we will call the direct path) and a contribution due to backscatter from the skin of the aircraft. We have also lumped the scatterers' contributions together. We assume that no interference other than additive noise falls in the receiver band.

The received signal $r(t)$ is given by

$$r(t) = \sum_i c_i x(t-\tau_i) + Bx(t-\tau_D) + \alpha y(t-\tau_R) + n(t) \quad (4.15)$$

where

$x(t)$	\triangleq	transmitted signal
$y(t)$	\triangleq	rusty bolt linear output signal
τ_i	\triangleq	propagation delay of scattered path
τ_R	\triangleq	propagation delay of rusty bolt path
τ_D	\triangleq	propagation delay of direct path
c_i	\triangleq	attenuation of scattered path
B	\triangleq	attenuation of the direct free space path
α	\triangleq	rusty bolt signal attenuation
$n(t)$	\triangleq	white Gaussian noise.

The lumped rusty bolt output signal is given by

$$y(t) = \int_{-\infty}^{\infty} h_1(\tau) x(t-\tau) d\tau \quad (4.16)$$

where $h_1(\tau)$ is the rusty bolt impulse response.

Thus if we could extract $y(t)$ from the received signal, we would be able to identify the rusty bolt linear transfer function.

As shown in Equation (4.15) the received time domain signal is made up of the input which is known, the rusty bolt output, which is due to the rusty bolt poles and the input, and the noise. This situation is therefore similar to the case where the unknown system contains a direct path between the input and the output. In such a case the unknown system poles can be identified using a linear system identification technique such as the pencil-of-functions method. While it is theoretically possible to extract the "rusty bolt" linear response, as shown in the next section, practical power constraints will introduce severe errors.

4.2.2 Received Power Levels

In the previous discussion we established that at least three signal paths combine at the receiver. We are interested in an estimate of the strength of the rusty bolt, the direct free space and the aircraft skin-reflected signals. A number of parameters such as transmitted power, transmitter and receiver antenna characteristics and the aircraft skin radar cross-section are required for the power calculation. In addition, and most important, one has to know the antenna characteristics of the rusty bolts. The determination of the rusty bolt antenna characteristics is a very difficult problem and no rigorous solutions

have been obtained to date. However, useful information can be obtained by treating the rusty bolt as an isotropic radiator and performing computations in the far field.

In interference analysis, the antenna gain of concern extends well beyond the main beam limits. Signals may couple through side lobes and back lobes. When detailed information on specific antennas is lacking, which is our case, one can use a coarse representation of an antenna pattern which involves two gain levels, one for the main beam and the other one for the remaining side lobe. In the analysis, we will assume that the main beam gain for both transmitter and receiver antennas is 0 dB and that the sidelobe gain is -13 dB relative to isotropic.

Another question that needs to be addressed deals with how the signals couple from the transmitter to the receiver for the three paths. The strongest rusty bolt signal occurs when it is irradiated by the transmitter main beam and its reradiated energy is received via the receiver main beam. This condition is referred to as main beam to main beam coupling and has a low probability of occurrence because it is highly likely that the rusty bolts are distributed over the large surface areas of the aircraft and only a small percentage would fall in the main antenna beam at any time. In order to improve the rusty bolt received signal with respect to the free space direct path signal, we can point the transmitter main beam away from the receiver main beam. In the analysis that follows, we will consider two situations.

The radar equation can be used to estimate the received power of the three linear signal paths. The direct free space path received power P_D is given by

$$P_D = \frac{P_T G_{TD} G_{RD}}{4\pi d^2} A_e \quad (4.17)$$

where

P_T	\triangleq	transmitted power in watts
G_{TD}	\triangleq	transmitter antenna gain for the direct path
G_{RD}	\triangleq	receiver antenna gain for the direct path
d	\triangleq	distance between transmitter and receiver in m
A_e	\triangleq	effective receiver antenna aperture in m^2 .

The received aircraft skin scattered power P_S is given by

$$P_S = \frac{P_T G_{TS}}{4\pi d_{TS}^2} \sigma \frac{G_{RS} A_e}{4\pi d_{RS}^2} \quad (4.18)$$

where P_T and A_e are the previously defined transmitter power and received antenna aperture and

G_{TS}	\triangleq	transmitter antenna gain for the scatterers
G_{RS}	\triangleq	receiver antenna gain for the scatterers
d_{TS}	\triangleq	distance from transmitter to center of the lumped scatterers, m
d_{RS}	\triangleq	distance from lumped scatterers to receiver, m
σ	\triangleq	radar cross section of the scatterers (aircraft skin), m^2 .

The received power P_{RB} due to the reradiation of the lumped rusty bolt is given by

$$P_{RB} = \left(\frac{P_T G_{TR}}{4\pi d_{TR}^2} \right) N A_R \frac{G_{RR}}{4\pi d_{RR}^2} A_e \quad (4.19)$$

Where P_T is the total transmitted power and

G_{TR}	\triangleq	transmitter antenna gain for the rusty bolt
G_{RR}	\triangleq	receiver antenna gain for the rusty bolt
A_R	\triangleq	area of a single rusty bolt which captures and reradiates the signal energy, m^2
N	\triangleq	total number of rusty bolts
A_e	\triangleq	effective receiver antenna aperture, m^2
d_{TR}	\triangleq	distance between transmitter and lumped rusty bolt, m
d_{RR}	\triangleq	distance between receiver and lumped rusty bolt, m.

We next consider two measurements, namely antenna sidelobe to sidelobe rusty bolt coupling and main lobe to main lobe rusty bolt coupling. The analysis will be performed with the following assumed parameter values,

G_{mb} (main beam gain) = 0 dB above isotropic
 G_{Sl} (side lobe gain) = -13 dB above isotropic
 d (distance between transmitter and receiver) = 50 ft = 15.2 m
 d_{TS} (distance between transmitter and scatterers) = $1/2 d$
 d_{TR} (distance between transmitter and rusty bolt) = $1/4 d$
 A_R (rusty bolt area) = $1 \text{ mm}^2 = 10^{-6} \text{ m}^2$
 N (number of rusty bolts) = 10,000
 σ (skin radar cross section) = 1 m^2 .

Sidelobe to sidelobe rusty bolt coupling is shown in Figure 4-6. This situation has the highest probability of occurrence. The received power ratio between the free space path and the rusty bolt signal for the case shown in Figure 4-6 is given by

$$\frac{P_D}{P_{RB}} = \left(\frac{G_{TD} G_{RD}}{d^2} \right) \frac{4\pi d_{TR}^2 d_{RR}^2}{G_{TR} G_{RR} N A_R} = \frac{G_{mb} 9\pi d^2}{G_{Sl} N A_R 64} \quad (4.20)$$

The ratio in dB is equal to

$$\begin{aligned}
 10 \log 9 + 10 \log \pi d^2 - (-13 \text{ dB}) - 18.06 \text{ dB} - 10 \log N_{AR} \\
 = 9.54 + 16.79 - 5.06 + 20 = 41.27 \text{ dB}.
 \end{aligned}$$

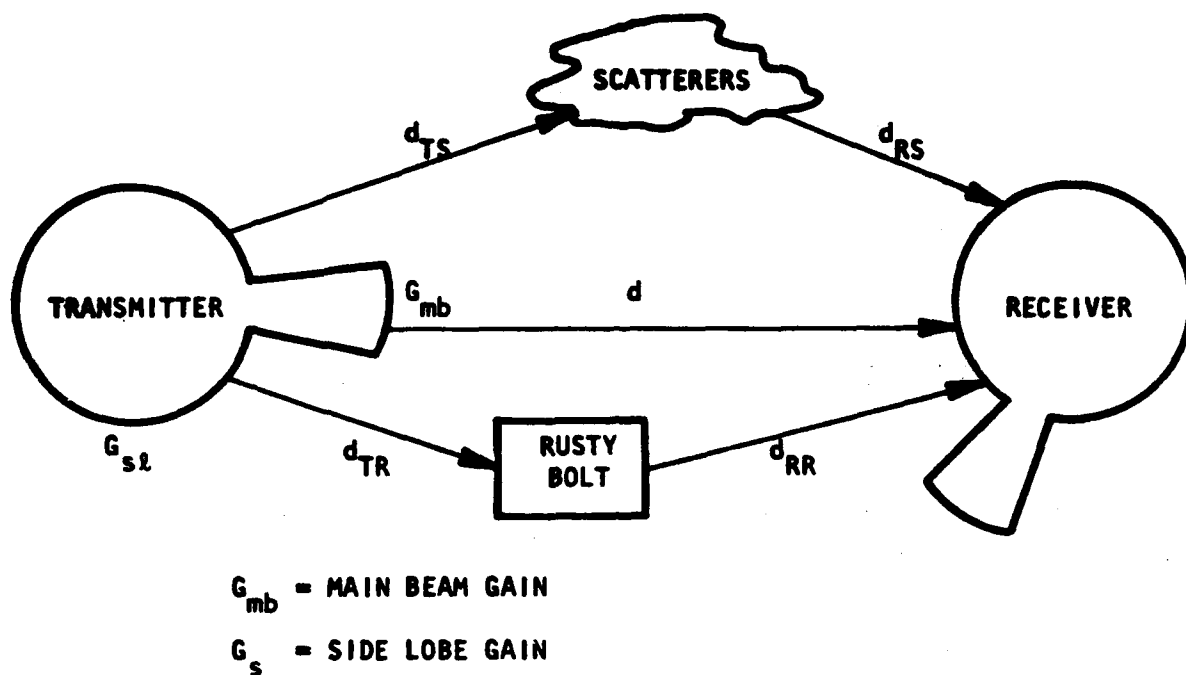


Figure 4-6 SIDE LOBE TO SIDE LOBE "RUSTY BOLT" COUPLING

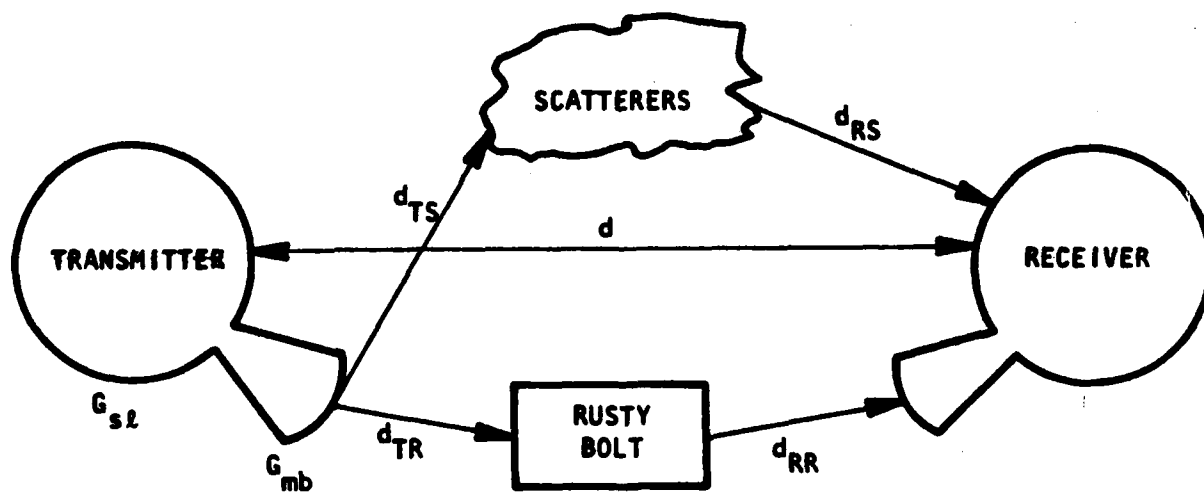


Figure 4-7 MAIN BEAM TO MAIN BEAM "RUSTY BOLT" COUPLING

Similarly, the received power ratio between the skin scatterers and the rusty bolt for the first case is given by

$$\begin{aligned} \frac{P_S}{P_{RB}} &= \frac{G_{TS}}{d_{TS}^2} \frac{G_{RS}}{d_{RS}^2} \left(\frac{\sigma}{NA_R} \right) \frac{d_{TR}^2}{G_{TR}} \frac{d_{RR}^2}{G_{RR}} \\ &= \frac{\sigma}{NA_R} \frac{9}{64} \end{aligned} \quad (4.21)$$

The scatter to rusty bolt power ratio in dB for the given parameters is then equal to

$$10 \log 10^2 + 10 \log 9 - 10 \log 64 = 29.54 - 18.06 = 11.48 \text{ dB.}$$

The second case is for main beam to main beam rusty bolt coupling as shown in Figure 4-7. As previously mentioned this case has a very low probability of occurrence. The free space path to rusty bolt received power ratio for this case is equal to

$$\begin{aligned} 20 \log G_{sl} + 10 \log 9\pi d^2 - 10 \log 64 NA_R &= \\ &= -26 + 26.33 + 1.94 = 2.27 \text{ dB.} \end{aligned}$$

The received scattered to rusty bolt power ratio for the second case is equal to $-13 + 11.48 = -1.52 \text{ dB}$.

It was pointed out in Section 4.2.1 that a linear identification technique such as the pencil of functions method could be used to extract the rusty bolt poles. However, as shown in this

section, the free space direct path signal in most cases will be some 40 dB stronger than the rusty bolt signal. Identification of the rusty bolt system poles based on such a relatively weak rusty bolt output signal would not be feasible in practice.

The above analysis showed that even in the absence of noise, it will be extremely difficult to extract the linear rusty bolt response because it will not be the strongest signal component. Furthermore it is highly likely that the propagation delay of all three paths will be very close to each other which makes it impossible to separate the signal components. In view of this, it is proposed to measure the nonlinear rusty bolt response directly. The most efficient measurement technique for the rusty bolt will be to measure the third harmonic or third-order intermodulation product. This should provide the strongest signal because the rusty bolt model has an almost symmetrical nonlinear i-v characteristic. Note that intermodulation product measurements avoid the problem of spectral impurities (harmonics) caused by some local oscillators.

SECTION 5

RUSTY BOLT NLTF IDENTIFICATION

It was shown in Section 4 that for the lumped parameter rusty bolt circuit the higher order transfer function poles depend only on the linear transfer function poles. This is always true for the case where the nonlinear system is a lumped parameter circuit with zero-memory nonlinearities between circuit nodes. Under normal conditions, linear identification can be used to identify the linear system poles and from this the nonlinear system poles can be determined. However, this procedure cannot be applied to the rusty bolt. The problem is the fact that estimation of the linear transfer function is complicated by the presence of the highly dominant direct path transmission signal as described in Section 4.2. Therefore, the "Rusty Bolt" can only be identified from direct measurements on the nonlinear response.

5.1 RUSTY BOLT IDENTIFICATION TECHNIQUES

In a general sense, identification procedures can be based on either the transient response or the sinusoidal steady state response of the system. In the next subsections we will discuss rusty bolt identification based on both the transient and sinusoidal steady state response. It is concluded that identification based on the sinusoidal steady state response is better suited for the rusty bolt problem.

5.1.1 Transient Probe Waveform Analysis for the Rusty Bolt

Suppose that the rusty bolt is excited by an input $x(t)$. Assuming a third-order rusty bolt model, the received signal is given by

$$y(t) = \int_{-\infty}^{\infty} h_1(u) x(t-u) du + \iiint_{-\infty}^{\infty} h_3(u_1, u_2, u_3) x(t-u_1) x(t-u_2) x(t-u_3) du_1 du_2 du_3 + d(t) + n(t) \quad (5.1)$$

where $d(t)$ denotes the signal due to the direct transmission of $x(t)$, $n(t)$ denotes additive noise, and $h_1(u)$, $h_3(u_1, u_2, u_3)$ are, respectively the first and third-order impulse responses of the rusty bolt.

As pointed out in Section 4.2, the identification of the linear response of the rusty bolt is not practicable because the received signal will be primarily due to the free space transmission and the aircraft skin scattered signal and not due to the output of the rusty bolt's linear transfer function. Consequently, direct identification, using transient analysis of the rusty bolt third-order transfer function, was considered.

For simplicity suppose that the linear transfer function has only one pole and is given by

$$H_1(s) = \frac{1}{s+p} . \quad (5.2)$$

Then, the rusty bolt third-order transfer function, assuming a symmetrical nonlinearity and a third order coefficient of unity, is equal to

$$\begin{aligned}
 H_3(s_1, s_2, s_3) &= - H_1(s_1) H_1(s_2) H(s_3) H_1(s_1 + s_2 + s_3) \\
 &= \frac{-1}{s_1 + p} \frac{1}{s_2 + p} \frac{1}{s_3 + p} \frac{1}{s_1 + s_2 + s_3 + p} . \quad (5.3)
 \end{aligned}$$

In an attempt to provide separation between the linear, direct path and third-order responses, we let the input be a pulsed carrier

$$x(t) = 2e^{\alpha t} \cos \omega_c t u(t) \quad (5.4)$$

where α determines the rise time of the pulse and $u(t)$ is the unit step. Using the association of variables it can be shown that the third-order response in the Laplace transform domain has poles at:

$$-3p$$

$$-2p + \alpha \pm j\omega_c$$

$$-p + 2\alpha \pm j2\omega_c$$

$$3\alpha \pm j3\omega_c$$

$$3\alpha \pm j\omega_c$$

$$-p + 2\alpha .$$

The direct path components have poles at $\alpha \pm j\omega_c$. Thus, although the system pole is for one term associated with frequency $2\omega_c$, the difference between $2\omega_c$ and the frequency of the direct path component ω_c is insufficient to separate the third-order component from the direct path component. Because of the high power level of the direct path component such a separation is necessary in order to use a transient response based technique such as the pencil-of-functions to identify the system pole of the third-order response. Therefore, the most promising identification technique consists of the identification of the third-order transfer function based on sinusoidal steady state measurements. In this approach, the third-order response can be separated from the direct path component.

It should, however, be noted that in applications where the direct path component is absent, the use of a pulsed carrier may facilitate the separation of the linear and third-order responses thereby permitting the identification of the residues of the third-order transfer function.

5.1.2 Sinusoidal Steady State Analysis for the Rusty Bolt

Sinusoidal steady state probing can be used to measure a system frequency response. The measurement allows the separation of some of the different order responses. For example, contributions of different orders of nonlinearities can be separated by measuring certain harmonic or intermodulation responses. In the discussions that follow, we will discuss sinusoidal steady state techniques to estimate the poles and zeros of the rusty bolt. We will then present a method which uses the estimated rusty bolt poles and zeros to identify the constants that are necessary to predict the NLTF specification parameters such as harmonic and intermodulation distortion.

5.1.2.1 Third-Order Transfer Function Identification Using Sinusoidal Steady-State Measurements

Suppose that the linear and third-order transfer function of the rusty bolt are, respectively, given by

$$H_1(s) = \frac{K(\frac{s}{a} + 1)}{(\frac{s}{b_1} + 1)(\frac{s}{b_2} + 1)} \quad (5.5)$$

$$H_3(s_1, s_2, s_3) = H_1(s_1)H_1(s_2)H_1(s_3)H_1(s_1 + s_2 + s_3).$$

Assume, for simplicity that the output due to input $\alpha(t)$ is equal to the sum of the first and third-order responses.

$$y(t) = \int h_1(u) \alpha(t-u) du + \iiint h_3(u_1, u_2, u_3) \alpha(t-u_1) \alpha(t-u_2) \alpha(t-u_3) du_1 du_2 du_3 \quad (5.6)$$

Then, if the input is

$$\alpha(t) = A_1 \cos \omega_1 t + A_2 \cos \omega_2 t \quad (5.7)$$

the steady-state output contains the terms listed in Tables 3-1 and 3-2 of Section 3. We select the third order intermodulation component for further analysis. The output components at frequencies $2f_1 + f_2$ and $-(2f_1 + f_2)$ have, respectively, amplitudes

AD-A147 659

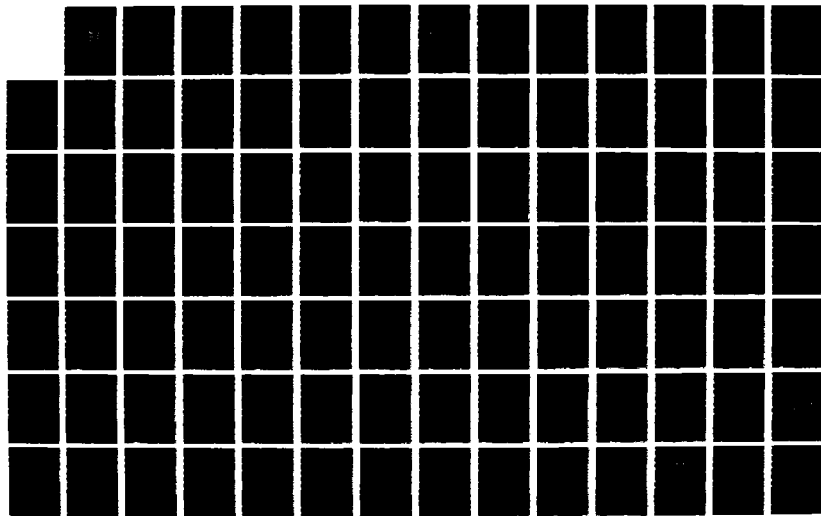
EMC (ELECTROMAGNETIC COMPATIBILITY) SPEC CRITERIA IN
VOLTERRA SYSTEMS(U) SIGNATRON INC LEXINGTON MA
L D TROMP ET AL. JUN 84 RADC-TR-84-147 F30602-82-C-0163

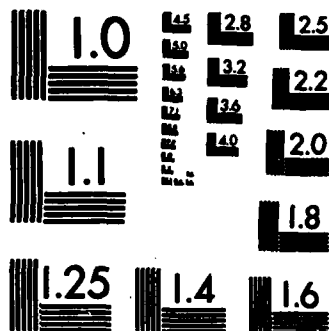
2/3

UNCLASSIFIED

F/G 20/14

NL





MICROCOPY RESOLUTION TEST CHART
NATIONAL BUREAU OF STANDARDS-1963-A

$$\frac{3}{4} A_1^2 A_2 H_3 (f_1, f_1, f_2), \quad (5.8)$$

and

$$\frac{3}{4} A_1^{*2} A_2^* H_3 (-f_1, -f_1, -f_2) \quad (5.9)$$

where the * denotes complex conjugate.

Consequently, the steady state response at $\pm(2f_1 + f_2)$ is given by

$$y_{2f_1+f_2}(t) = \frac{1}{2} \left[\frac{3}{4} A_1^2 A_2 H_3 (f_1, f_1, f_2) e^{j2\pi(2f_1+f_2)t} + \frac{3}{4} A_1^{*2} A_2^* H_3 (-f_1, -f_1, -f_2) e^{-j2\pi(2f_1+f_2)t} \right] \quad (5.10)$$

where,

$$H_3(f_1, f_1, f_2) = \frac{\kappa^4 \left(\frac{j2\pi f_1}{a} + 1 \right)}{\left(\frac{j2\pi f_1}{b_1} + 1 \right) \left(\frac{j2\pi f_1}{b_2} + 1 \right)} \frac{\left(\frac{j2\pi f_1}{a} + 1 \right)}{\left(\frac{j2\pi f_1}{b_1} + 1 \right) \left(\frac{j2\pi f_1}{b_2} + 1 \right)} \cdot \frac{\left(\frac{j2\pi f_2}{a} + 1 \right)}{\left(\frac{j2\pi f_2}{b_1} + 1 \right) \left(\frac{j2\pi f_2}{b_2} + 1 \right)} \frac{\left[\frac{j2\pi(2f_1+f_2)}{a} + 1 \right]}{\left[\frac{j2\pi(2f_1+f_2)}{b_1} + 1 \right] \left[\frac{j2\pi(2f_1+f_2)}{b_2} + 1 \right]} \quad (5.11)$$

Note that this is the only component of the output at this frequency.

In the above,

$$\begin{aligned}
 H_3(f_1, f_1, f_2) &= |H_3(f_1, f_1, f_2)| e^{j\phi_3(f_1, f_1, f_2)} \\
 H_3(-f_1, -f_1, -f_2) &= |H_3(-f_1, -f_1, -f_2)| e^{j\phi_3(-f_1, -f_1, -f_2)} \\
 &= H_3^*(f_1, f_1, f_2) \\
 &= |H_3(f_1, f_1, f_2)| e^{-j\phi_3(f_1, f_1, f_2)} \quad (5.12)
 \end{aligned}$$

If we assume that A_1 , A_2 are real, we have the result

$$\begin{aligned}
 y_{2f_1+f_2}(t) &= \frac{3}{8} A_1^2 A_2 |H_3(f_1, f_1, f_2)| [e^{j[2\pi(2f_1+f_2)t + \phi_3]} \\
 &\quad + e^{-j[2\pi(2f_1+f_2)t + \phi_3]}] \\
 &= \frac{3}{4} A_1^2 A_2 |H_3(f_1, f_1, f_2)| \cos [2\pi(2f_1+f_2)t + \phi_3] \quad (5.13)
 \end{aligned}$$

where

$$|H_3(f_1, f_1, f_2)| = \frac{K^4 \left| \frac{j2\pi f_1}{a} + 1 \right|^2 \left| \frac{j2\pi f_2}{a} + 1 \right|}{\left| \frac{j2\pi f_1}{b_1} + 1 \right|^2 \left| \frac{j2\pi f_1}{b_2} + 1 \right|^2 \left| \frac{j2\pi f_2}{b_1} + 1 \right| \left| \frac{j2\pi f_2}{b_2} + 1 \right|} \\ \times \frac{\left| \frac{j2\pi(2f_1 + f_2)}{a} + 1 \right|}{\left| \frac{j2\pi(2f_1 + f_2)}{b_1} + 1 \right| \left| \frac{j2\pi(2f_1 + f_2)}{b_2} + 1 \right|} \quad (5.14)$$

Now let us fix f_1 such that

$$2f_1 < \min \left\{ \frac{|a|}{2\pi}, \frac{|b_1|}{2\pi}, \frac{|b_2|}{2\pi} \right\} \quad (5.15)$$

and sweep with respect to f_2 . Then the Bode amplitude plot of the frequency response will exhibit breaking frequencies at

$$f_2 = \frac{a}{2\pi}, \frac{b_1}{2\pi}, \frac{b_2}{2\pi} \quad (5.16)$$

and

$$f_2 = \left(\frac{a}{2\pi} \right) - 2f_1, \left(\frac{b_1}{2\pi} \right) - 2f_1, \left(\frac{b_2}{2\pi} \right) - 2f_1. \quad (5.17)$$

If the poles $-b_1, -b_2$ are real, the amplitude frequency response should permit the estimation of a, b_1, b_2 and K .

The identification procedure may be repeated for different values of f_1 to improve the estimates. Note that if the poles are not real the procedure will estimate $|b_1|$ and $|b_2|$. If the higher order responses are significant they will also contribute to the output at frequency $\pm(2f_1 + f_2)$ thus complicating the procedure. Similarly, if f_2 is fixed and f_1 is swept, the frequency response will exhibit breaks at

$$f_1 = \frac{a}{2\pi}, \frac{b_1}{2\pi}, \frac{b_2}{2\pi} \quad (\text{double breaks}) \quad (5.18)$$

and

$$f_1 = \frac{1}{2} \left(\frac{a}{2\pi} - f_2 \right), \frac{1}{2} \left(\frac{b_1}{2\pi} - f_2 \right), \frac{1}{2} \left(\frac{b_2}{2\pi} - f_2 \right). \quad (5.19)$$

The poles and zeros identification just described can also be carried out using numerical curve fitting techniques [Shanmugan and Jong (1975)]. We assume that we have a minimum phase transfer function. The basic procedure is as follows. We are given the amplitude $|H(f)|$ of a minimum phase transfer function $H(f)$, at P values of $f=f_k, k=1,2,\dots,P$. From this data we want to determine $H(f)$ in the form

$$H(f) = \sum_{i=0}^M (c_i f^i) / (1 + \sum_{n=1}^N d_n f^n), \quad (5.20)$$

such that the error between function $|H(f)|$ and the P measured values of $|H(f)|$ is minimized. If the least square error criterion is used in the above equation to find the coefficients c's and d's, a set of nonlinear equation results. Different algorithms have been proposed to solve the set of nonlinear equations but most of the methods require both amplitude and phase measurements. Convergence can be a problem when the available data spans a few decades in frequency. Shanmugan and Jong have proposed a method which avoids these problems. The method uses the magnitude squared function and the minimum phase transfer function assumption. The method is described in detail in [Shanmugan and Jong (1975)].

5.1.2.2 Sinusoidal Steady State Identification Including The Effects of the Fifth Order NLTF.

Third-order transfer function poles and zeros identification using a sinusoidal steady-state procedure was discussed in the previous subsection. In this Section we give results for the procedure in the absence of noise. We also consider the effects of the fifth order Volterra NLTF on the identification of the third order transfer function. The case where the measurements contain a noise component is examined in Section 5.2.

Assume that we have a symmetrical nonlinearity (only odd order nonlinear coefficients are important) and consider a response up to fifth order. Note that there is much evidence in the literature that MIM junctions have almost symmetrical i-v characteristics. A system model with up to a fifth order nonlinearity is shown in Figure 5-1. If the input $x(t)$ is the sum of four complex exponentials

$$x(t) = \frac{1}{2} \sum_{m=1}^{M=4} A_m e^{j2\pi f_m t}, \quad (5.21)$$

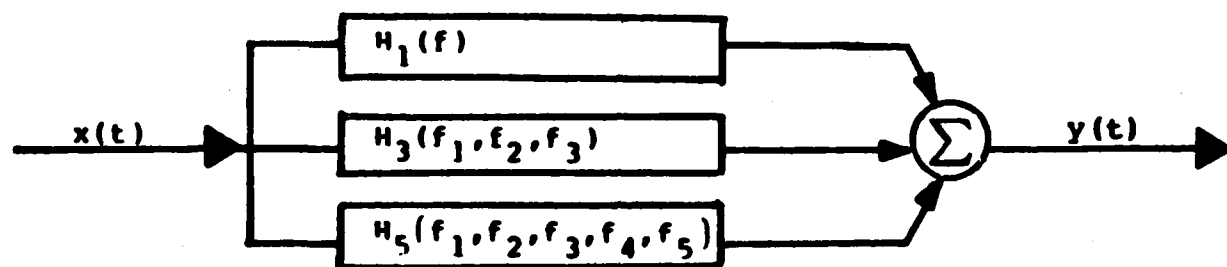


Figure 5-1 Fifth Order System Model

then, as described in Section 3.1 the output $y(t)$ is given by

$$y(t) = \frac{1}{2} \sum_n B_n(\underline{m}) H_n e^{j2\pi f_\Sigma t}$$

$$f_\Sigma = \sum_{i=1}^M m_i f_i, \quad \sum_{i=1}^M m_i = n \quad (5.22)$$

where B_n depends on the input signal amplitudes A_m and is independent of frequency. The frequency dependence is entirely given by the n 'th order nonlinear transfer function H_n .

5.1.2.2.1 Two-Tone Input Example

Multitone testing can be used to characterize nonlinear distortion. The most important case is two-tone testing. In this section we will give the nonlinear response when the system is excited by two sinusoids. In Eq. (5.21) we let $A_3 = A_1^*$, $A_4 = A_2^*$, $f_3 = -f_1$ and $f_4 = -f_2$. We are interested in the intermodulation product (nonlinear response) occurring at frequency $f_\Sigma = 2f_1 - f_2$. Using Eq. 5.22, we have

$$IM = \frac{3}{4} A_1^2 A_2^* H_3(f_1, f_1 - f_2) + \frac{5}{4} A_1^2 A_2^* |A_1|^2 H_5(f_1, f_1, f_1, -f_1, -f_2)$$

$$+ \frac{15}{8} A_1^2 A_2^* |A_2|^2 H_5(f_1, f_1, f_2, -f_2, -f_2) \quad (5.23)$$

The third and fifth order nonlinear transfer functions, assuming only third and fifth order nonlinear coefficients k_3 and k_5 , are given by

$$H_3(s_1, s_2, s_3) = -k_3 H_1(s_1)H_1(s_2)H_1(s_3)H_1(s_1+s_2+s_3) \quad (5.24)$$

and

$$H_5(s_1, s_2, s_3, s_4, s_5) = \overbrace{\left\{ \frac{-3}{10} k_3 H_1(s_1)H_1(s_2)H_3(s_3, s_4, s_5) \right.} \\ \left. - k_5 \prod_{i=1}^5 H_1(s_i) \right\}} H_1(s_1+s_2+s_3+s_4+s_5) \quad (5.25)$$

where the overbar is a compact symmetrization notation, corresponding to taking all permutations of the arguments.

Let the linear transfer function be given by

$$H_1(s) = \frac{1000}{(s+10)(s+100)} \quad (5.26)$$

This corresponds to linear system poles at frequencies 1.6 and 16 Hz. We select the amplitudes of the input A_1 and A_2 to be real. The magnitude of the third order response at frequency $2f_1 - f_2$ is then equal to

$$\frac{3}{4} A_1^2 A_2 |H_3(f_1, f_1, -f_2)| \quad (5.27)$$

We now hold f_1 constant and sweep with respect to f_2 . The magnitude of the third order transfer function is then given by

$$|H_3(f_1, f_1, -f_2)|$$

$$= \frac{K}{|-j2\pi f_2 + 10| |-j2\pi f_2 + 100| |j2\pi(2f_1 - f_2) + 10| |j2\pi(2f_1 - f_2) + 100|}$$

(5.28)

where K is a constant and the Bode amplitude plot of the third order frequency response will exhibit breaking frequencies in Hz at

$$f_2 = 1.6, 16 \quad (5.29)$$

and

$$f_2 = 2f_1 + 1.6, 2f_1 + 16. \quad (5.30)$$

Thus if f_1 is small, the third order frequency response will exhibit double breaks at 1.6 and 16 Hz.

For the identification procedure, one can choose to fix either f_1 or f_2 . The frequency that is fixed must be much smaller than the breaking frequencies of the linear transfer function and therefore one chooses it to be as small as possible. In practice the frequency resolution imposes a constraint as to how small the fixed frequency can be. For the results to be presented, we choose f_1 equal to 0.05 Hz.

The magnitude of the intermodulation (IM) response at $2f_1 - f_2$ for a third order Volterra model (only the first term in Eq. (5.23) is considered) is shown in Figure 5-2. Here we select unit signal amplitudes ($A_1 = A_2 = 1$). From the Bode plot shown in Figure 5-2 we see that the third order magnitude response falls off at a rate of -80 dB/decade at high f_2 frequency values. A single pole contributes -20 dB per decade. We can thus conclude that there are 4 poles in the system. By fitting the model to the IM amplitude Bode plot shown in Figure 5-2 we can graphically obtain the result that there exists a double pole around 1.5 Hz and a double pole around 16 Hz. From this result and the model we can identify the poles of the linear transfer function with good accuracy.

Next we consider the effects of the fifth order nonlinear transfer function (NLTF) on the identification of the poles via the third order intermodulation response. Figure 5-3 shows the magnitude (Bode plot) of the IM response at $2f_1 - f_2$ including all the terms in Eq. (5.23). The fifth order nonlinear coefficient k_5 is 20 dB below the third order coefficient. Frequency plots of the IM magnitude versus f_2 are shown for different choices of input signal amplitudes. The frequency plot for unit input signal amplitudes shown in Figure 5-3 closely agrees with the one shown in Figure 5-2. For this case, the fifth order contribution is small and there is no problem in carrying out the identification. As the input signal amplitudes are increased, the fifth order contribution becomes more significant at low frequencies and the relative phase between the terms in Equation (5.23) may become important. The fifth order contribution has a smaller impact at the higher f_2 frequencies; as we can see from Figure 5-3, the slope is only slightly changed from the -80 dB per decade roll-off. The reason is that for frequencies outside the linear transfer function passband, the fifth order transfer function is attenuated much more than the third order transfer function because it has more poles.

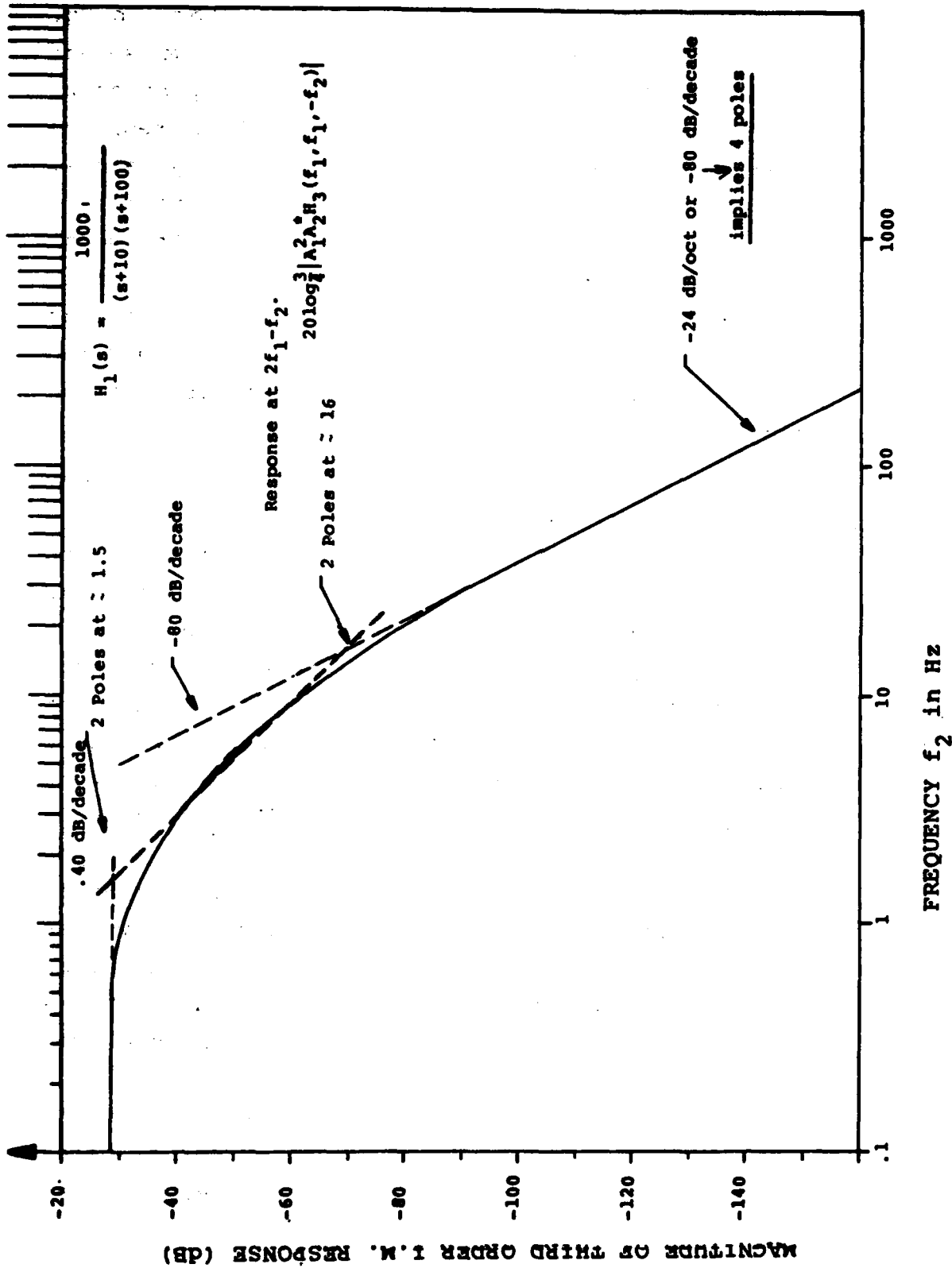


Figure 5-2 Third Order Intermodulation Magnitude as a Function of f_2

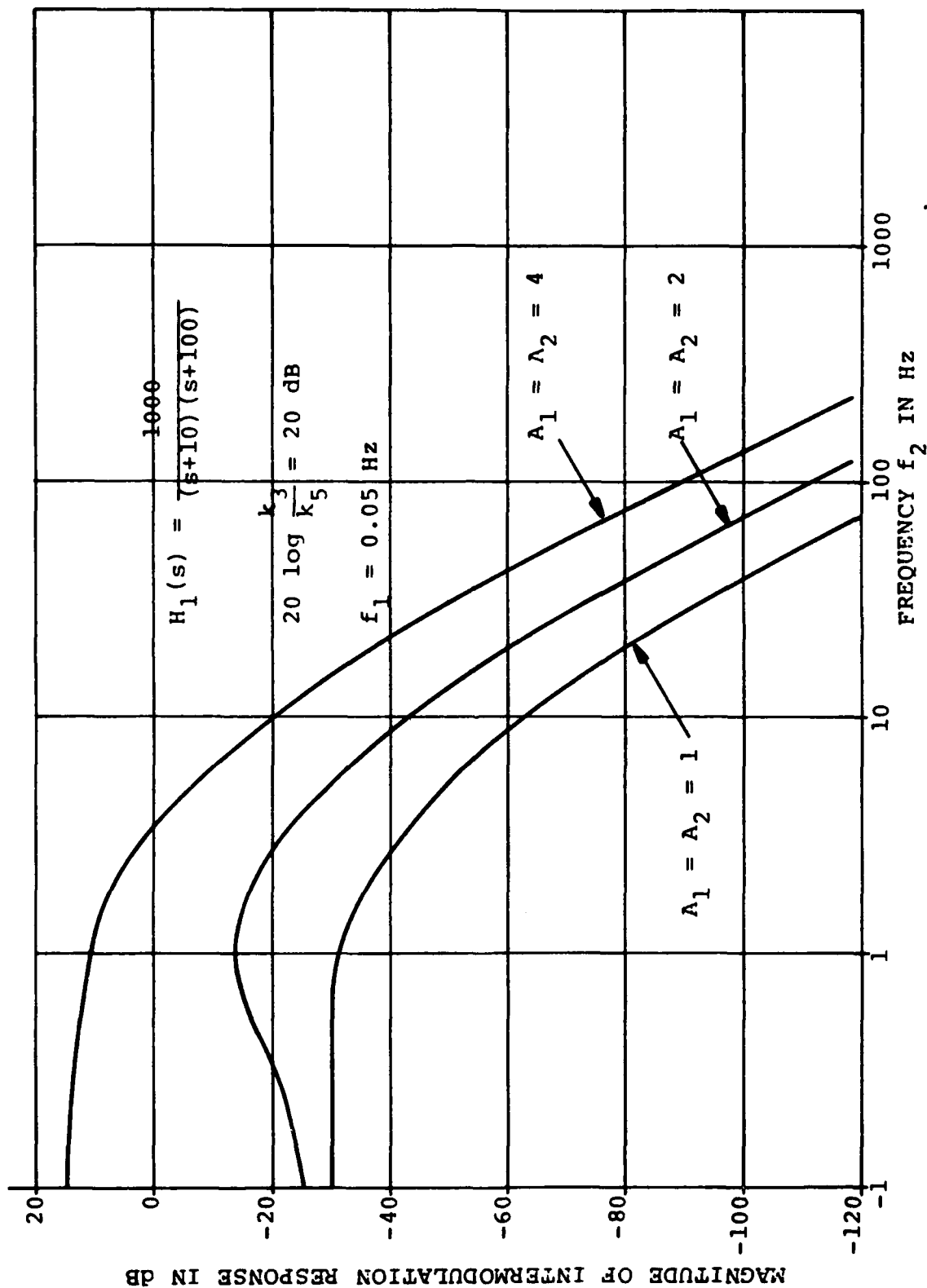


Figure 5-3 Intermodulation Magnitude at Frequency $2f_1 - f_2$, $20 \log(\frac{k_3}{k_5}) = 20 \text{ dB}$

Another case showing the effects of the fifth order NLTF contribution to the IM response at $2f_1 - f_2$ is shown in Figure 5-4. Here the third order nonlinear coefficient k_3 is 10 dB stronger than the fifth order coefficient k_5 . Frequency f_1 is again fixed at 0.05 Hz and we sweep f_2 . The three terms in Eq. 3.0 are all in phase for the range of frequencies of f_2 shown in Figure 5-4. As we increase the input signal amplitudes, the magnitude of the IM response also increases and the slopes exhibit a larger change compared to the results shown in Figure 5-3. This is consistent with the fact that the fifth order contribution in Figure 5-4 has been increased by 10 dB compared to the case shown in Figure 5-3. However the third order transfer function still dominates for frequencies outside the passband.

5.1.2.3 Sinusoidal Steady State Poles and Zero Identification Using Phase Information

The method discussed in Section 5.1.2.1 uses magnitude measurements to estimate the poles and zeros of the rusty bolt linear transfer function. Another sinusoidal steady state method which uses phase measurement was developed by V.K. Jain. This alternate method is discussed in detail in Appendix A. Basically, sinusoidal steady state phase measurements are performed at the third harmonic frequency. These measurements are used to solve a set of nonlinear equations which yield the estimated poles and zeros.

5.1.2.4 Identification of Rusty Bolt NLTF Specification Parameters Constants

The sinusoidal steady state identification technique just discussed can be used to estimate the poles and zeros of a selected nonlinear response and from this one can determine the poles and zeros of the linear transfer function. In the case of

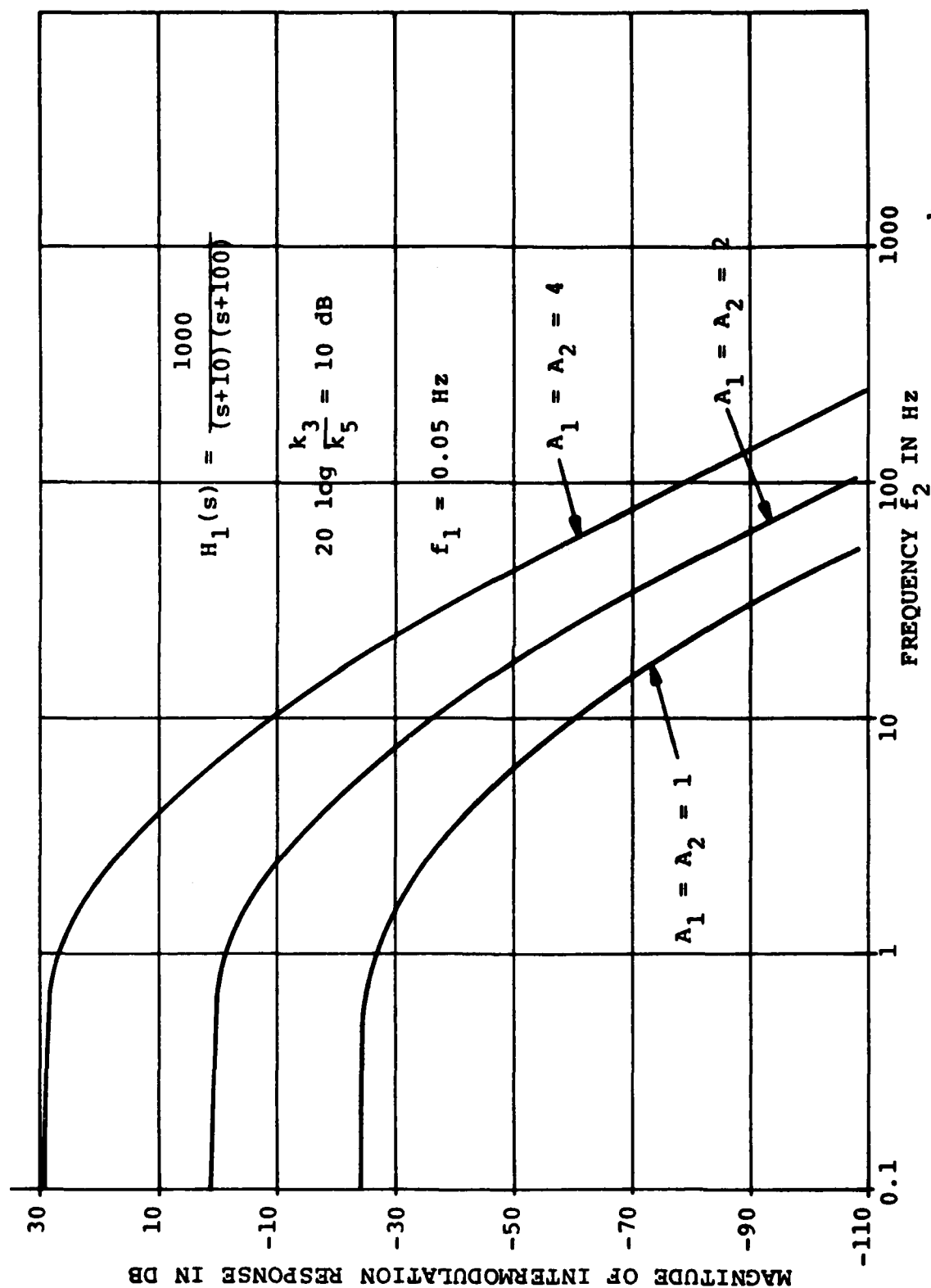


Figure 5-4 Intermodulation Magnitude at Frequency $2f_1 - f_2$, $20 \log(\frac{k_3}{k_5}) = 10 \text{ dB}$

voltage to voltage measurements, one can also determine the normalized antenna impedance of the lumped parameter circuit. The objective is to use the lumped parameter "rusty bolt" circuit model to predict nonlinear effects, which requires the determination of the gains of the Volterra transfer functions in addition to its poles and zeros. In the following section we discuss an approach to and the difficulties in determining the gains of the transfer functions. We assume a fifth order rusty bolt model.

5.1.2.4.1 Nonlinear Response Measurements

Harmonic and intermodulation measurements can be used to determine the parameters of the "rusty bolt" lumped parameter circuit necessary to specify the EMC performance. The third and fifth harmonic responses $y_{3f}(t)$ and $y_{5f}(t)$ due to the input

$$x(t) = A \sin(2\pi ft) \quad (5.31)$$

are given by

$$y_{3f}(t) = \frac{A^3}{4} |H_3(f, f, f)| \sin(2\pi(3f)t + \phi_3) \quad (5.32)$$

$$y_{5f}(t) = \frac{A^5}{16} |H_5(f, f, f, f, f)| \sin(2\pi(5f)t + \phi_5) \quad (5.33)$$

where H_3 and H_5 are the third and fifth order Volterra transfer functions. Similarly the intermodulation response at frequency $2f_1-f_2$ due to the input $x(t) = A_1 \sin 2\pi f_1 t + A_2 \sin 2\pi f_2 t$ is given by

$$y_{2f_1-f_2}(t) = \left[\frac{3}{4} A_1^2 A_2 H_3(f_1, f_1-f_2) + \frac{5}{4} A_1^4 A_2 H_5(f_1, f_1, f_1-f_1, f_2) + \right. \\ \left. \frac{15}{8} A_1^2 A_2^3 H_5(f_1, f_1, f_2-f_2-f_2) \right] \sin(2\pi(2f_1-f_2)t + \phi) \quad (5.34)$$

where we have assumed that the input amplitudes A_1 and A_2 are real.

In the discussion that follows, we present expressions using voltage-to-voltage transfer functions. To get the voltage to current expression one sets the antenna impedance (αZ_{en}) in the expressions to unity.

Let the linear transfer function be given by

$$H_1(s) = \frac{K(\frac{s}{a} - 1)}{(\frac{s}{b_1} - 1)(\frac{s}{b_2} - 1)} = KG_1(s) \quad (5.35)$$

where s is the Laplace variable.

The equivalent antenna impedance is given by

$$Z_e(s) = \alpha \left(\frac{s}{s_0} - 1 \right) = \alpha Z_{en}(s) \quad (5.36)$$

where α is the normalized equivalent antenna impedance constant.

We can estimate $G_1(s)$ and $Z_{en}(s)$ using the sinusoidal steady state technique. The magnitudes of the third order and fifth order Volterra transfer functions take the following form

$$|H_3| = |\alpha k_3 K^4| |D_1| |Z_{en}(s_1 + s_2 + s_3)| \quad (5.37)$$

$$|H_5| = |\alpha K^6| |D_2| |3K \alpha k_3^2 D_3 - k_5| |Z_{en}(s_1 + s_2 + s_3 + s_4 + s_5)| \quad (5.38)$$

where the D_i s are complex constants that depend on the linear transfer function term G_1 , k_3 and k_5 are the nonlinear coefficients, K is the gain constant of the linear transfer function and α is the normalized antenna impedance constant.

5.1.2.4.2 Determination of Gain Constants From Harmonic Measurements

Suppose that $G_1(s)$ and $Z_{en}(s)$ have been identified, then the measurement of $|F[y_{3f}(t)]|$, where F denotes the Fourier transform, would yield the identification of $|\alpha k_3 K^4| = B$. Measurement of the magnitude square of the Fourier transform of $y_{5f}(t)$ gives

$$|\alpha^2 K^{12}| C_1(f) \{ |k_3^4 K^2 \alpha^2| C_2(f) + k_5^2 + \alpha k_3^2 k_5 K C_3(f) \} \quad (5.39)$$

where

$$C_1(f) = \left(\frac{A^5}{16} |G_1(f)|^5 |G_1(5f)|^2 |z_{en}(5f)|^2\right) \quad (5.40)$$

$$C_2(f) = 9 |G_1(3f)|^2 |z_{en}(3f)|^2 \quad (5.41)$$

$$C_3(f) = -6 \operatorname{Re}\{G_1(3f)z_{en}(3f)\} \quad (5.42)$$

are knowns (A is the input signal amplitude).

Make fifth harmonic measurements with three fundamental frequencies f_1 , f_2 and f_3 . Let M_1 , M_2 and M_3 be the measured values (magnitude square of the Fourier transform). We then have the equations

$$\begin{aligned} & |\alpha^4 K^{14} k_3^4| C_2(f_i) + |\alpha^2 K^{12} k_5^2| + |\alpha K^6| |\alpha^2 K k_3^2 k_5 C_3(f_i)| \\ &= \frac{M_i}{C_1(f_i)} \quad i = 1, 2, 3 \quad (5.43) \end{aligned}$$

These equations can be solved for $|\alpha^4 K^{14} k_3^4|$, $|\alpha^2 K^{12} k_5^2|$ and $|\alpha K^5| |\alpha K k_3^2 k_5|$ by inverting a matrix whose elements are determined by $C_2(f_i)$ and $C_3(f_i)$. It has already been established that the third harmonic measurement yields $|\alpha k_3 K^4| = B$. We now have four equations

$$|\alpha K^4 k_3| = B \quad (5.44)$$

$$|\alpha^4 K^{14} k_3^4| = F_1 \quad (5.45)$$

$$|\alpha^2 K^{12} k_5^2| = F_2 \quad (5.46)$$

$$|\alpha K^6|^2 \alpha K k_3^2 k_5 = F_3 . \quad (5.47)$$

To solve for K, we can use Equations (5.44) and (5.45) which yield

$$K = \frac{B^2}{\sqrt{F_1}} . \quad (5.48)$$

It then follows that $|\alpha|$, $|K|$, $|k_3|$ and $|k_5|$ can be obtained from Equations (5.44) through (5.48). The unknown constants are raised to several powers in the Equations to be solved. Therefore, the accuracy of the solution is sensitive to errors. However, the goal is to predict specification parameters such as harmonic and intermodulation distortion and for this we need the combined constants $|\alpha K^4 k_3|$, $|\alpha^2 K^7 k_3^2|$, and $|\alpha K^6 k_5|$. The first combined constant is obtained from equation (5.44) while the other two can be obtained by taking the square root of the right-hand side of Equations (5.45) and (5.46). The combined constants should be less sensitive to measurement errors.

5.2 SPECIFICATION PARAMETERS INVESTIGATION FOR THE RUSTY BOLT

The relationship between nonlinear transfer functions (NLTF) and the EMC specification parameters was discussed in Section 3. The sensitivity to LTF identification errors was analyzed for the general problem. The goal was to evaluate the effects of errors in pole locations on the quality of linear identifications and on the predictions of nonlinear EMC specification parameters such as intermodulation and harmonic distortion assuming that the coefficients of the nonlinearity were known.

In this section, we present intermodulation and harmonic distortion results for the rusty bolt problem. Third order harmonic and intermodulation are predicted using estimates of the voltage-to-voltage Volterra transfer functions of the lumped parameter rusty bolt circuit. The estimates are based on a fifth order Volterra model and the sinusoidal steady state identification technique of Section 5.1.

5.2.1 Intermodulation and Harmonic Distortion Prediction Assuming a Third Order i-v Characteristic

Calculations using rusty bolt parameters found in the literature [Long and Schwartz (1974), Bond et al., (1979)] indicate that the poles of the equivalent lumped parameter circuit are real and that they are separated by a few orders of magnitude in frequency. The parameters also indicate that the singularity of the antenna impedance (zero at the sum frequencies in the voltage-to-voltage NLTF) is about equal to the highest frequency pole of the rusty bolt.

Let the rusty bolt linear voltage-to-voltage transfer function and antenna impedance be given by

$$H_1(s) = \frac{100}{(s+1)(s+100)} \quad (5.49)$$

$$Z_e(s) = (s+100) . \quad (5.50)$$

Note that it has been assumed in this case that the antenna impedance zero is exactly equal to the higher frequency pole of $H_1(s)$. We now will consider two different i-v characteristics for the rusty bolt (MIM junction). First, assume that the i-v relationship for the circuit shown in Figure 4-2 is given by

$$i_d = k_1 v_d + k_3 v_d^3 . \quad (5.51)$$

In order to predict intermodulation and harmonic distortion, we need estimates of the linear transfer function poles, the normalized antenna impedance and the combined constants $C_1 = |\alpha K^4 k_3|$ and $C_2 = |\alpha^2 K^7 k_3^2|$. From equations (5.35), (5.36), (5.49), and (5.50) we can see that the true values of the normalized linear transfer function gain and the normalized antenna impedance constant are, respectively, $K=1$ and $\alpha=100$. For the examples to be presented, we select $k_3 = 0.05 \text{ mhos/V}^2$. This gives combined constants $C_1=5$ and $C_2=25$.

A computer program was developed to implement the combined constants estimation technique described in Section 5.1.2.4. In the program, the harmonic measurements are corrupted by additive white Gaussian noise. The combined constant identification algorithm gave correct estimates for the noiseless (SNR > 60 dB) case

(the correct normalized linear transfer function and antenna impedance were used in the estimation). Next, we performed estimation in the presence of additive noise. Let the poles be identified as $\hat{s}_1 = -1.11$ and $\hat{s}_2 = -101.5$ and the antenna impedance singularity as $\hat{s}_0 = \hat{s}_2$. Using the identified poles, normalized impedance and a SNR = 30 dB, we estimated the combined constants as $C_1 = 4.257$ and $C_2 = 18.344$. The true and estimated third order harmonic is shown in Figure 5-5. The predicted result is labeled estimated Case I in Figure 5-5. As we can see, the predicted results are quite good. The error between the true and estimated third harmonic ranges between 2 and 2.5 dB. Third order intermodulation results are shown in Figure 5-6. The predicted result is labeled as estimated Case I in the figure. The intermodulation result is of the same quality as the predicted third order harmonic. In other words the errors range between 2 and 2.5 dB.

In the next case, the poles and antenna impedance singularity are identified as $\hat{s}_1 = -3.53$, $\hat{s}_2 = -70$, $\hat{s}_0 = -70$. Notice that the low frequency pole is 250 percent in error, while the higher frequency pole and the antenna impedance singularity are 30 percent in error. Using the identified singularities and a SNR of 10 dB, we identified the constants as $\hat{C}_1 = 3.66 \times 10^{-2}$ and $\hat{C}_2 = 4.60 \times 10^{-3}$. The estimated constants depend on the identified linear transfer function poles, the antenna impedance, the SNR and the fundamental frequencies used in the harmonic measurement (see Section 5.1.2.4.2). The same frequency (2Hz) was used in all cases to identify the combined constants of the voltage-to-voltage rusty bolt NLTF. This frequency is about midway between the two pole location frequencies on a log scale. The true combined constants (using the correct poles and antenna impedance) are $C_1 = 5$ and $C_2 = 25$. Thus there is a large difference between the estimated and true constants. This difference is due to the large errors associated with the identified poles

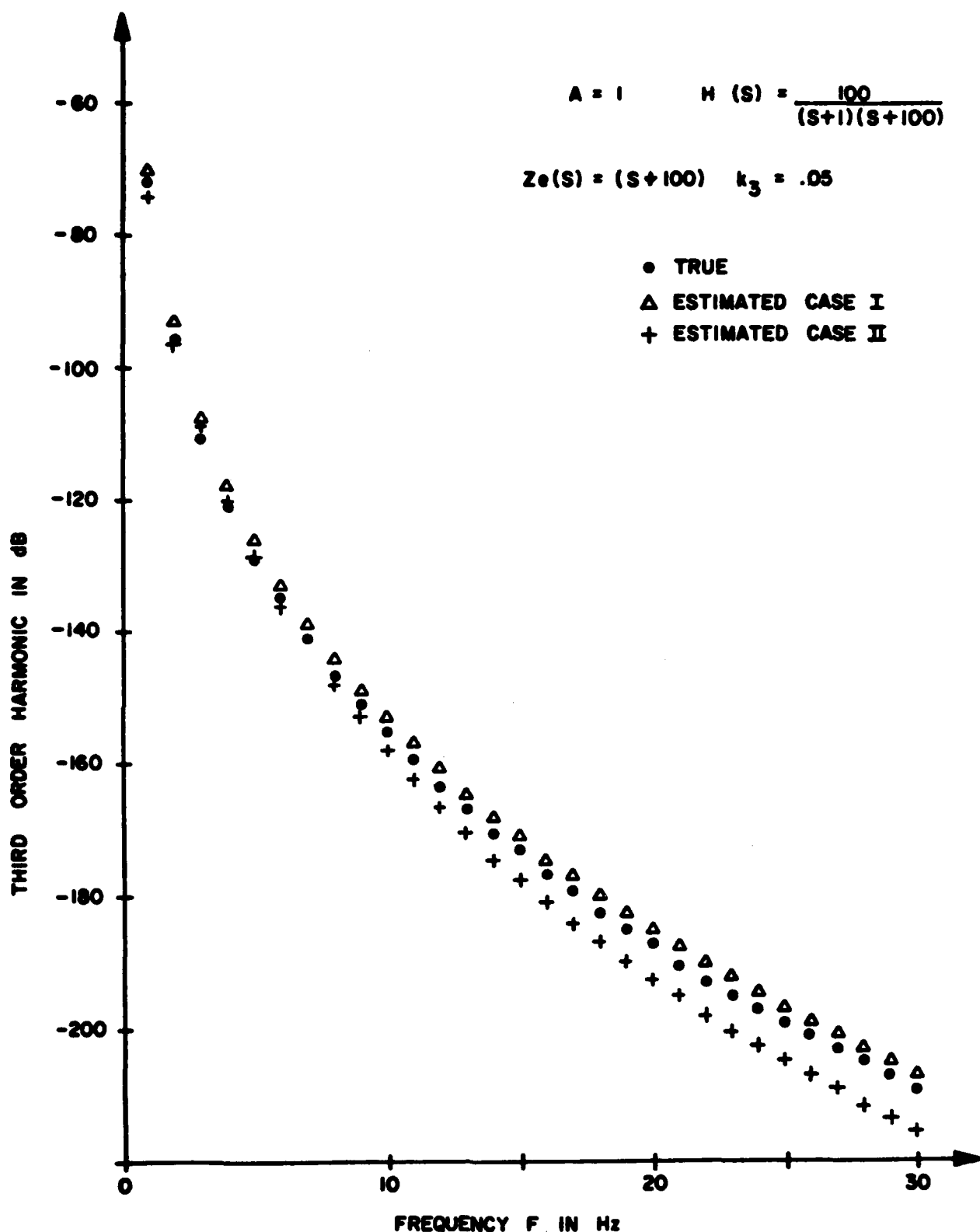


Figure 5-5 Third Order Harmonic Using Volterra Voltage to Voltage Transfer Function.

1. Estimate based on poles at $s_1 = -1.11$, $s_2 = -101.5$, Antenna impedance zero at $s = -101.5$
2. Estimate based on poles at $s_1 = -3.53$, $s_2 = -70$, Antenna impedance zero at $s = -70$.

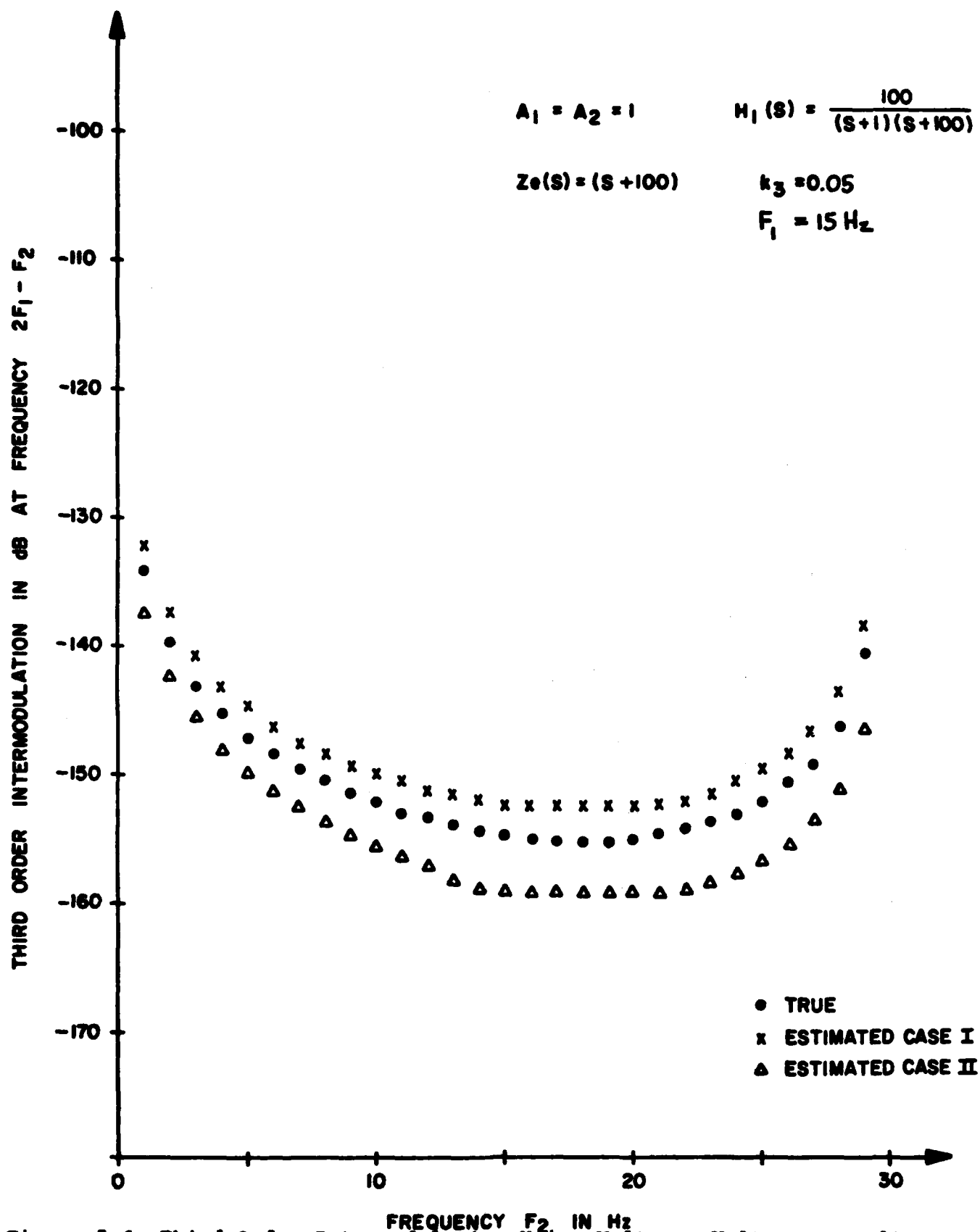


Figure 5-6 Third Order Intermodulation Using Volterra Voltage to Voltage Transfer Function.

1. Estimate based on poles at $s_1 = -1.11$, $s_2 = -101.5$, Antenna Impedance zero at $s_0 = -101.5$
2. Estimate based on poles at $s_1 = -3.53$, $s_2 = -70$, Antenna Impedance zero at $s_0 = -70$.

and antenna impedance. Harmonic and intermodulation results for this second case are shown in Figures 5-5 and 5-6. The predicted third order harmonic and intermodulation EMC specification parameters are reasonable for this case despite the large errors in pole location, antenna impedance and the combined constants. The error in the prediction of the third harmonic for the frequency range shown varies between 0 and 6.5 dB. The error in the prediction of the third order intermodulation ranges between 2.7 and 6 dB. The estimated constants appear to compensate for the errors in pole locations and the antenna impedance.

Next, we present a case where the system is severely misidentified. Let the linear system be identified as a single pole at $\hat{s} = -26.6$. The antenna impedance is identified as pure real ($Z_{en} = 1$). Using the identified pole and a SNR = 5 dB, the constants are estimated as $\hat{C}_1 = 1.5 \times 10^{-4}$ and $\hat{C}_2 = 2.38 \times 10^{-7}$. The true and predicted third order harmonic and intermodulation are shown in Figures 5-7 and 5-8. The error in predicting the third harmonic for this case ranges from 0 to 43 dB, while the errors in predicting third order intermodulation ranges from 15 to 32 dB. Thus the errors are severe. This is to be expected since the number of poles and the pole locations have been misidentified.

5.2.1.1 Caution in Using Severely Misidentified Poles to Estimate Constants to Predict Nonlinear Performance

In the previous subsection we showed third order harmonic and intermodulation results for the case where the poles are identified as $p_1 = -3.53$ and $p_2 = -70$. The predicted intermodulation and harmonic results with the estimated constants gave acceptable errors even though the identified poles and combined constants were significantly different from the true ones.

The constants were identified using harmonic measurements with a fundamental frequency of 2Hz (12.56 radians/sec). The

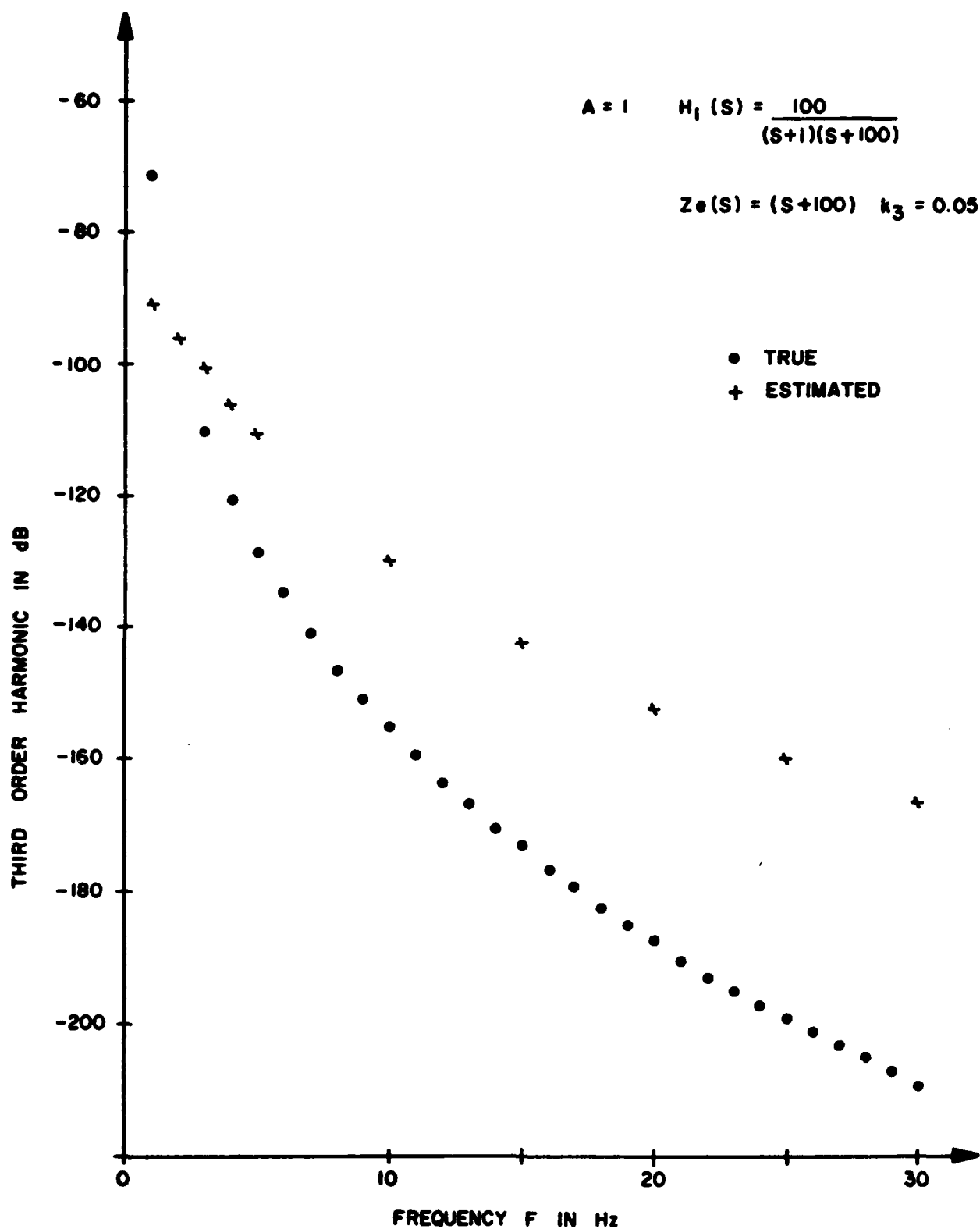


Figure 5-7 Third Order Harmonic Using Volterra Voltage to Voltage Transfer Function. Estimate based on a single pole at $s = -26.6$.

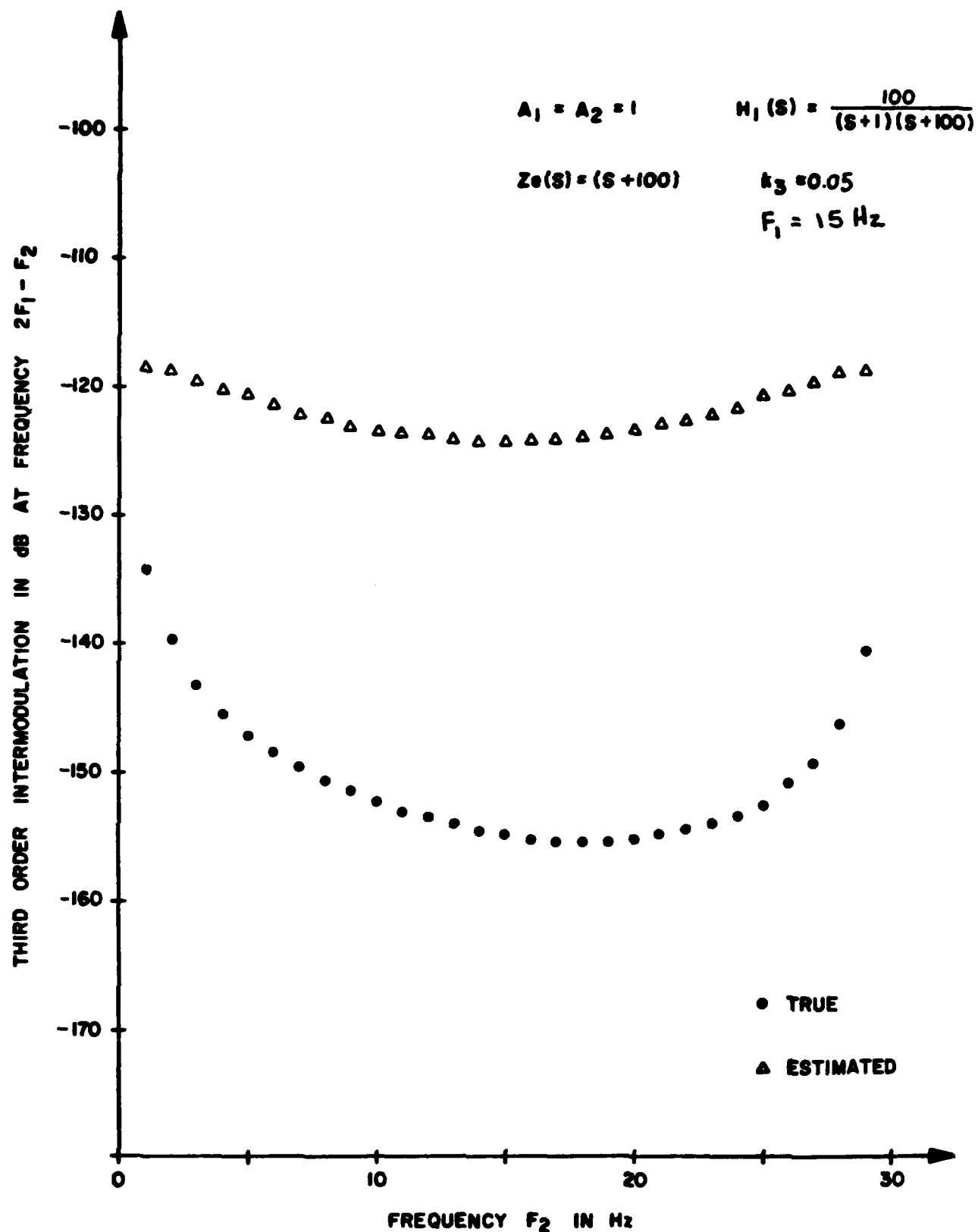


Figure 5-8 Third Order Intermodulation Using Volterra Voltage to Voltage Transfer Function. Estimate based on identification of a single pole at $s = -26.6$.

fundamental frequency used in the harmonic measurements was varied to investigate the sensitivity of the estimated constants as a function of the frequency used in the measurements. The obtained results are shown in Table 5-1. The results indicate that the estimated constants are not too sensitive to the fundamental frequency used in the harmonic measurements unless the error in pole locations is large. Predicted third harmonic and intermodulation for the cases shown in Table 5-1 were reasonable except for the case where the poles are estimated as $\hat{s}_1 = -3.53$, $\hat{s}_2 = -70$ and the constants are estimated as $\hat{C}_1 = .541$, $\hat{C}_2 = .376$ with a fundamental measurement frequency of .2 Hz. The error in predicting intermodulation for this case varied from 18 to 20 dB, while the error in predicting the third order harmonic ranged from 16 to 23.6 dB. These results should be compared with the results shown in Figures 5-5 and 5-6. There, the largest error in predicting third order intermodulation and harmonic distribution was about 6 dB.

The previously discussed example showed that when the errors in the identified poles are large, the nonlinear transfer function combined constants can be very sensitive to the frequency used in the harmonic measurements. This can cause large errors in the predicted third order harmonic and intermodulation specification parameters.

5.2.2 Intermodulation and Harmonic Distortion Prediction Assuming a Fifth Order i-v MIM Characteristic

In the previous Section 5.2.1, we presented harmonic and intermodulation results assuming a third order MIM junction i-v characteristic which is the case mostly discussed in the literature. We now extend the i-v characteristic. Assume that the i-v relationship for the circuit shown in Figure 4-2 is given by

$$i_d = k_1 v_d + k_3 v_d^3 + k_5 v_d^5 \quad (5.52)$$

Table 5-1 Estimated constants as a function of fundamental measurement frequency

$$H_1(s) = \frac{100}{(s+1)(s+100)}$$

TRUE PARAMETERS									
poles $s_1 = -1$, $s_2 = -100$, Antenna Singularity $s_0 = -100$, constants $C_1 = 5$, $C_2 = 25$									
Estimated Parameters									
Fundamental Frequency used in Harmonic Measurements	$\hat{s}_1 = -1$, $\hat{s}_2 = -100$, $\hat{s}_0 = \hat{s}_2$ (SNR = 60 dB)		$\hat{s}_1 = -1.11$, $\hat{s}_2 = -101.5$, $\hat{s}_0 = \hat{s}_2$ (SNR = 30 dB)		$\hat{s}_1 = -3.53$, $\hat{s}_2 = -70$, $\hat{s}_0 = \hat{s}_2$ (SNR = 10 dB)				
	C_1	C_2	C_1	C_2	C_1	C_2			
	5	25	3.77	15.08	5.41×10^{-1}	3.76×10^{-1}			
	5	25	4.26	18.34	3.66×10^{-2}	4.60×10^{-3}			
	5	25	3.21	11.5	6.82×10^{-2}	1.26×10^{-2}			
f (Hz)	w (rad/sec)								
.2	1.26								
2	12.6								
20	126								

In addition to the singularities of the linear transfer function and the normalized antenna impedance, the prediction of the third order harmonic and intermodulation specification parameters for this case requires estimates of the combined constants $C_1 = |\alpha K^4 k_3|$, $C_2 = |\alpha^2 K^7 k_3^2|$ and $C_3 = |\alpha K^6 k_5|$.

In the example of Section 5.2.1, the combined constants could be determined using harmonic measurements with the assumption that $k_5 = 0$. Now because the MIM i-v characteristic contains a fifth order term, both third and fifth harmonic measurements with the assumption that k_5 is present are required to estimate the combined constants. A procedure for estimating the combined constants was outlined in Section 5.1.2.4.2. The system of equations derived in that section to solve for the combined constants becomes singular when the linear transfer function contains a single pole and k_5 is present. The system also becomes singular when the linear transfer function contains two poles and the antenna impedance singularity is equal to one pole. Thus, because of k_5 , the system of equations for the rusty bolt case discussed in the previous example is singular. The problem is that $C_3(f)$ is a multiple of $C_2(f)$ in Equations (5.39) through (5.43). In practice the measurements will be corrupted by noise and the system will be highly ill condition (close to singular).

We now discuss the previous rusty bolt case when the i-v characteristic is expanded to include k_5 . The true linear transfer function poles and antenna singularity s_0 are assumed to be at $s_1 = 1$, $s_2 = -100$ and $s_0 = s_2 = -100$. The i-v nonlinear coefficients are taken as $k_3 = .05$ and $k_5 = .0158$. Thus k_3 is about 10 dB stronger than k_5 . Theoretically, the combined constants cannot be determined by the procedure of Section 5.1.2.4.2 because the system is singular. We can however determine C_1 , C_2 which depend only on k_3 , and we ask the question, how well can we predict the third order intermodulation and harmonic distortion if we assume that only k_3 is present and we identify the combined

constants using the harmonic measurements. We performed the identification assuming the same pole and normalized antenna impedance estimates as for the case discussed in Section 5.2.1. The predicted third order intermodulation and harmonic distortion estimates were very close to those predicted in Section 5.2.1. It is not surprising that the third harmonic estimates agreed with the results obtained in Section 5.2.1 since the third harmonic is not a function of k_5 . This is not so for the third order intermodulation. The third order intermodulation is given by Equation (5.23). It contains three contributions, one from the third order Volterra NLTF and two from the fifth order Volterra NLTF. For real and equal input signal amplitudes A , the third order NLTF term is weighted by A^3 and the fifth order terms are weighted by A^5 . For the examples presented, we used unit input signal amplitudes. The fifth order NLTF depends on both k_3 and k_5 (See Equation (4.12)). The fact that the predicted third order intermodulation was close to that predicted in Section 5.2.1 indicates that the sum of the third order NLTF and fifth order NLTF contributions due to k_3 is much stronger than the fifth order NLTF function contribution due to k_5 . We increased the input signal amplitudes by a factor of 10 and the results still did not change significantly from those obtained in Section 5.2.1. For frequencies outside the linear transfer function (LTF) passband, the contribution due to the third order NLTF dominates because the fifth order NLTF H_5 contains more poles and thus H_5 is much more attenuated.

Next, we attempted to predict the fifth order harmonic using the combined constants obtained from harmonic measurements with the assumption that $k_5 = 0$. We assumed that the poles and the normalized antenna impedance of the previous example were known exactly. First, assume that $k_3 = 0.05$ and $k_5 = .005$. Then the true combined constants are $C_1 = 5$, $C_2 = 25$, and $C_3 = 0.5$. The estimated combined constants using harmonic measurements with

the assumption $k_5 = 0$ and a SNR = 60 dB are $\hat{C}_1 = 5$, $\hat{C}_2 = 25.6$ and $\hat{C}_3 = 0$. The computed true and estimated fifth harmonic for this case indicated that the error between the true and predicted harmonic increases as a function of the fundamental frequency. The largest error for the frequency range 1 to 30 Hz was 11.6 dB. Next, we changed the value of k_5 to 0.0158. The new true combined constants are $C_1 = 5$, $C_2 = 25$ and $C_3 = 1.58$. The estimated combined constants using the harmonic measurements with the assumption $k_5 = 0$ were $\hat{C}_1 = 5$, $\hat{C}_2 = 31.5$ and $C_3 = 0$. The true and predicted fifth harmonic is shown in Figure 5-9. Again the error between the predicted and true fifth harmonic increases with an increase in fundamental frequency. The maximum error for the frequency range shown has increased to 19.5 dB. This is understandable since the fifth order nonlinear i-v characteristic coefficient was increased by 10 dB. These results show that for a fifth order i-v characteristic, it is important to have an estimate of the combined constant related to k_5 if fifth order EMC specification parameters are to be accurately predicted.

5.2.2.1 Determination of Combined Constant Associated with k_5

It was just shown that when the MIM i-v characteristic contains a fifth order coefficient k_5 it is important to have an estimate of the combined constant associated with k_5 when predicting fifth order EMC specification performance. The highly ill-conditioned system of equations was solved to get an idea of the accuracy of the solution. The results are shown in Table 5-2 where they are compared with those obtained from harmonic measurements with the assumption that $k_5 = 0$. When the poles and the normalized antenna impedance are known exactly, the third and fifth harmonic measurements at an SNR = 60 dB yield good result. Even though the system is ill-conditioned, the first and third combined constants (C_1 and C_3) are estimated correctly. The estimate of the second combined constant is about 19 percent

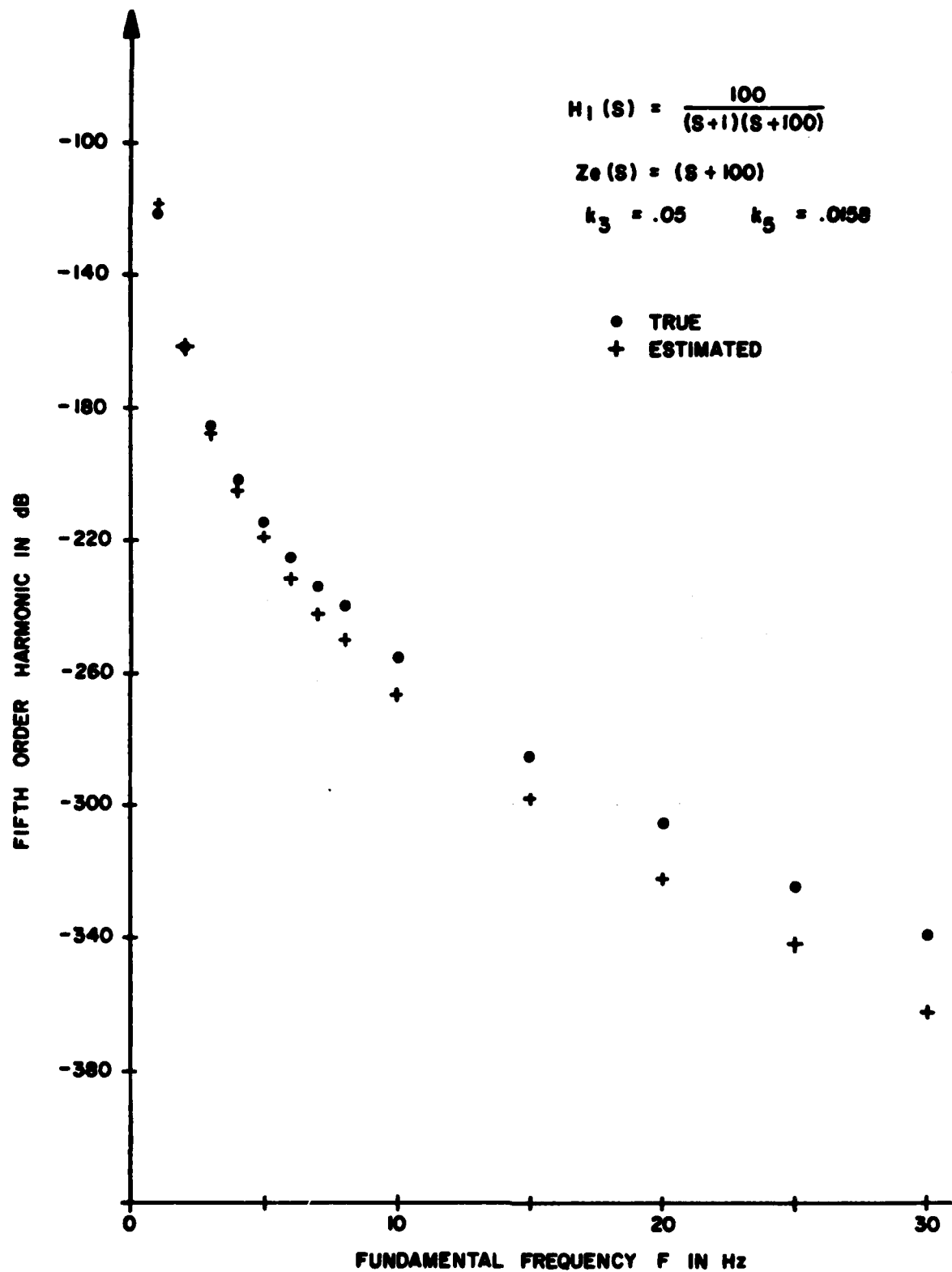


Figure 5-9 Fifth Order Harmonic Using Volterra Voltage to Voltage Transfer Functions. Estimate based on true poles, true antenna impedance and constants obtained from Harmonic measurements with the assumption $k_5 = 0$.

Table 5-2 Comparison of estimated constants using a highly ill condition system of equations and only third harmonic measurements

$$H_1(s) = \frac{100}{(s+1)(s+100)} \quad k_3 = 0.05 \quad k_5 = .0158$$

Type of Measurements Used to Estimate Constants	TRUE PARAMETERS									
	poles $s_1 = -1$, $s_2 = -100$, Antenna Singularity $s_0 = -100$, constants $C_1 = 5$, $C_2 = 25$, $C_3 = 1.58$									
	Estimated Parameters									
	(SNR = 60 dB)			(SNR = 30 dB)			(SNR = 10 dB)			
	$\hat{s}_1 = -1$, $\hat{s}_2 = \hat{s}_0 = -100$, $\hat{s}_0 = \hat{s}_2$	$\hat{s}_1 = -1.11$, $\hat{s}_2 = \hat{s}_0 = -101.5$	$\hat{s}_1 = -3.53$, $\hat{s}_2 = \hat{s}_0 = -70$							
	C_1	C_2	C_3	C_1	C_2	C_3	C_1	C_2	C_3	
Harmonic Measurements Assuming $k_5=0$.	5	31.5	0	3.29	15.22	0	3.66×10^{-2}	5.77×10^{-3}	0	
Harmonic Measurements Assuming k_5 is present	5	20.26	1.58	3.30	1011.8	0.836	3.66×10^{-2}	5.95	1.10×10^{-3}	

Third harmonic measurements made with a fundamental frequency of 2 Hz.

Fifth harmonic fundamental frequencies used 2, 4 and 6 Hz

in error. Prediction of the EMC specification parameters will yield good results. However, when the estimated poles and normalized impedance are in error, the second combined constant is severely misidentified. If we compare the estimated second constants for the cases $\text{SNR} = 30$ and $\text{SNR} = 10$ dB with those obtained by performing harmonic measurements under the assumptions $k_5 = 0$ and k_5 is present we see that the estimates differ by a multiplicative factor of about 70 in one case and by about 1000 in the other case.

Third order EMC specification parameters where one of the frequencies is outside the passband of the linear rusty bolt transfer function depends mostly on the third order Volterra transfer function. The fifth order NLTF plays a role only when the amplitude of the input signal is very strong. Thus for frequencies outside the passband only the combined constant C_1 is important. In this case the error in the second combined coefficient C_2 is not important and thus prediction of the third order EMC specification parameters using the estimated constants shown in Table 5-2 will give acceptable results. In contrast, the prediction of fifth order EMC specification parameters depend on both C_2 and C_3 . In the previous sub-section, it was shown that predicting the fifth harmonic using constants estimated from harmonic measurements with the assumption $k_5 = 0$ gave large errors (max. 19.5 dB) even if the poles and the normalized impedance were correct. The reason is that the third combined constant C_3 cannot be estimated from harmonic measurements with the assumption that $k_5 = 0$. Prediction of the fifth order EMC specification parameters when the poles are in error and the constants are estimated from the ill condition system of equations also yields very large errors. For a fundamental frequency in the range of 1 to 30 Hz, the maximum error for the $\text{SNR} = 30$ dB case was 37 dB at a fundamental frequency f_0 of 1 Hz and the minimum error in predicting the fifth harmonic was 17.5 dB at

$f_0 = 30$ Hz. The error in predicting the fifth harmonic for the SNR = 10 dB case was a minimum of 30 dB at $f_0 = 30$ Hz and a maximum of 60 dB at 2 Hz. This is due to the inaccurate estimate of C_2 . However, if we estimate C_1 and C_2 from harmonic measurements with the assumption that $k_5 = 0$ and estimate C_3 from the ill-conditioned system of equations, we get good results in the prediction of up to fifth order EMC parameters. The maximum error in predicting the fifth harmonic for the SNR = 30 dB case was reduced from 37 dB to 1.7 dB. Similarly the maximum error in predicting the fifth harmonic for the SNR = 10 dB case was reduced from 60 dB to 10.3 dB, the maximum error in this case occurred at 30 Hz instead of 2 Hz.

5.3 CONCLUSION

We have presented intermodulation and harmonic distortion results for the lumped parameter rusty bolt problem. A third order and a fifth order metal-insulator-metal (MIM) i-v characteristic was considered. For a third order i-v characteristic, the EMC specification parameter up to fifth order can be predicted with good quality provided that the number of poles is identified correctly and that the errors in the estimates of the linear transfer function poles and the antenna impedance singularity are reasonable (say less than 30 percent).

When the MIM i-v characteristic contains both a third order and a fifth order coefficient the combined constants necessary to predict the EMC specification parameters can be estimated from the procedure described in Section 5.1.2.4. The combined constants are obtained by inverting a matrix and by using third and fifth harmonic measurements. The elements of the matrix are obtained from estimates of the linear transfer function and antenna impedance singularities. In general, the matrix is non-singular except when the linear transfer function consists of a single pole or when it has two poles and the antenna impedance

singularity is equal to one of the poles. One of the most difficult cases, the case when the matrix is highly ill-conditioned, was studied. The solution obtained by inverting the highly ill-conditioned matrix gives reasonable estimates for the combined constants $C_1 = |\alpha^4 k_3|$ and $C_3 = |\alpha^6 k_5|$. However, the second combined constant $C_2 = |\alpha^2 k_3^2|$ is very inaccurate and unreliable.

Third order EMC specification parameters such as intermodulation which have a contribution due to the fifth order Volterra NLTF can be predicted with good quality using combined constants obtained from harmonic measurements and assuming that $k_5=0$. This is especially true if the EMC specification parameters are to be predicted at frequencies outside the passband of the linear transfer function. The reason is that the contribution due to the third order Volterra NLTF dominates because the fifth order NLTF contains more poles and thus its magnitude response is much more attenuated.

Prediction of fifth order EMC specification parameters when the MIM i-v characteristic contains k_5 requires estimates of both the combined constants C_2 and C_3 . In this case, the EMC parameters can be predicted with good quality if C_2 is estimated from harmonic measurements with the assumption that $k_5=0$ and C_3 is estimated by inverting the highly ill-conditioned matrix. Good results are obtained provided that reasonable estimates are used for the poles and the normalized antenna impedance.

SECTION 6

MEASUREMENT AND INSTRUMENTATION CRITERIA

The traditional EMC specification parameters such as harmonic distortion, gain compression, intermodulation and cross modulation all depend on a common factor, namely the amplitude of the signal or signals which interact with the nonlinearity. The NLTF on the other hand are in most cases independent of the signal amplitude. Therefore, once the NLTF are identified, the traditional parameters for nonlinear elements are predictable for any given signal amplitude. Techniques to predict the EMC specification parameters were discussed in the previous sections. The "rusty bolt" equivalent circuit falls in the class of lumped parameter circuits with zero-memory nonlinearities between circuit nodes. For this class of systems, the relevant features of the NLTF are the poles, zeros or residues of the LTF and the combined constants of the NLTF. The combined constants are always functions of the LTF gain and the coefficients of the nonlinearity. The experiment criteria must take the relevant features of the NLTF into account. In addition, the experiment criteria must relate to the following:

- System Dynamic Range
- System Bandwidth
- System Gain
- Signal(s) Amplitude
- Signal(s) Waveform
- Pertinent Output Characteristics
- Degree of Known Nonlinearity.

6.1 TEST PROCEDURES AND REQUIREMENTS

MIM junctions (rusty bolt) in the coupling path(s) between co-located transmitters and receivers on board Air Force C³I platforms cause very low level nonlinear interference. Even though the interference is low level it still can degrade receiver performance, because the receivers are highly sensitive. Receiver sensitivities can be about -170 dBm/Hz. Rusty bolt experiment criteria require special attention and care because of the low level rusty bolt signals and the large system dynamic range.

The proposed test procedure includes three steps. First, the i-v characteristics of a rusty bolt would be measured on a laboratory bench. Second, a rusty bolt would be identified in an anechoic chamber and the nonlinear performance would be predicted. The model and the identification procedure would be refined as necessary. Finally, upon the successful identification of the rusty bolt in step 2, the identification would be carried out on board an aircraft. It should be noted that even if the results of step 2 indicate that a lumped parameter model is adequate to represent the rusty bolt in an anechoic chamber the success of the experiment on board the aircraft is not guaranteed. The reason is that the aircraft rusty bolt will probably be of a distributed nature. This may necessitate the development of a distributed parameter (transmission line) rusty bolt nonlinear model. Furthermore, the characteristics may be time varying.

6.1.1 Intermodulation and Harmonic Measurements

The parameters of the rusty bolt equivalent circuit are best identified from sinusoidal steady state intermodulation and harmonic measurements. These external nonlinear interference products must be separated from internal products generated in

the transmitter if the principal features of the lumped parameter rusty bolt circuit are to be successfully identified. In addition, the rusty bolt nonlinear response measurements must be performed with adequate signal-to-noise ratio (SNR). The total thermal noise power N in a bandwidth B in Hz is equal to

$$N = kTB \quad (6.1)$$

where k is Boltzman's constant and T is the noise temperature in degrees Kelvin. The thermal noise floor at room temperature (290°K) is equal to -174 dBm/Hz. This is close to the -170 dBm/Hz sensitivities of some Air Force receivers.

AL-AL₂O₃-AL MIM junction intermodulation levels of -110 to -135 dBm for a transmitter power of about 1 Watt (30 dBm) have been measured by Bond et al., (1979). Harmonic measurements have been performed by Flemming et al., (1977), and Watson (1980).

A block diagram for rusty bolt harmonic generation measurement is shown in Figure 6-1. We recommend making third order and fifth order rusty bolt harmonic measurements. The necessary combined constants to predict up to fifth order nonlinear EMC specification performance can be identified from these measurements. Special filters are required to remove or substantially attenuate internally generated nonlinear products. Ideally, the residual harmonic level (without the rusty bolt present) should be reduced below the receiver noise level. A block diagram for third order rusty bolt intermodulation measurement is shown in Figure 6-2. Again special attention should be paid to the screening and filtering of the equipment, the cabling and connectors.

Measurements of the properties and identification of the MIM junction (rusty bolt) parameters will be based on harmonic and intermodulation detection and measurements with the following

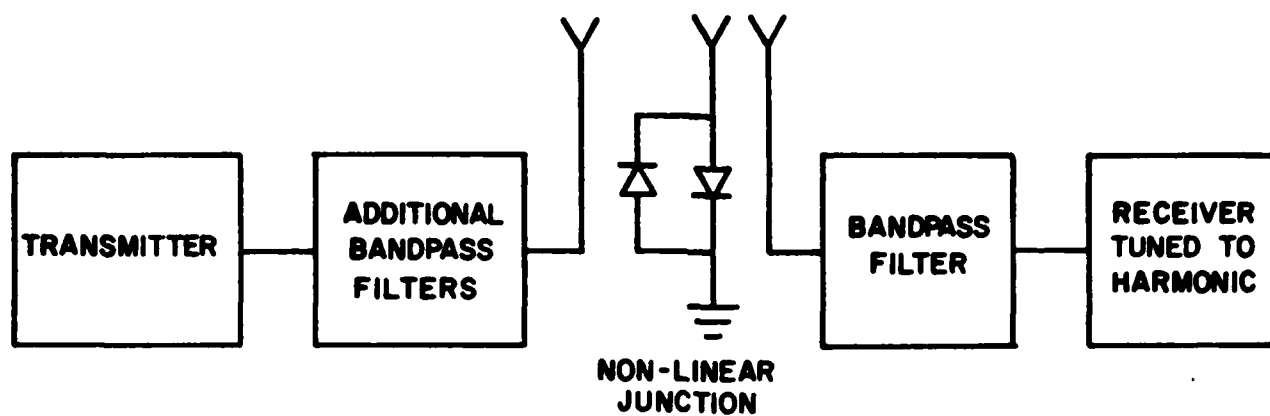


Figure 6-1 Harmonic Generation Measurement.

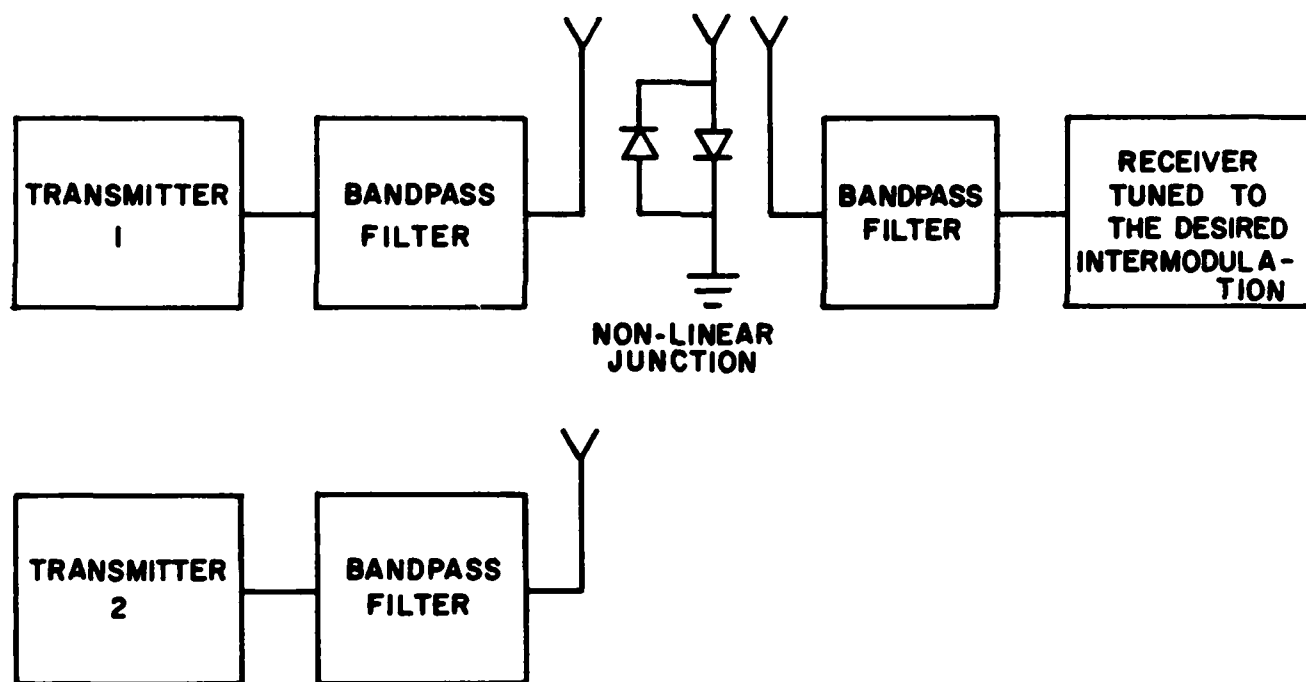


Figure 6-2 Intermodulation Generation Measurement.

conditions. Signal sources (transmitters) in a UHF range of 225 to 400 MHz at power levels typically up to 50 Watts (47 dBm) will be used. The receiver should be tunable up to at least L-band (1 to 2 GHz) with sensitivities in the range of -110 to -140 dBm. This corresponds to receiver bandwidths of 1 kHz to 1 MHz for receiver sensitivities of -170 dBm/Hz. Based on information about rusty bolt measurements available in the literature [Flemming, et al., (1977), Bond et al., (1979)], the AL-AL₂O₃-AL third order rusty bolt nonlinear products are expected to be 110 to 130 dB down from the transmitted power, while the fifth order products are expected to be in the range of 125 to 145 dB down from transmitted power. Assume that the transmitted power is 47 dBm (50 Watts) and that the nonlinear product to be measured is 145 dB down from transmitted power, in other words -98 dBm and that the receiver sensitivity is -110 dBm (bandwidth of 1 MHz for receiver sensitivities of -170 dBm/Hz). The signal-to-thermal noise ratio (assuming room temperature) for the nonlinear product measurement with a receiver bandwidth of 1 MHz is $SNR = -98 + 117 = 19$ dB. The signal-to-noise ratio can be improved by using a bandpass filter with a smaller bandwidth tuned to the desired nonlinear response or by averaging the measurement over a period of time. The same measurement with a receiver bandpass filter of 1 kHz can be performed with a $SNR = 49$ dB.

The above discussion on the levels of the nonlinear products generated by the AL-AL₂O₃-AL MIM junction (rusty bolt) indicates that a large isolation between transmitters and receivers is required in the measurements. For a transmitted power of 47 dBm and a receiver sensitivity of -140 dBm, an isolation of about 200 dB between source and receiver is required to reduce the residual interference (without the rusty bolt present) 10 dB below the receiver noise level. The only way this can be achieved is by performing the measurements in a special anechoic chamber and by paying special attention to the screening and

filtering of the equipment, the cabling and the connectors. An isolation approaching 200 dB between source and receiver, positioned well within 10 meters in a special anechoic chamber, has been achieved by Watson (1980). This indicates that the required isolation and measurement of the rusty bolt nonlinear harmonic and intermodulation response is feasible.

6.1.2 Rusty Bolt Experimental Criteria and Methodology

In the previous subsection, we discussed the procedures and requirements of the rusty bolt measurements. In this subsection we summarize and describe the measurement methodology.

6.1.2.1 Probe Waveform and NLTF Specification Measurement

Sinusoidal steady state probe waveforms will be used to measure the third and fifth rusty bolt harmonic and the third order intermodulation. The intermodulation measurement will be performed with equal level signal sources.

6.1.2.2 System Dynamic Range and Transmitted Power

Transmitter signal sources with a maximum power of 50 W (47 dBm) in the UHF range 225 to 400 MHz will be used. The receiver will be tunable and highly sensitive -110 to -140 dBm. The maximum isolation required to avoid interferences in the measurement is at least 187 dB.

6.1.2.3 Rusty Bolt Identification and Model Validation

The rusty bolt harmonic and intermodulation measurements performed at a given set of frequencies will be used to identify the rusty bolt lumped parameter circuit linear transfer function (LTF) singularities, the equivalent antenna impedance and the combined constants of the Volterra NLTF's up to fifth order. The identified rusty bolt parameters will then be used to predict

harmonic and intermodulation at other frequencies. Measurements will then be performed at these frequencies and compared with the predicted results.

SECTION 7

CONCLUSIONS AND RECOMMENDATIONS

Lumped parameter nonlinear systems which can cause interference and degrade Air Force C³I systems were analyzed and identified. The nonlinear system features which are relevant to the EMC performance of equipments were identified in terms of nonlinear Volterra transfer functions. Particular emphasis was placed on the "rusty bolt" (Metal-Insulator-Metal junction) nonlinearity. This nonlinearity occurs in the coupling paths between co-located transmitters and receivers on board Air Force airplanes and can be a primary factor in limiting Air Force C³I systems performance. In addition to the rusty bolt, nonlinearities in transmitters and receivers contribute to the degradation of the EMC performance. Because of this, two different situations were treated in this report.

In the first, the output of the linear part of the system can be measured. In this case, a linear system identification technique, such as the pencil-of-functions method [Jain (1980)], can be used to identify the poles of the linear system based on the system's transient response. These poles then specify the NLTFs. A survey of linear system identification techniques was presented, criteria to be used in specifying the probe waveform were described, and the types of identification errors that can occur were described. A sensitivity analysis of the linear system function identification errors on the NLTFs and the EMC specification parameters, such as intermodulation and harmonic distortion, was performed.

The second case of interest is the identification of the rusty bolt. Because of the strong direct transmission between the transmitting and receiving antennas, the "rusty bolt" linear response cannot be measured directly. Under this condition, it

is necessary to estimate the poles of the LTF and NLTFs from sinusoidal steady state third order nonlinear response measurements. A lumped parameter circuit model of the rusty bolt and the corresponding NLTFs were derived. It was shown that sinusoidal steady state probing allows the separation of the responses of different orders and that it can be used to measure the frequency response of the third order nonlinear transfer function. Based on the rusty bolt circuit model and on the third order NLTF frequency response, the poles of the LTF can be identified. The rusty bolt NLTF specification parameter constants can then be determined from harmonic measurements. The errors that can be encountered in the identified parameters and the predicted EMC specification parameters were then examined. Finally, the measurement and instrumentation criteria to be used in the sinusoidal steady state identification of the rusty bolt were presented.

The results of the study indicate the following:

1. Mean squared error between measured output and the output of the identified system is a more reliable predictor of the errors in the NLTF specification parameters than errors in pole locations.
2. Global mean squared error cannot be used to predict the error in the specification parameters in all cases, specially when the number of poles is misidentified. Instead, an error criterion which is segmented in frequency should be used.
3. For the rusty bolt lumped parameter circuit and a MIM i-v characteristic up to fifth order, the EMC specification parameters up to fifth order can be predicted with good quality provided that the number of poles are identified correctly and that the errors in the estimates of the linear transfer function poles and the antenna impedance are reasonable (say less than 30 percent).

Based on the results of this effort it is recommended that the following topics be studied:

1. Develop and implement algorithms for the sinusoidal steady state poles and zeros identification techniques developed under this present contract and evaluate their performance in noise. The first technique uses magnitude measurements while the other technique uses phase measurements of a third order response to identify the poles and zeros.
2. Measure a MIM junction on a laboratory bench.
3. Identify and measure the nonlinear performance of the same MIM junction in an anechoic chamber. Predict the system nonlinear performance based on a lumped parameter circuit model and refine the model if necessary.
4. Upon successful identification of the rusty bolt and adequate prediction of the nonlinear system performance in step 3, perform identification on board an aircraft. A word of caution is in order. It should be noted that even if the results of step 3 indicate that a lumped parameter is adequate to represent a rusty bolt in anechoic chambers, the success of the experiment on board an aircraft is not guaranteed. The reason is that the aircraft rusty bolt will probably be of a distributed nature and the characteristics may be time varying. This would require the development of a distributed parameter (transmission line) rusty bolt nonlinear model and possibly time varying. Nevertheless, usefull information can be obtained by performing the experiment.

REFERENCES

- Arazm, Farrokh and Benson, Frank A., (1980) "Nonlinearities in Metal Contacts at Microwave Frequencies", IEEE Trans. on EMC, Vol. EMC-22, pp. 142-149, August 1980.
- Bedrosian, E. and Rice, S.O., (1971), "The Output Properties of Volterra Systems driven by Harmonic and Gaussian Inputs", Proc. IEEE, Vol. 59, No. 12, pp. 1688 to 1707, December 1971.
- Bohm, D., (1951), Quantum Theory, Prentice-Hall, Inc., Englewood Cliffs, NJ, 1951, p. 275.
- Bond, Clarence D., Guenzer, Charles S. and Carosella, Carmine A., (1979), "Intermodulation generation by Electron Tunneling through Aluminum-Oxide Films", Proc. IEEE, Vol. 67, No. 12, pp. 1643-1652, December 1979.
- Bor-Long, T.W.U. and Schwartz, S.E., (1974), "Mechanism and Properties of Point-Contact Metal-Insulator-Metal diode detectors at 10.6 μ ", Appl. Phys. LETT., Vol. 25, No. 10, November 1974.
- Bucker, H.P., (1977), "Comparison of FFT and Prony algorithms for bearing estimation of narrow-band signals in a realistic ocean environment", J. Acoust. Soc. Amer., Vol. 61, pp. 756-762, Mar. 1977.
- Busgang, J.J., Ehrman, L. and Graham, J.W., (1974), "Analysis of Nonlinear Systems with Multiple Inputs", Proc. IEEE, Vol. 62, pp. 1088-1119, August 1974.
- Chow, J.C., (1972), "On Estimating the orders of an autoregressive moving-average process with uncertain observations", IEEE Trans. Automat. Contr., Vol. AC-17, pp. 707-709, Oct. 1972.
- Chuang, C.W. and Moffatt, D.L., (1976), "Natural resonances of radar targets via Prony's method and target discrimination", IEEE Trans. Aerospace Electron, Syst., Vol. AES-12, pp. 583-589, Sept. 1976.
- Dudley, D.G., (1979), "Parametric modeling of transient electromagnetic systems", Radio Science, Vol. 14, No. 3, pp. 387-396, May-June 1979.

REFERENCES (Continued)

- Elchinger, G.M., Sanchez, A., Davis, C.F. and Javan, A., (1976), "Mechanism of Detection of Radiation in a High Speed Metal-Oxide-Metal Junction in the Visible Region and at Longer Wavelengths," J. Appl., Phys., Vol. 47, No. 2, February 1976.
- Ewen, E., (1975), "Black-Box Identification of Nonlinear Volterra Systems", Ph.D. Dissertation, Syracuse University, December 1975.
- Ewen, E., (1979), "Nonlinear System Identification Study", Parts 1 and 2, RADC Report RADC-TR-79-199, December 1979 and February 1980.
- Flemming, M.A., Mullins, F.H., Watson, A.W.D., (1977), "Harmonic Radar Detection Systems", IEE Radar Conference, London, England, October 1977.
- Forlani, F. and Minnaja, N., (1964), "Rectification by means of metal-dielectric-metal sandwiches", Nuovo Cimento, Vol. 31, pp. 1246-1257, March 1964.
- Friedlander, B., Morf, M., Kailath, T. and Ljung, L., (1979), "New inversion formulas for matrices classified in terms of their distance from Toeplitz matrices", Linear Algebra and Its Applications, Vol. 27, pp. 31-60, 1979.
- Graham, J.W. and Ehrman, L., (1973), "Nonlinear System Modeling and Analysis with Applications to Communication Receivers", RADC Report RADC-TR-73-178, June 1973.
- Jackson, L.B. et al., (1978), "Frequency estimation by linear prediction", 1978 Int. Conf. Acoustics, Speech and Signal Processing, pp. 352-356.
- Jackson, L.B. and Soong, F.K., (1978), "Observations on linear estimation", in Rec. 1978 IEEE Int. Conf. Acoustics, Speech, and Signal Processing, pp. 203-207.
- Jain, V.K., (1974), "Filter Analysis by Use of Pencil-of-Functions: Part I", IEEE Trans. Circuits and Systems, Vol. CAS-21, pp. 574-579, September 1974.
- Jain, V.K., (1980), "Advanced Techniques for Black Box Modeling", RADC Report TR-80-343, August 1980.

REFERENCES (Continued)

- Kay, S.M. and Marple, S.L., (1981), "Spectrum Analysis - A Modern Perspective", Proc. IEEE, Vol. 69, pp. 1380-1419, November 1981.
- McDonough, R.N., (1963), "Representations and analysis of signals, Part XV. Matched exponents for the representation of signals", Ph.D. dissertation, Dep. Elec. Eng., Johns Hopkins Univ., Baltimore, MD, Apr. 30, 1963.
- McDonough, R.N. and Huggins, W.H., (1968), "Best least-squares representation of signals by exponentials", IEEE Trans. Automat. Contr., Vol. AC-13, pp. 408-412, Aug. 1968.
- Mehra, R.K., (1974), "Optimal Inputs for Linear System Identification", IEEE Trans. Automatic Control, AC-19, pp. 192-200, June 1974.
- Mehra, R.K., (1976), "Frequency-Domain Synthesis of Optimal Inputs for Linear System Parameter Estimates", ASME Journal of Dynamic Systems, Measurement and Control, pp. 130-138, June 1976.
- Mehra, R.K. and Lainiotis, D.G., (1976), editors, "System Identification Advances and Case Studies", Academic Press, N.Y. 1976.
- Mittra R. and Pearson, L.W., (1978), "A variational method for efficient determination of SEM poles", IEEE Trans. Antennas Propagat., Vol. Ap. 26, pp. 354-358, Mar. 1978.
- Morf, M., (1974), "Fast algorithms for multivariable systems", Ph.D. dissertation, Stanford University, Stanford, VA, Dep. Elec. Eng., Aug. 1974.
- Morf, M., Kailath, T. and Ljung, L., (1976), "Fast algorithms for recursive identification", in Proc. 1976 IEEE Conf. Decision and Control (Clearwater, FL), Dec. 1-3, 1976, pp. 916-921.
- Morf, M., Dickinson, B., Kailath, T. and Vieira, A., (1977), "Efficient solution of covariance equations for linear prediction", IEEE Trans. Acoust., Speech, Signal Process., Vol. ASSP-25, pp. 429-433, Oct. 1977.
- Morf, M., Vieira, A. and Lee, D.T., (1977), "Ladder forms for identification and speech processing", in Proc. 1977 Conf. Decision and Control (New Orleans, LA), pp. 1074-1078, Dec. 1977.

REFERENCES (Continued)

- Morf, M., Vieira, A., Lee, D.T. and Kailath, T., (1978), "Recursive multichannel maximum entropy spectral estimation", IEEE Trans. Geosci. Electron., Vol. GE-16, pp. 85-94, Apr. 1978.
- Prado, G. and Moroney, P., (1978), "The application of linear predictive methods of spectral analysis to frequency estimation", in Rec. 1978 NAECON.
- Prado, G. and Moroney, P., (1978), "The accuracy of center frequency estimators using linear predictive methods", in Rec. 1978 IEEE Int. Conf. Acoustics, Speech and Signal Processing, pp. 361-364.
- Prony, G.R.B., (1795), "Essai experimental et analytique, etc.", Paris, J. de L'Ecole Polytechnique, Vol. 1, cahier 2, pp. 24-76, 1795.
- Rudko, M. and Bussgang, J.J., (1982), "Nonlinear System Identification Technique Validation", RADC Report TR-81-391, January 1982.
- Sankar, A., (1978), "A Prediction Model for Ship Generated Intermodulations", IEEE Conf. on EMC, 1978.
- Scahubert, D.H., (1979), "Application of Prony's method to time-domain reflectometer data and equivalent circuit synthesis", IEEE Trans. Antennas Propagat., Vol. AP-27, pp. 180-184, Mar. 1979.
- Shanmugan, K.S., Jong, M.T., (1975), "Identification on Nonlinear System in Frequency Domain", IEEE Trans. Aerospace and Electronic Systems, Vol. AES-11, pp. 1218-1225, November 1975.
- Simmons, John G., (1963), "Generalized Formula for the Electric Tunnel Effect Between Similar Electrodes Separated by a Thin Insulating Film", Journal Appl. Physics, Vol. 34, No. 6, June 1963.
- Uslenghi, P., (1980), editor, "Nonlinear Electromagnetics", Academic Press, pp. 303-341, New York, 1980.
- Van Blaricum, M.L. and Mittra, R., (1978), "Problems and solutions associated with Prony's method for processing transient data", IEEE Trans. Antennas Propagat., Vol. AP-26, pp. 174-182, Jan. 1978.

REFERENCES (Concluded)

- Van Blaricum, M.L., (1978), "A review of Prony's method techniques for parameter estimation"; in Proc. Rome Air Development Center Spectrum Estimation Workshop, Griffiss Air Force Base, May 24-26, 1978, pp. 125-139.
- Van Blaricum, M.L. and Mittra, R., (1980), Correction to "Problems and solutions associated with Prony's method for processing transient data", IEEE Trans. Antennas Propagat., Vol. AP-28, p. 949, Nov. 1980.
- Watson, A.W.D., (1980), "The Measurement, Detection, Location and Suppression of Exernal Nonlinearities which Affects Radio Systems", Conference on EMC, IERE, London, England, September 1980.
- Weiner, D.D. and Spina, J., (1980), "Sinusoidal Analysis and Modelling of Weakly Nonlinear Circuits", New York: Van Nostrand, 1980.

APPENDIX A

LINEAR IDENTIFICATION TECHNIQUES, AND A DFT-BASED
'RUSTY-BOLT' TESTING TECHNIQUE

BY: DR. V.K. JAIN

NOTE: The contents of this Appendix were developed under Contract F30602-82-C-0163 by Dr. V.K. Jain, a Consultant to SIGNATRON, Inc.

APPENDIX A
LINEAR IDENTIFICATION TECHNIQUES, AND A
DFT-BASED 'RUSTY BOLT' TESTING TECHNIQUE

A.1 INTRODUCTION

System identification technology is critical to the efficient characterization of networks and systems from test data. This appendix presents a summary of some carefully selected linear system identification (or black box modeling) techniques. A particularly interesting part of the appendix is a new discrete-Fourier-transform based technique which employs sinusoidal probing to estimate 'Rusyt-Bolt' linear TF from third harmonic measurement. This is necessary to avoid the influence of corrupting signals, for example the direct transmission signal which is a few orders of magnitude more dominant than the linear component of the RB.

A.2 LINEAR SYSTEM IDENTIFICATION PROBLEM

Linear system identification represents the most well developed area in the field of black-box modeling. Almost always the measured signals are in a sampled (digital) form, therefore it is usual to consider a model of the type $B(z)/A(z)$ where $B(z)$ and $A(z)$ are polynomials in the z -transform variable. In line with this convention, we will consider the problem of identification in discrete-time, even though the physical network under test may in fact be a continuous-time system. After a satisfactory model of this type is obtained, a z -domain to s -domain conversion is easily performed [Jain, et al., (1983); Jain (1980)] if desired.

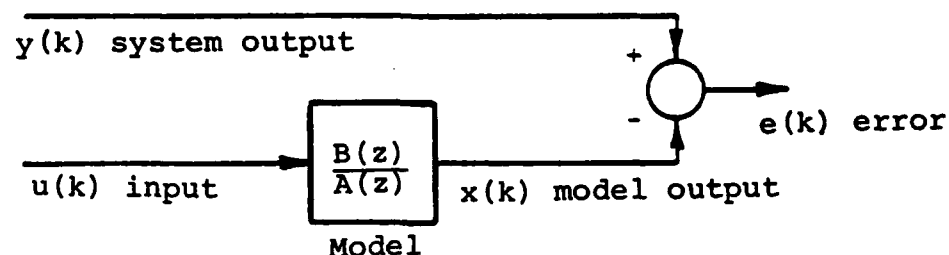


Figure A-1 Linear Identification Problem

The linear identification problem may be stated with the help of Figure A-1. The parameters of the model are to be found such that the error between the observed response and the model response (to the same input as applied to the test system), is minimized in some sense. Assuming the model order to be n , the model response is given by the difference equation

$$x(k) + a_1 x(k-1) + \dots + a_n x(k-n) = -[b_0 u(k) + b_1 u(k-1) + \dots + b_n u(k-n)] \quad (\text{A.1a})$$

or by the rational z-transfer function

$$\frac{X(z)}{U(z)} = \frac{b_0 + b_1 z^{-1} + \dots + b_n z^{-n}}{1 + a_1 z^{-1} + \dots + a_n z^{-n}}$$

$$\hat{=} \frac{B(z)}{A(z)} \quad (\text{A.1b})$$

From (A.1a) the model output can be written as

$$x(k) = -\underline{f}^T(k)\underline{\theta} \quad (\text{A.2a})$$

where the $(2n+1)$ dimensional vectors \underline{f} and $\underline{\theta}$ are defined as

$$\underline{f}(k) = [x(k-1) \dots x(k-n) \quad u(k) \quad u(k-1) \dots u(k-n)]^T \quad (\text{A.2b})$$

$$\underline{\theta} = [a_1 \quad \dots a_n \quad b_0 \quad b_1 \dots b_n]^T \quad (\text{A.2c})$$

for $k < n$. It is assumed that the data are observed for $k = 0, 1, \dots, K-1$.

A natural performance criterion is the sum-of-squares error (SSE)*

$$J = \sum_{k=n}^{K-1} [e(k)]^2 \quad (\text{A.3a})$$

$$= \sum_{k=n}^{K-1} [y(k) - x(k)]^2 \quad (\text{A.3b})$$

$$= \sum_{k=n}^{K-1} [y(k) + \underline{f}^T(k) \underline{\theta}]^2 \quad (\text{A.3c})$$

* The error $e(k)$ from $k=0$ to $k=n-1$ is misleading and is therefore not included in Equation (A.3).

Minimization of J , for instance by setting its gradient to zero, leads to a set of equations whereby the optimal parameters can be determined. Unfortunately, these equations are nonlinear and can only be solved by iterative means (even in the noiseless case). There are however methods in which the actual SSE is not directly minimized; rather, a related error is minimized, and the solution becomes relatively simple.

Three solutions will be given below. These are

1. Equation error method
2. Quasi-linearization method
3. Pencil-of-functions method.

The first technique minimizes the equation error, the second minimizes the true error, and the third minimizes the error in the approximation of the observed output by a novel set of basis functions.

A.3 IDENTIFICATION TECHNIQUES

A.3.1 Equation Error Method

Instead of minimizing the sum of squares of the output error e , the sum-of-squares of the equation error (SSEE)

$$J_{\epsilon} = \sum_{k=n}^{K-1} \epsilon^2(k) \quad (\text{A.4a})$$

is minimized where

$$\epsilon(k) = y(k) + a_1 y(k-1) + \dots + a_n y(k-n) + b_0 u(k) + \dots + b_n u(k-n) \quad (\text{A.4b})$$

The equation error $\epsilon(k)$ is related to $e(k)$ as shown in Figure A-2(a) or equivalently as in Figure A-2(b).

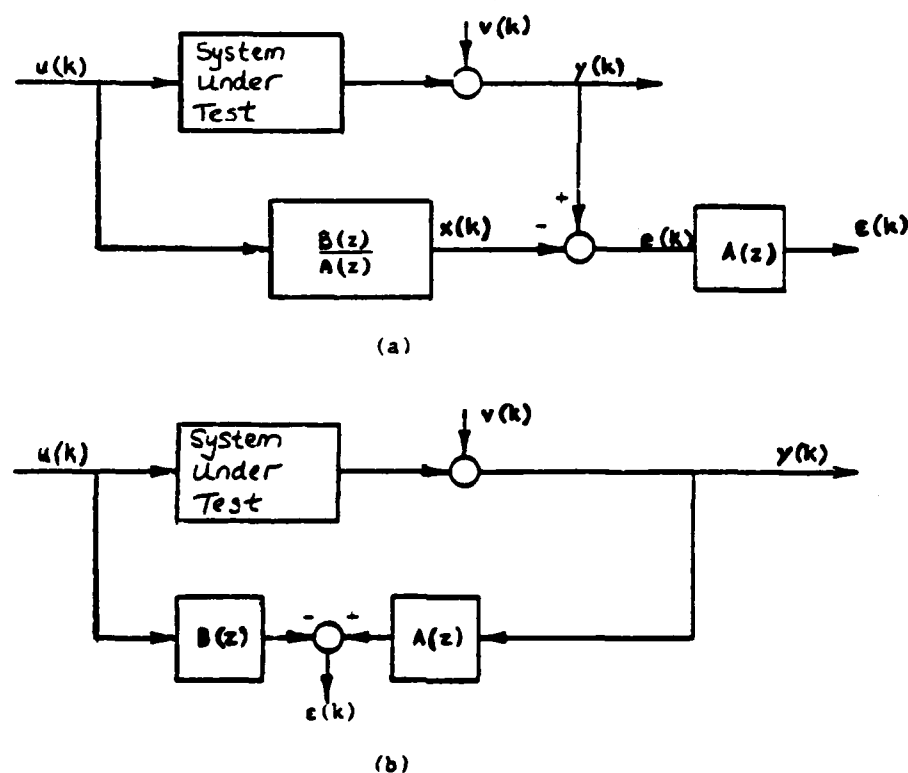


Figure A-2 Definition of the equation error

Minimization of the SSEE with respect to $\underline{\theta}$ straightforwardly yields the solution

$$\underline{\theta} = (F^T F)^{-1} F^T \underline{y} \quad (A.5a)$$

where

$$\underline{y} = [y(n) \dots \dots \dots y(K-1)]^T \quad (A.5b)$$

and

$$F = \begin{bmatrix} -y(n) & -y(n-1) & \dots & -y(1) & u(n) & u(n-1) & \dots & u(0) \\ -y(n+1) & -y(n) & \dots & -y(2) & u(n+1) & u(n) & \dots & u(1) \\ \cdot & & & \cdot & \cdot & & & \cdot \\ \cdot & & & \cdot & \cdot & & & \cdot \\ \cdot & & & \cdot & \cdot & & & \cdot \\ -y(K-1) & -y(K-2) & \dots & -y(K-n) & u(K) & \dots & \dots & u(K-n) \end{bmatrix} \quad (A.5c)$$

Thus identification is completed by the inversion of a $(2n+1)$ dimensional square matrix. In the absence of noise, or at very low levels of noise (say SNR = 50 dB or higher), good results can be obtained if the assumed system order is reasonable. A flow-chart of the method is given in Figure A-3.

At practical noise levels, the true output error must be minimized to achieve reasonable results; an iterative method for this is discussed next.

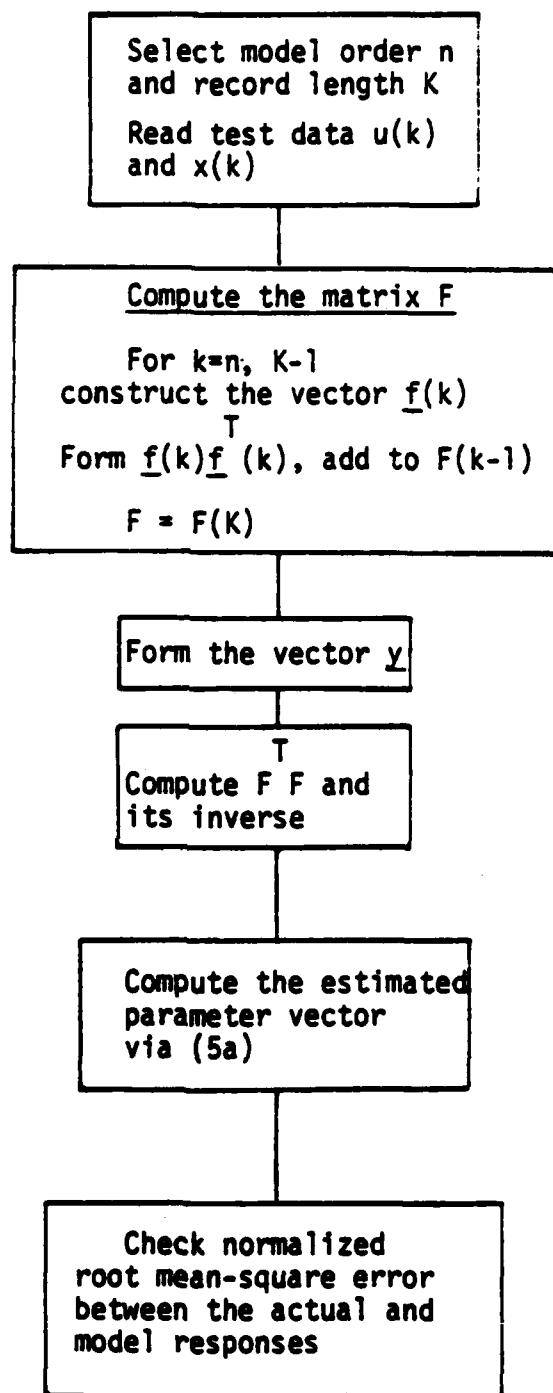


Figure A-3 Flowchart for implementation of the equation-error method

A.3.2 Quasi-Linearization Method [Cadzow (1976)]

This method is based upon the fact that the model output is a function of the model parameters. That is, $x(k) = x(k; \underline{\theta})$. Suppose that $\tilde{\underline{\theta}}$ denotes the initial guess (or current estimate) of the model parameters. Then, expanding $x(k)$ in a Taylor series about $\tilde{\underline{\theta}}$ and retaining only the first two terms gives

$$x(k) = \tilde{x}(k) + \underline{s}^T(k) (\underline{\theta} - \tilde{\underline{\theta}}) \quad (\text{A.6a})$$

where

$$\tilde{x}(k) = x(k; \tilde{\underline{\theta}}),$$

$$\underline{s}(k) = \underline{s}(k) \Big|_{\underline{\theta} = \tilde{\underline{\theta}}} \quad (\text{A.6b})$$

and

$$\underline{s}(k) = \frac{\partial x(k, \underline{\theta})}{\partial \underline{\theta}} \quad (\text{A.6c})$$

Substituting into (A.3b) and setting the gradient with respect to $\underline{\theta}$ to zero gives the update equation

$$\underline{\theta} = \tilde{\underline{\theta}} - \alpha \tilde{P}^{-1} \tilde{q} \quad (\text{A.7a})$$

where

$$\tilde{P} = \sum_{k=n+1}^K \underline{\tilde{s}}(k) \underline{\tilde{s}}^T(k) \quad (A.7b)$$

and

$$\tilde{q} = \sum_{k=n+1}^K \underline{\tilde{s}}(k) [y(k) - \tilde{x}(k)] \quad (A.7c)$$

Computation of the Sensitivity Matrix

To obtain the sensitivity vector let us examine the model equation (A.1a) closely:

$$x(k) = - \sum_{i=1}^n a_i x(k-i) - \sum_{i=0}^n b_i u(k-i) \quad (A.8)$$

The entries of $\underline{s}(k)$ consist of two types; rows 1 through n consist of partial derivatives with respect to a_i , and rows n+1 through 2n+1 consist of derivatives with respect to b_i . These entries can be computed as follows:

$$p_i(k) = \partial x(k) / \partial a_i \quad .$$

These $p_i(k)$ can be computed by solving the difference equation obtained by differentiating (A.8) with respect to a_i :

$$p_i(k) = - \sum_{j=1}^n a_j p_i(k-j) - x(k-i) \quad (\text{A.9a})$$

Note that $p_i(k) = p_1(k-i+1)$. This observation together with (A.9a) suggest the block diagram of Figure A-4(a) for the computation of $p_i(k)$.

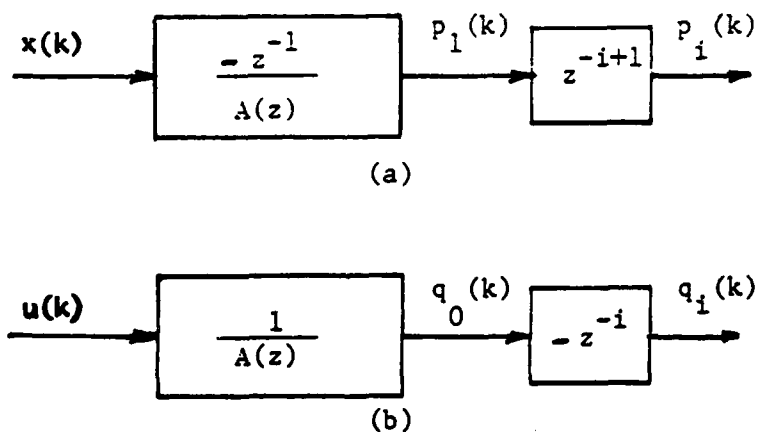


Figure A-4 Computation of the sensitivity vector

$$q_i(k) = \partial x(k) / \partial b_i \quad .$$

These $q_i(k)$ can be computed by solving the difference equation obtained by differentiating (A.8) with respect to b_i :

$$q_i(k) = - \sum_{j=1}^n a_j q_i(k-j) - u(k-i) \quad . \quad (A.9b)$$

Note that $q_i(k) = q_0(k-i)$. This observation together with (A.9b) suggests the block diagram of Figure A-4(b) for the computation of $q_i(k)$.

Both Equations (A.9a) and (A.9b) are solved with zero initial conditions. Also, in actuality, $\tilde{A}(z)$ is used in place of $A(z)$ and $\tilde{x}(k)$ in place of $x(k)$ in Figure A-4 so that the entries of $\underline{s}(k)$ are evaluated.

The method is quite robust to noise in the measured data. However like most iterative methods, convergence to the correct solution is not assured and is critically dependent on (a) the initial guess for the parameter vector, and (b) proper selection of the step size α at each iteration. Frequently, the equation-error method is first used to yield a parameter vector that is used as an initial guess for the quasi-linearization method. We also remark that the method is also known by the name 'Modified Newton-Raphson method for system identification'. A flowchart of the method is given in Figure A-5.

Next we discuss what may be considered as an advanced method. It uses a set of refined basis functions for the identification procedure. The method is the pencil-of-functions method. It is robust to additive noise in measured data, and is non-iterative and therefore computationally efficient.

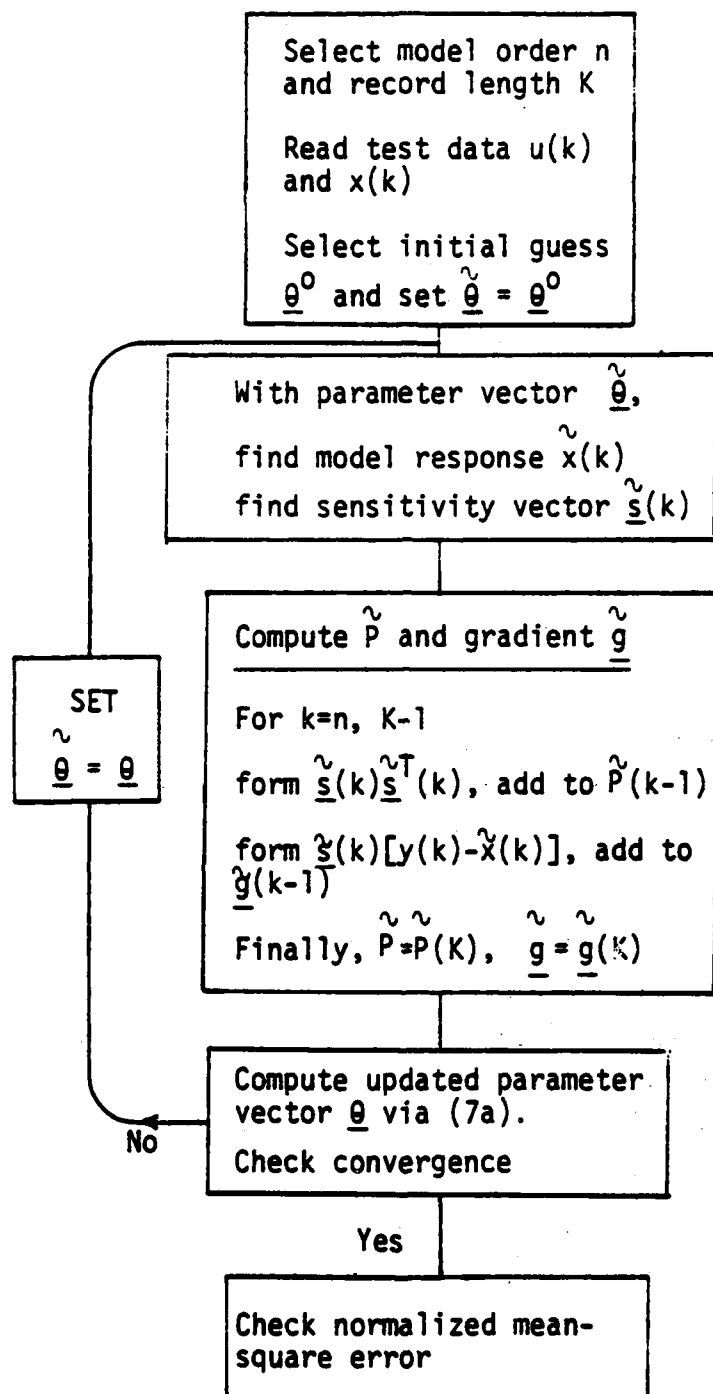


Figure A-5 Flowchart for implementation of the quasi-linearization method

**A.3.3 Pencil-of-Functions Method [Jain et al., (1983);
Jain (1980)]**

The pencil-of-functions technique is best explained by means of Figure A-6. The measured input and response signals (of the network under test) are impressed upon the two identical cascades of filters as shown. The transfer function of each of the processing filters is $Q(z) = 1/(1-qz^{-1})$, where the pole q lies between -1 and 1 . More will be said about its selection later.

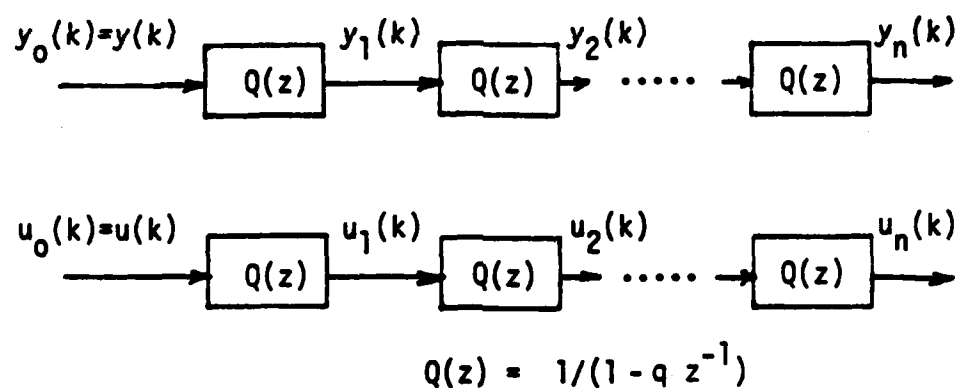


Figure A-6 Generation of information signals

The signals generated at the nodes of the cascades are called information signals. Their Gram matrix is defined as

$$F = \sum_{k=0}^{K-1} \underline{f}(k) \underline{f}^T(k) \quad (\text{A.10a})$$

where

$$\underline{f}(k) = [y_0(k) \dots y_n(k) \quad u_0(k) \dots u_n(k)]^T \quad (\text{A.10b})$$

Note that the vector \underline{f} is $(2n+2)$ dimensional, so that the matrix F is $(2n+2) \times (2n+2)$ dimensional and clearly symmetric. The information signals are generated by the first order recursive equations

$$y_i(k) = q y_i(k-1) + y_{i-1}(k), \quad y_i(K) = 0 \quad (\text{A.11a})$$

$$u_i(k) = q u_i(k-1) + u_{i-1}(k), \quad u_i(K) = 0 \quad (\text{A.11b})$$

The theoretical development of the method is somewhat involved and can be found in [Richmond, Jain (1983); Jain (1974)]. Here, we state the solution directly. The transfer function of the model is given by*

$$H(z) = \frac{\sum_{i=0}^n \sqrt{D_{n+1+i}} (1 - qz^{-1})^{n-i/D}}{\sum_{i=0}^n \sqrt{D_{i+1}} (1 - qz^{-1})^{n-i/D}} . \quad (\text{A.12})$$

The numbers D_i are the diagonal cofactors of the Gram matrix F of the information signals, and $D = \sqrt{D_1} + \dots + \sqrt{D_{n+1}}$. Remarks:

- The pole q determines the type of information, or basis, signals generated. If the network under test is primarily lowpass (compared to the sampling frequency), then a value between 0 and 1 is desirable. Note that the approximate -3 dB frequency of the processing filters is then given by $\ln(1/q)/T$ Radians/s where T denotes the sampling interval.
- In the absence of noise the model coincides with the true system function if the system is indeed linear, rational and if the model order equals the true order.
- When the data are noisy, a noise correction procedure may be applied as described in [Richmond, Jain (1983)].

* Equation (A.12) assumes that the term b_0 in Equation (A.1b) is not zero; when $b_0 = 0$, then Equation (A.12) should be modified slightly to include a z^{-1} term in the numerator [Richmond, Jain (1983)].

A flowchart of the implementation of the method is given in Figure A-7. A complete user oriented program can be found in [Jain, et al., (1983)].

A.4 A HIGH ACCURACY DFT-BASED TONE TESTING TECHNIQUE

A high accuracy tone testing technique is developed here. This method will be shown to be particularly suited for the rusty-bolt modeling problem. The primary reference for this is a paper by Jain et al. (1979) which permits high accuracy measurement of single and multiple tones, even in the presence of noise. The technique gives values of frequency, amplitude and phase of each sinusoid.

The key formulas are given here only for the single sinusoid case: for the multi-tone case one may refer to [Jain, et al., (1979)]. Suppose the tone is

$$x(t) = A_1 \sin(2\pi f_1 t + \phi_1) \quad (\text{A.13a})$$

and its sampled values

$$x(kT) = A_1 \sin(2\pi f_1 kT + \phi_1), \quad k = 0, 1, \dots, K-1 \quad (\text{A.13b})$$

where we have taken the time reference ($t=0$) to be the instant of the first sample. It is convenient to rewrite (A.13b) as

$$x_k = A_1 \sin\left(\frac{2\pi}{K} \lambda k + \phi_1\right) \quad (\text{A.13c})$$

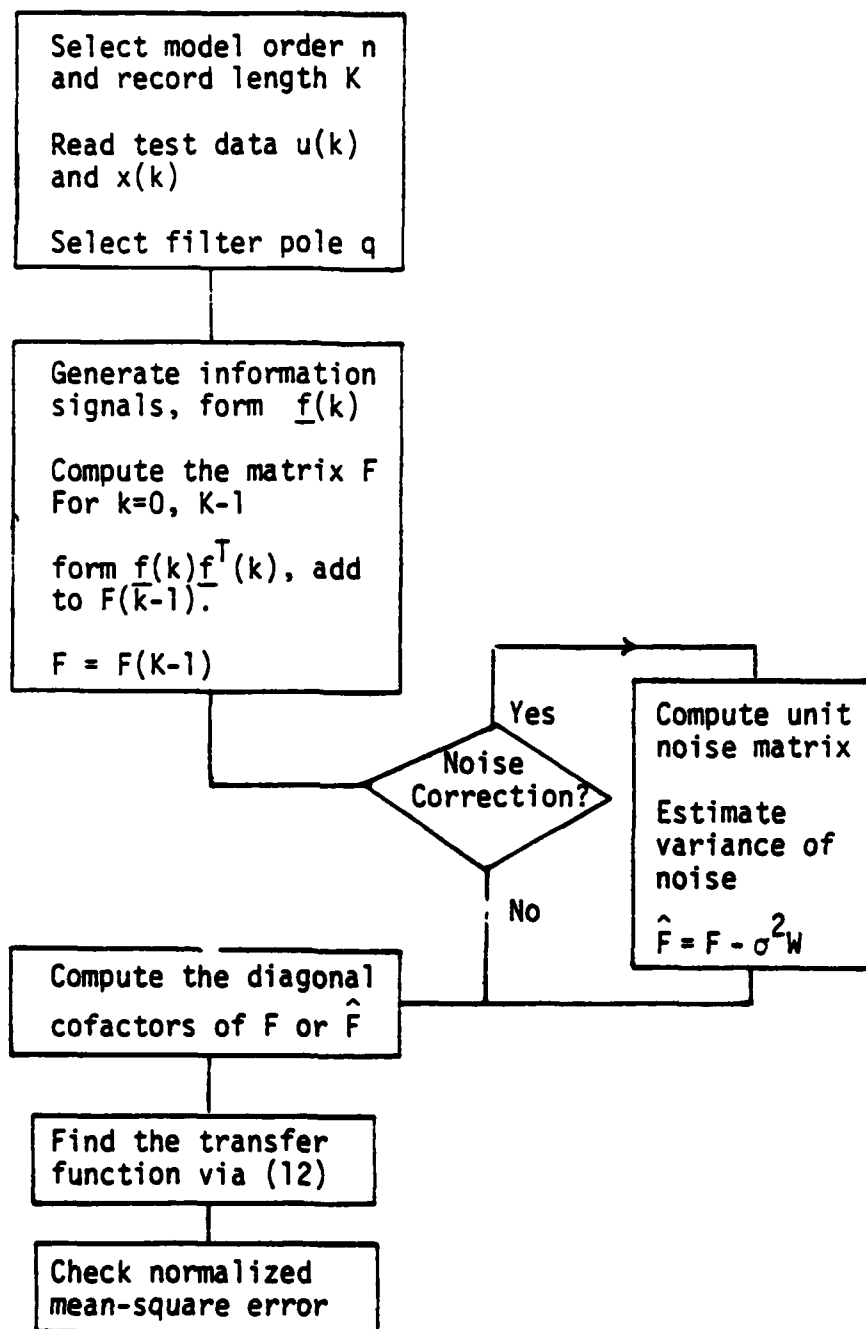


Figure A-7 Flowchart for the implementation of pencil-of-functions method

where

$$\lambda = f_1/f_0 = \ell + \delta \quad (\text{A.13d})$$

Here $f_0 = 1/KT$ is the frequency resolution of the DFT and $\ell = \lfloor \lambda \rfloor$, i.e., ℓ is the truncated integer value of λ (note that $0 \leq \delta < 1$).

A typical value of K for high accuracy measurement is $2048 = 2^{11}$. Also, the sampling interval is so chosen that all frequencies of interest lie between bin 10 and 100 (so that 10 to 100 cycles of each of the sinusoids is encompassed in the data).

The steps involved in the computation of high accuracy values are the following:

Step 1

Compute the discrete Fourier transform (DFT) via the fast algorithmic version (FFT). Recall that the definition of the DFT is

$$X(m) = \sum_{k=0}^{K-1} x_k e^{-j \frac{2\pi}{K} km} \quad (\text{A.14a})$$

In general, the DFT values are complex. Convert them to polar form

$$X(m) = S(m) e^{j\alpha_m} \quad (\text{A.14b})$$

Step 2

The largest two values of the magnitude DFT are detected. These values will be found to be consecutive, $S(l)$ and $S(l+1)$, and the signal frequency will be sandwiched between the frequencies lf_0 and $(l+1)f_0$.

The frequency is then computed as

$$\hat{\delta} = \frac{1}{1 + \frac{S(l)}{S(l+1)}} \quad (\text{A.15a})$$

$$\hat{f}_1 = (l + \hat{\delta})f_0 \quad (\text{A.15b})$$

Step 3

The amplitude and phase are next computed. If $S(l)$ is larger than $S(l+1)$, then (A.16a) is used, otherwise (A.16b) is used.

$$\hat{A}_1 = \frac{2\pi\hat{\delta}}{K} \frac{S(l)}{\sin \pi\hat{\delta}}, \quad \hat{\phi}_1 = \alpha_l - a\hat{\delta} + \frac{\pi}{2} \quad (\text{A.16a})$$

$$\hat{A}_1 = \frac{2(1-\hat{\delta})}{K} \frac{S(l+1)}{\sin \pi(1-\hat{\delta})}, \quad \hat{\phi}_1 = \alpha_{l+1} - a(\hat{\delta}-1) + \frac{\pi}{2} \quad (\text{A.16b})$$

where $a = \pi(K-1)/K$.

**A.5 ESTIMATION OF LINEAR TF OF 'RUSTY BOLT' BY TONE TESTING
(VIA THE DFT APPROACH OF SECTION A.4)**

It was shown in Section 4.2.2 of the main text that the estimation of the linear transfer function of the 'rusty-bolt' is complicated by the presence of the highly dominant direct transmission signal. The DFT approach is ideally suited here for sinusoidal measurements. Specifically, we will show that the linear transfer function may be computed from phase measurement at the third-harmonic frequency. The cases where the RB LTF is either a single pole or two-pole TF are discussed in detail.

Consider the block diagram of Figure A-8 where we have ignored the presence of fifth and higher order nonlinearities. Their presence, however, may be incorporated without complicating the procedure because of the resolvability of the DFT approach.

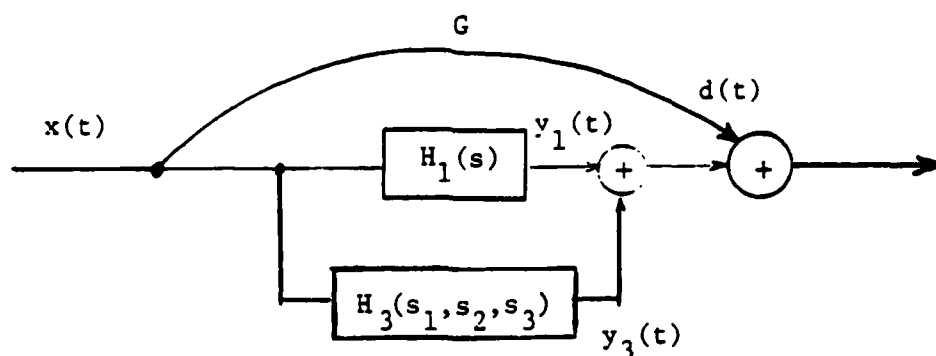


Figure A-8 Simplified diagram of the 'rusty-bolt'

Suppose the applied signal is

$$x(t) = A \cos(\Omega_1 t + \alpha) \quad (\text{A.17})$$

so that the overall response becomes

$$y(t) = d(t) + y_1(t) + y_3(t) \quad (\text{A.18})$$

Here, $d(t)$ is the direct transmission component, $y_1(t)$ is the linear response of the RB, and $y_3(t)$ is the third order response of the RB. The expressions for these components are given below:

$$d(t) = GA \cos(\Omega_1 t + \alpha) \quad (\text{A.19a})$$

$$y_1(t) = A |H_1(\Omega_1)| \cos(\Omega_1 t + \alpha + \phi_1) \quad (\text{A.19b})$$

$$y_3(t) = \frac{A^3}{4} \{ |H_3(\Omega_1, \Omega_1, -\Omega_1)| \cos(\Omega_1 t + \alpha + \phi_2) \\ + |H_3(\Omega_1, \Omega_1, \Omega_1)| \cos(3\Omega_1 t + 3\alpha + \phi_3) \} \quad (\text{A.19c})$$

where the phase angles ϕ_i , $i = 1, 2, 3$ are phases of the complex numbers within the modulus signs. Also note that

$$H_3(\omega_1, \omega_2, \omega_3) = \beta H(\omega_1) H(\omega_2) H(\omega_3) H(\omega_1 + \omega_2 + \omega_3) \quad (\text{A.20})$$

The third harmonic component is the second term in (A.19c) and will be denoted as $y_3'(t)$.

Using the DFT approach the following measurements can be made very accurately:

$$\Omega_1, A, \alpha \quad (\text{A.21a})$$

$$B_3' = \frac{A^3}{4} |H_3(\Omega_1, \Omega_1, \Omega_1)| \quad (\text{A.21b})$$

$$\phi_3' = 3\alpha + \phi_3 \quad (\text{A.21c})$$

Two cases are discussed below in detail, the single pole case and the two pole case. Of these, perhaps only the latter is useful from a practical standpoint.

Single Pole Case:

Only one test with a tone $A \cos(\Omega_1 t + \alpha)$ is required to be conducted. Let

$$H_1(s) = \frac{K}{(s+p)} \quad (A.22)$$

so that (A.21c) can be written explicitly as

$$\phi_3' = 3\alpha - 3 \operatorname{Arctan}(\Omega_1/p) - \operatorname{Arctan}(3\Omega_1/p) . \quad (A.23a)$$

Since α and ϕ_3' can be calculated by the DFT measurements on the input and output waveforms, we can solve for p . Even though (A.23a) is nonlinear, the solution is straightforward on the computer.

Now using (A.21b) we obtain

$$K^4 = 4B_3' |(j\Omega_1+p)^3 (j3\Omega_1+p)|/A^3 \quad (A.23b)$$

so that βK^4 , or $(\beta)^{1/4}K$, can be computed. Clearly, K cannot be computed separately. However, in the prediction of third order effects, we actually need K^4 . With this observation in mind, the estimation of $H_1(s)$ is now complete.

Two-Pole Case:

Let

$$H_1(s) = \frac{K(s+q)}{(s+p_1)(s+p_2)} \quad (\text{A.24})$$

Three tests are conducted, each with a single-tone input, as listed below:

Test	Input	Computed Quantities
1	$A \cos(\Omega_1 t + \alpha_1)$	$\phi_3'(1), B_3'(1)$
2	$A \cos(\Omega_2 t + \alpha_2)$	$\phi_3'(2)$
3	$A \cos(\Omega_3 t + \alpha_3)$	$\phi_3'(3)$

Then from (A.21c) we have

$$\begin{aligned} \phi_3'(i) = & 3\alpha_i + 3 \operatorname{Arctan}(\Omega_i/q) - 3 \operatorname{Arctan}(\Omega_i/p_1) \\ & - 3 \operatorname{Arctan}(\Omega_i/p_2) + \operatorname{Arctan}(3\Omega_i/q) \quad (\text{A.25}) \\ & - \operatorname{Arctan}(3\Omega_i/p_1) - \operatorname{Arctan}(3\Omega_i/p_2), \quad i = 1, 2, 3 \end{aligned}$$

These three equations can be solved for q , p_1 and p_2 . Finally, βK^4 can be determined from (A.21b) and $B_3'(1)$.

APPENDIX A
REFERENCES

- V.K. Jain, A.M. Bush, and D.J. Kenneally, "Volterra transfer from pulse tests for mildly nonlinear channels", RADC-TR-83-157, July, 1983.
- C. Richmond, and V.K. Jain, "System modeling by digital signal processing", Proc. Intntl. Conf. on ASSP, 1983.
- V.K. Jain "Advanced techniques for black-box modeling", RADC-TR-80-343, November 1980.
- V.K. Jain, W. Collins, and D. Davis, "High accuracy analog measurements via Interpolated FFT", IEEE Trans. IM, June 1979.
- J.A. Cadzow, "Recursive digital filter synthesis via gradient based algorithm", IEEE Trans. ASSP, pp. 349-355, October 1976.
- V.K. Jain, "Filter analysis by pencil-of-functions method", IEEE Trans. CT., pp. 574-579, September 1974.

APPENDIX B

**THE ELECTRIC TUNNELING EFFECT AND PROPERTIES
OF A METAL-INSULATOR-METAL (MIM) JUNCTION**

APPENDIX B

THE ELECTRIC TUNNELING EFFECT AND PROPERTIES OF A METAL-INSULATOR-METAL (MIM) JUNCTION

B.1 THE ELECTRIC TUNNELING EFFECT

The theory of electronic tunneling through an insulating layer goes back to the early 1930's. However, up to the present time there is no general agreement regarding the correct form of the tunneling equation for thin insulating films ($< 50 \text{ \AA}$). Some of the problems include the following [Bond, et al., 1979]:

1. The applicability of parameters such as the dielectric constant (which is a macroscopic parameter) to a few atomic layers.
2. Accurate evaluation of contaminant effects on the electron scattering surfaces.
3. Integral expression which can presently only be solved with approximations.

The equilibrium conditions for two metallic conductors separated by a thin insulator film (MIM junction) require that the top of the energy gap of the insulator be positioned above the Fermi level of the conductors. The insulating film introduces a potential barrier between the two metals which interferes with the flow of electrons between the two metal conductors. There are two conditions for which an electric current can flow through the insulator film between the two metal conductors, namely:

1. The electrons in the metals have enough thermal energy to surmount the potential barrier and flow in the conduction band.
2. The barrier is thin enough to permit its penetration by the electric tunnel effect. (In other words, if a particle (electron) with energy E is incident on a thin energy barrier of height greater than E , there is a finite probability of a particle penetrating the barrier).

Simmons [1963] conducted an analysis of the above two conditions for low temperature conditions under which the thermal current can be neglected, thus restricting the current flow between the two metals to the tunnel effect.

The probability $P(E_x)$ that an electron can penetrate a potential barrier height $V(x)$, as shown in Figure B-1, is approximately given by Bohm [1951]

$$P(E_x) = \exp \left\{ \frac{4\pi}{h} \int_{s_1}^{s_2} [2m(V(x) - E_x)]^{1/2} dx \right\} \quad (B.1)$$

where

m = mass of electron

h = Planck's constant

$V(x)$ = potential barrier height

E_x = $\frac{mv_x^2}{2}$ energy component of the incident electron in the x direction.

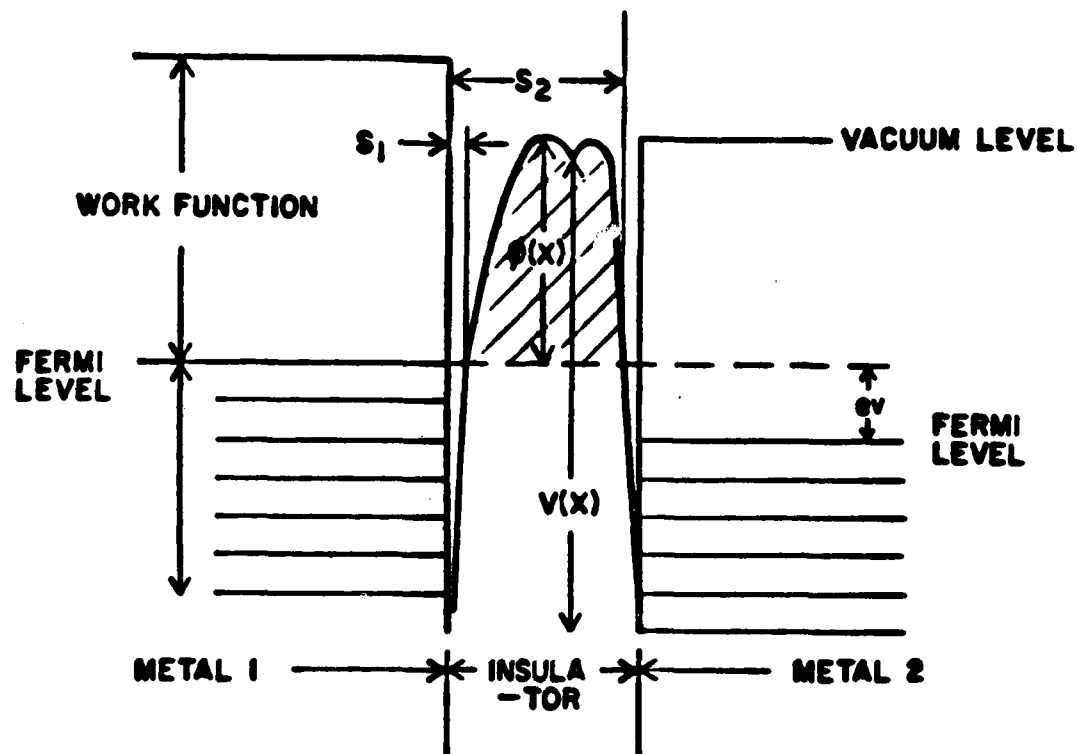


FIGURE B-1 GENERAL BARRIER IN INSULATION FILM BETWEEN TWO METAL CONDUCTORS

s_1, s_2 = limits of barrier at Fermi level.

The number of electrons N_1 tunneling from metal 1 to metal 2 is given by

$$N_1 = \int_0^{v_m} v_x n(v_x) p(E_x) dv_x = \frac{1}{m} \int_0^{E_m} n(v_x) P(E_x) dE_x \quad (B.2)$$

where E_m is the maximum energy of electrons in the metal and $n(v_x)dv_x$ is the number of electrons per unit volume with a velocity between v_x and $v_x + dv_x$. The number of electrons tunneling from metal 2 to metal 1 can be determined in a similar manner since the probability $P(E_x)$ is the same in either direction. If we assume that metal 2 is at a positive potential V with respect to metal 1 then the net electron flow through the barrier is given by $N = N_2 - N_1$.

Simmons [1963] derived the following current-voltage relationship for the generalized barrier

$$J = J_0 \{ \bar{\phi} \exp(-A\bar{\phi}^{1/2}) - (\bar{\phi} + eV) \exp[-A(\bar{\phi} + eV)^{1/2}] \} \quad (B.3)$$

where

$$J_0 = \frac{e}{2\pi h \Delta S^2}$$

$$A = \left(\frac{4\pi \Delta S}{h} \right) \sqrt{2m}$$

$$\bar{\phi} = \frac{1}{\Delta s} \int_{s_1}^{s_2} \phi(x) dx.$$

and

- J = tunnel current density
- e = charge of electron
- $\bar{\phi}$ = mean barrier height
- s_1, s_2 = limits of barrier at Fermi level
- Δs = $s_2 - s_1$
- m = mass of electron
- V = voltage across insulating film
- h = Planck's constant.

The interpretation of the above equation is that a current density $J_0 \bar{\phi} \exp[-A\bar{\phi}^{1/2}]$ (first term) flows from metal 1 to metal 2 and the second term in the above equation is a current density flowing from metal 2 to metal 1 which results in a net current density J . The current-voltage characteristics can be obtained by integrating the current density. The mean potential barrier height will be a function of the insulator (dielectric constant).

The current-voltage characteristics for metal-to-metal junctions may be approximated (Sankar [1978]) as

$$i = \alpha [\exp(\beta_1 V) - \exp(-\beta_2 V)] \quad (\text{B.4})$$

where α , β_1 and β_2 are the characteristic constants of a particular nonlinear junction. When the nonlinear current-voltage characteristic is symmetrical, then $\beta_1 = \beta_2$.

B.2 PROPERTIES OF THE METAL JUNCTION NONLINEARITY

There have been many investigations carried out by measurement of the properties of the metal junction nonlinearity. Watson [1980] measured harmonic and intermodulation products generated by metal-to-metal and carbon fibre junctions, in structures irradiated by radio transmitters at HF, VHF and microwave frequencies. He found that except for very high incident power where saturation and higher order effects occur, the results of very many measurements of backscatter power show that for external nonlinearities, the power law of a given harmonic or intermodulation product is the same as the order of that product. This implies that a small-signal nonlinear model, such as provided by a Volterra series, can be applied. This is not necessarily the case for nonlinear products that are generated internally in transmitters and receivers. Another interesting result is the fact that measurements of harmonic generation for metal junctions show significant temporal variations even when the junctions are stationary.

The average power of the received harmonics or intermodulation products is given by the back-scatter equations (Watson [1980])

$$P_r(nf_t) = \frac{\left[\frac{P_t G_t}{4\pi R_t^2}\right]^n \sigma_n G_r \lambda_r^2}{(4\pi)^2 R_r^2} \quad (B.5)$$

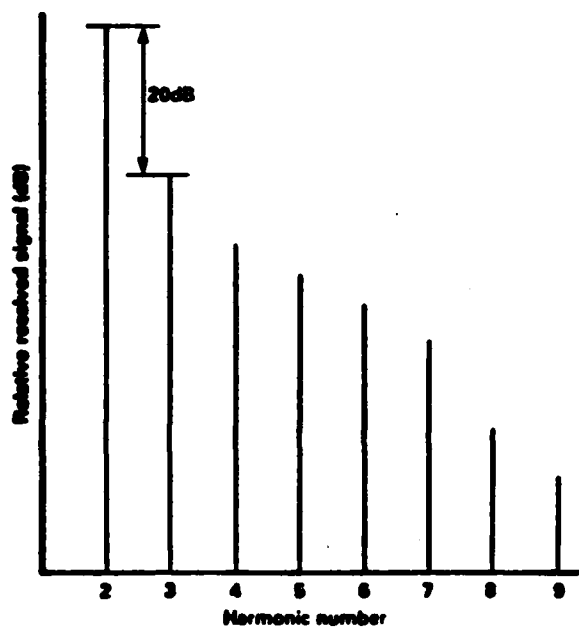
$$P_r(nf_{t_1} \pm mf_{t_2}) = \frac{\left[\frac{P_{t1} G_{t1}}{4\pi R_{t1}^2}\right]^n \left[\frac{P_{t2} G_{t2}}{4\pi R_{t2}^2}\right]^m \sigma_{n,m} G_r \lambda_r^2}{(4\pi)^2 R_r^2} \quad (B.6)$$

where

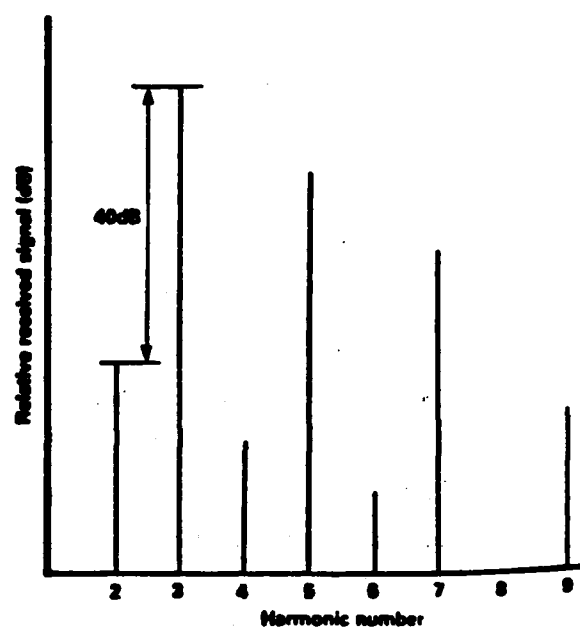
$P_r(nf_t)$	=	power of the received harmonic
P_t	=	transmitter power
G_t	=	transmitter aerial gain
G_r	=	received aerial gain
λ_r	=	receiving wavelength
n,m	=	the power law
$\sigma_{n,m}$	=	harmonic cross section.

The subscripts 1 and 2 refer to the parameters of transmitter 1 and transmitter 2.

Flemming et al., [1977] used harmonic radar detection to locate nonlinear metallic junctions. For a metal junction to be observable as a harmonic target it must receive the incident radiation in such a way that a voltage is generated across the nonlinear junction. The nonlinearity produces currents at harmonic frequencies which transmit the signals to the receiver. The rusty bolt nonlinearity, therefore, may be considered as three parts: a receiving aperture, a nonlinear element and a re-radiating aperture (antenna). Spectra measured by Flemming et al., using semi-conductor and metallic targets are shown in Figure B-2. Notice the suppression of even harmonics in the case of the metallic target. This is because a typical metal junction has almost symmetrical transfer characteristics; that is, electrical conduction is equal in either direction. When a power series approximation is used, the symmetrical characteristic will contain only odd-order terms.



(a) Semi-conductor target



(b) Metallic target

(From Flemming et al., (1977))

Figure B-2 Measured Harmonic Spectra

Watson and Flemming et al., have derived harmonic and intermodulation backscatter equations that could be used to predict intermodulation interference at given communications platform sites, but these cannot be used in practice because they predict received power for individual junctions. In general there will be many contributing junctions on a site and therefore the ranges between the target and the transmitting and receiving antennas will be indeterminate. Furthermore many junctions may be in the near field because of the electronically dense platforms. Watson has suggested an alternative way of quantifying the nonlinearity of a site in the form of relative levels of the fundamental and the harmonics or intermodulation products in terms of a coupled network, i.e.,

$$\frac{P_r(nf_1)}{P_r(f_1)} = \left[\frac{S_{21}(nf_1)}{S_{21}} \right]^2 P_t^{n-1} \quad (B.7)$$

where

$P_r(nf_1)$ = the power of the received harmonic

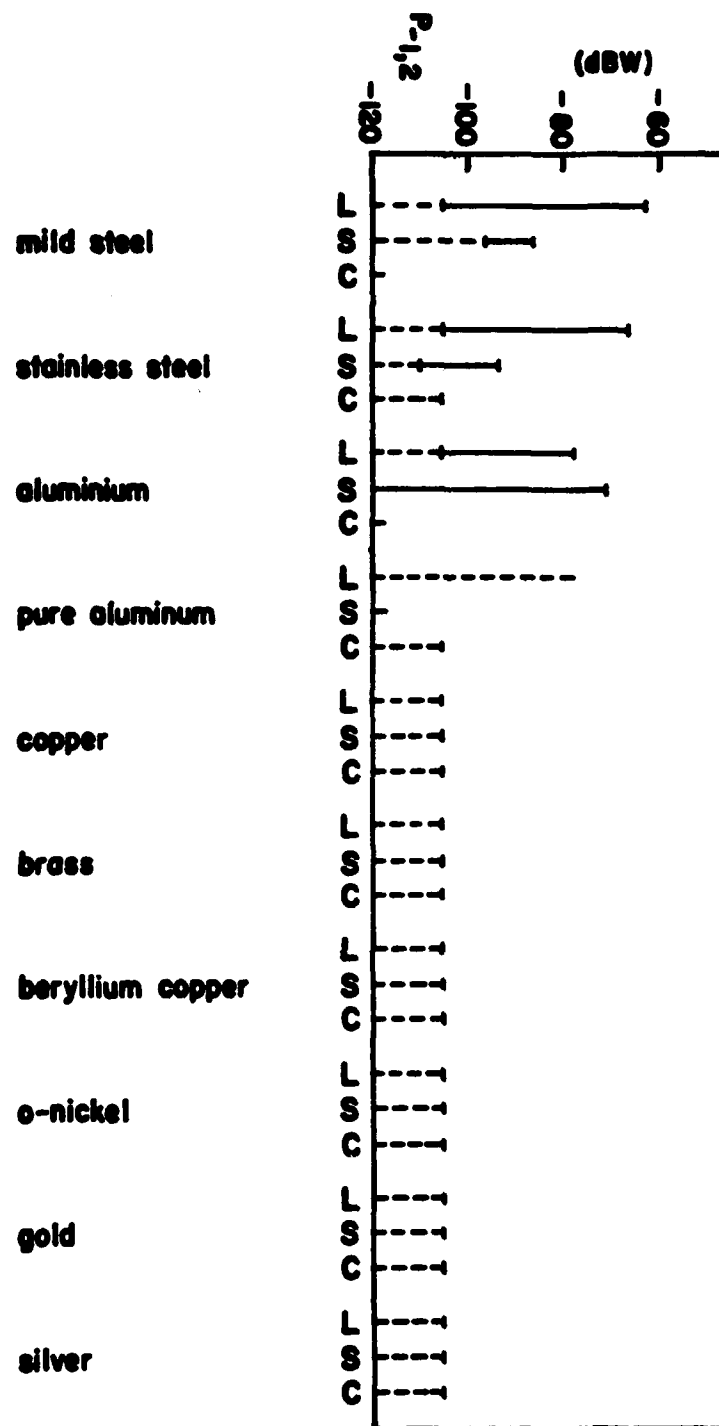
P_t = the transmitter power

$S_{21}(nf_1)$ = S parameter describing the overall harmonic coupling between transmitter and receiver due to a fundamental transmission.

S_{21} = conventional S parameter describing the fundamental frequency coupling between transmitter and receiver.

There were no indications of frequency dependencies for harmonic generation of actual junctions over the frequency ranges measured by Watson. However the size of the structure was important. Harmonic re-radiation decreased rapidly if the length of the structure is less than a quarter wavelength of the irradiation frequency.

Arazm and Benson [1980] published results that show some frequency dependence for the third order intermodulation products generated by contacting faces between similar metals. Their results are shown in Figure B-3.



$P_{in} = 3.2 \text{ W}$;
 $S = 10.65 \text{ N}$;
 Residual level = 106 dBW;
 O-nickel = oxygen-free nickel.

L = center frequency around 1.5 GHz;
 S = center frequency around 3 GHz;
 C = center frequency around 6 GHz;

Figure B-3 Relative amplitudes of 3rd-order IP at center frequencies around 1.5, 3 and 6 GHz.
 (from Arazm and Benson, 1980)

APPENDIX B
REFERENCES

- Arazm, Farrokh and Benson, Frank A., (1980), "Nonlinearities in Metal Contacts at Microwave Frequencies", IEEE Trans. on EMC, Vol. EMC-22, pp. 142-149, August 1980.
- Bohm, D., (1951), Quantum Therory, Prentice-Hall, Inc., Englewood Cliffs, NJ, 1951, p. 275.
- Bond, Clarence D., Guenzer, Charles S. and Carosella, Carmine A., (1979), "Intermodulation generation by Electron Tunneling through Aluminum-Oxide Films", Proc. IEEE, Vol. 67, No. 10, November 1974.
- Flemming, M.A., Mullins, F.H., Watson, A.W.D., (1977) "Harmonic Radar Detection Systems", IEEE Radar Conference, London, England, October 1977.
- Sankar, A., (1978), "A Prediction Model for Ship Generated Intermodulations", IEEE Conference on EMC, 1978.
- Simmons, John G., (1963), "Generalized Formula for the Electric Tunnel Effect Between Similar Electrodes Separated by a Thin Insulating Film", Journal Appl. Physics, Vol. 34, No. 6, June 1963.
- Watson, A.W.D., (1980), "The Measurement, Detection, Location and Suppresion of External Nonlinearities which Affects Radio Systems", Conference on EMC, IEEE, London, England, September 1980.

APPENDIX C

VOLTERRA TRANSFER FUNCTIONS FOR A "RUSTY BOLT" EQUIVALENT CIRCUIT

APPENDIX C

VOLTERRA TRANSFER FUNCTIONS FOR A "RUSTY BOLT" EQUIVALENT CIRCUIT

C.1 "RUSTY BOLT" MODELING

Some authors think of the "rusty bolt" (MIM junction) as a pair of back-to-back diodes with an antenna system as shown in Figure C-1. The i - v relationship of the back-to-back diode pair is then approximated as:

$$i_d = k_1 v_d + k_3 v_d^3 \quad (C.1)$$

thus neglecting nonlinear capacitive effects [Uslenghi (1980)]. Values are given to the constants k_1 and k_2 to match the computed and measured results. Still other authors define some ideal nonlinear element, usually memoryless, without any reference to any real existing device.

A commonly accepted and more sophisticated lumped parameter equivalent circuit for a MIM junction (rusty bolt) which was used by Long and Schwartz (1974) is shown in Figure C-2. An antenna and a shunting capacitance apply an a.c. voltage across a nonlinear resistor. The antenna is represented by its Thevenin equivalent impedance Z_a . The junction is modeled by a junction resistance r_d in series with a parallel combination of a junction capacitance impedance Z_c and a circuit element with nonlinear current characteristic $i_r(v)$. The capacitance is considered to be linear. This is not unreasonable since measurements by Bond et al. (1979), on $Al-Al_2O_3-Al$ junctions showed no measurable

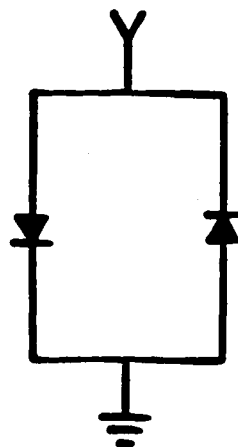


Figure C-1 Back-to-Back Diode Pair with an Antenna System which Represent a Symmetrical Nonlinearity.

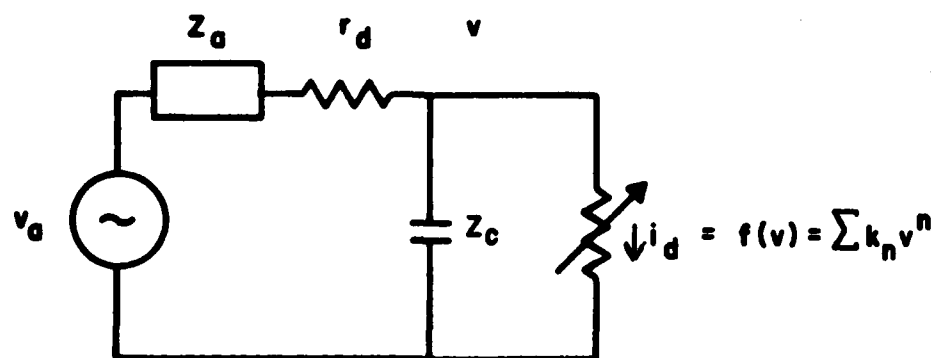


Figure C-2 Simplified Circuit Model for the MIM Junction.

change of junction capacitance as a function of applied bias voltage. Bond et al., concluded that the dielectric constant of Al_2O_3 is not a function of voltage and will conduct UHF signals in a linear manner. An oxide layer is a common insulator for many of the rusty bolts path nonlinearities on board Air Force airplanes.

There is evidence that typical MIM junctions have almost symmetrical i-v transfer characteristics. In other words electrical conduction is about equal in either direction. This implies that when a power series approximation is used, the symmetrical characteristics will contain only odd-order terms.

C.2 VOLTERRA TRANSFER FUNCTIONS OF THE RUSTY BOLT

Several methods for computing the Volterra transfer functions have been derived in the literature. Some of the methods are the method of exponential inputs (also known as the harmonic input method), the nonlinear current method [Bussgang, et al., (1974)] and the direct expansion method. Among those mentioned, the harmonic input method is particularly well known and allows the nonlinear transfer functions to be determined recursively. However, the calculations involved for higher than third order functions are cumbersome and seem difficult to implement on computers [Fliess et al., (1983)]. In the discussion that follows, we will use an expansion method where we manipulate the equations until they are brought into the form of a Volterra series expansion. The Volterra transfer functions can then be found by taking the n-fold Laplace or Fourier transform of the Volterra kernels.

A Norton's equivalent circuit for the MIM junction is shown in Figure C-3. The antenna impedance Z_a and the junction resistance r_d have been combined into an equivalent impedance Z_e . The driving current source $i_a(t)$ is the convolution of the antenna

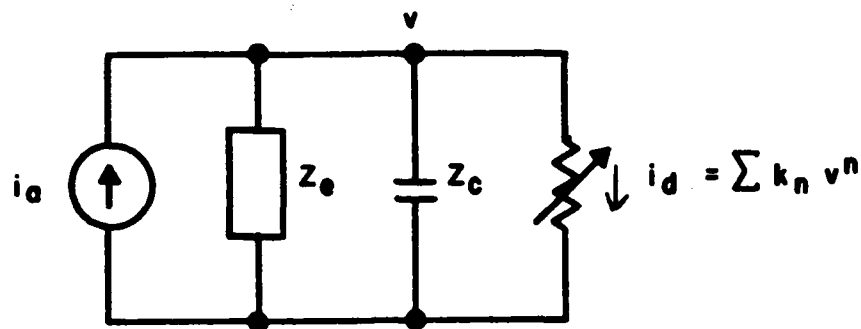


Figure C-3 Norton Equivalent Circuit for the MIM Junction.

$$I(s) = \frac{v_a(s)}{z_e(s)}$$

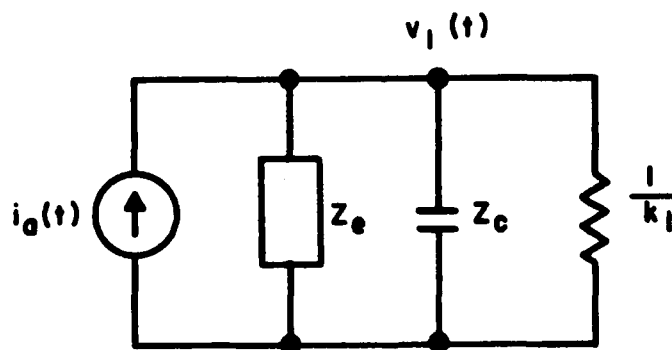


Figure C-4 Circuit used in Determining the Linear Voltage $v_1(t)$.

AD-A147 659

EMC (ELECTROMAGNETIC COMPATIBILITY) SPEC CRITERIA IN
VOLTERRA SYSTEMS(U) SIGNATRON INC LEXINGTON MA
L D TROMP ET AL. JUN 84 RADC-TR-84-147 F30602-82-C-0163

3/3

UNCLASSIFIED

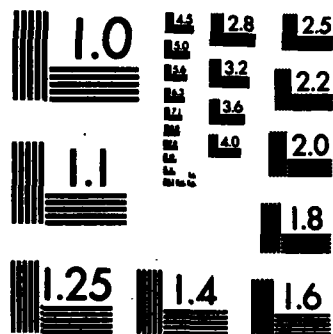
F/G 20/14

NL

END

FILMED

DTIC



MICROCOPY RESOLUTION TEST CHART
NATIONAL BUREAU OF STANDARDS-1963-A

driving voltage $v_a(t)$ and the equivalent admittance (inverse of the impedance Z_e). The nonlinear exponential current-voltage characteristic of the MIM junction discussed in Appendix B [Simmons (1963)] can be expanded into a power series

$$i_d = \sum_n k_n v^n \quad (C.2)$$

where k_n are the series coefficients which are a function of the dielectric material, work function of the metal, the electron charge and mass, Planck's constant, dielectric thickness and junction geometry. The current through the nonlinear resistor, i_d , can be interpreted as a set of voltage controlled circuit sources connected in parallel across the junction capacitor.

C.3 LINEAR RESPONSE AND TRANSFER FUNCTION

We will now obtain the linear impulse response of the equivalent circuit for the MIM junction by considering $i_a(t)$ as an input current source and $v(t)$ as the output. Ultimately we will be interested in the linear and nonlinear transfer functions between the input and output voltages.

In general the voltage response $v(t)$ can be expressed as

$$v(t) = \sum_{k=1}^{\infty} v_k(t)$$

where $v_k(t)$ denotes the k 'th order portion of the response. To determine the linear portion of the response, the nonlinear voltage controlled current sources can be ignored. The circuit to be analyzed is shown in Figure C-4.

The linear voltage, $v_1(t)$ is given by

$$v_1(t) = \int_{-\infty}^{\infty} h_1(\tau) i_a(t-\tau) d\tau \quad . \quad (C.3)$$

The Laplace transform of $v_1(t)$ is equal to

$$V_1(s) = H_1(s) I_a(s) \quad . \quad (C.4)$$

The transfer function $H_1(s)$ can be obtained from the node equation

$$\frac{V_1(s)}{Z_e(s)} + \frac{V_1(s)}{Z_C(s)} + k_1 V_1(s) = I_a(s) \quad (C.5)$$

$$H_1(s) = \frac{V_1(s)}{I_a(s)} = \frac{Z_e(s) Z_C(s)}{Z_e(s) + Z_C(s) + k_1 Z_e(s) Z_C(s)} \quad . \quad (C.6)$$

The voltage transfer function is then given by

$$H_{v1}(s) = \frac{V_1(s)}{V_a(s)} = \frac{H_1(s)}{Z_e(s)} = \frac{Z_C(s)}{Z_e(s) + Z_C(s) + k_1 Z_e(s) Z_C(s)} \quad . \quad (C.7)$$

C.4 SECOND ORDER RESPONSE AND VOLTAGE TO CURRENT TRANSFER FUNCTION

Next, we consider how the linear circuit in Figure C-4 must be modified if we add the second-order voltage controlled current source $k_2 v^2$ to the system and seek to determine the additional second order response $v_2(t)$ which is only due to the linear voltage $v_1(t)$. Clearly, we must add a current source $k_2 v_1^2$ to the linear circuit as shown in Figure C-5. The second order response is then given by

$$v_2(t) = -k_2 \int_{-\infty}^{\infty} h_1(\tau) v_1^2(t-\tau) d\tau \quad (C.8)$$

$$v_2(t) = -k_2 \int_{-\infty}^{\infty} h_1(\tau_3) \int_{-\infty}^{\infty} h_1(\tau_1) i_a(t-\tau_3-\tau_1) d\tau_1 \quad (C.9)$$

$$\int_{-\infty}^{\infty} h_1(\tau_2) i_a(t-\tau_3-\tau_2) d\tau_2 d\tau_3 .$$

If we let $\sigma_1 = \tau_1 + \tau_3$ and $\sigma_2 = \tau_2 + \tau_3$, then we can write the above equation as

$$v_2(t) = -k_2 \iiint h_1(\tau_3) \prod_{i=1}^2 h_1(\sigma_i - \tau_3) i_a(t - \sigma_i) d\sigma_i d\tau_3 \quad (C.10)$$

$$v_2(t) = \iint h_2(\sigma_1, \sigma_2) i_a(t - \sigma_1) i_a(t - \sigma_2) d\sigma_1 d\sigma_2 \quad (C.11)$$

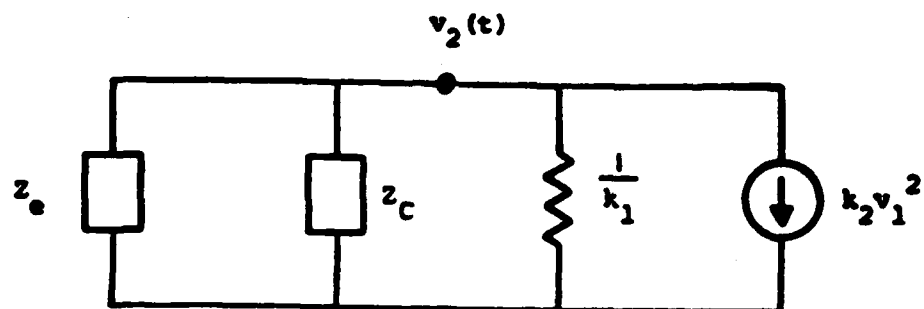


Figure C-5 Circuit Used in Determining the Second Order Response $v_2(t)$.

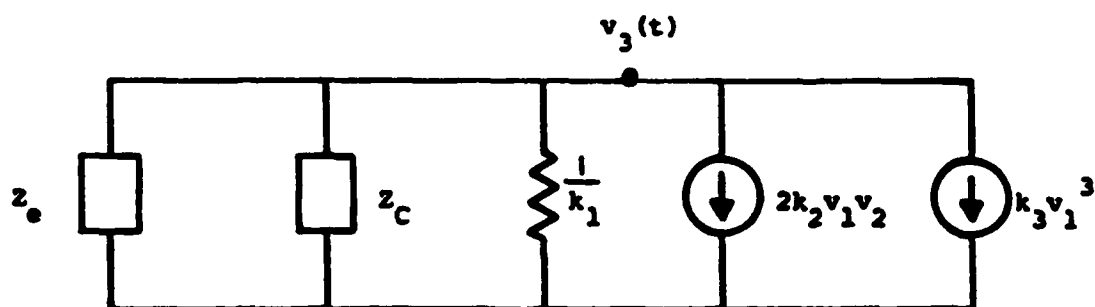


Figure C-6 Circuit Used in Determining the Third Order Response $v_3(t)$.

where

$$h_2(\sigma_1, \sigma_2) = -k_2 \int h_1(\tau) h_1(\sigma_1 - \tau) h_1(\sigma_2 - \tau) d\tau \quad (C.12)$$

and the limits of integration are understood to be from $-\infty$ to ∞ . The second order Volterra transfer function can be obtained by making use of the multi-dimensional Laplace transform. Taking the 2-dimensional transform of Equation (C.12) yields

$$H_2(s_1, s_2) = -k_2 H_1(s_1 + s_2) H_1(s_1) H_1(s_2) \quad (C.13)$$

The above equation shows that the second order output voltage to input current transfer function depends only on the constant k_2 and the linear transfer function $H_1(s)$. Therefore, the second order general transfer function depends only on $H_1(s)$ and the coefficient k_2 .

C.5 THIRD ORDER RESPONSE AND VOLTAGE TO CURRENT TRANSFER FUNCTION

In order to determine the third order response one needs to consider the voltage controlled current sources $k_2 v^2 + k_3 v^3$ as the driving source of the linear network. The third order voltage $v_3(t)$ can only be due to the combinations of voltages v_1 and v_2 . The source driving the network is

$$k_2 v^2 + k_3 v^3 = k_2 (v_1 + v_2)^2 + k_3 (v_1 + v_2)^3 \quad (C.14)$$

The terms that contribute to the third order response are shown in Figure C-6. The third order response $v_3(t)$ from Figure C-6 is then given by

$$v_3(t) = - \int_{-\infty}^{\infty} h_1(\tau) [2k_2 v_1(t-\tau) v_2(t-\tau) + k_3 v_1^3(t-\tau)] d\tau \quad (C.15)$$

Substituting Equations (C.3) and (C.11) into (C.15) yields

$$\begin{aligned} v_3(t) = & -2k_2 \iiint h_1(\tau_4) h_1(\tau_1) h_2(\tau_2, \tau_3) \prod_{i=1}^3 i_a(t-\tau_4-\tau_i) d\tau_i d\tau_4 \\ & - k_3 \iiint h_1(\tau_4) \prod_{i=1}^3 h_1(\tau_i) i_a(t-\tau_4-\tau_i) d\tau_i d\tau_4 . \end{aligned} \quad (C.16)$$

By making a change of variables $\sigma_1 = \tau_4 + \tau_1$, $\sigma_2 = \tau_4 + \tau_2$, $\sigma_3 = \tau_4 + \tau_3$ and rearranging we can write the expression in Equation (C.16) as

$$v_3(t) = \iiint h_3(\sigma_1, \sigma_2, \sigma_3) \prod_{i=1}^3 i_a(t-\sigma_i) d\sigma_i \quad (C.17)$$

where

$$h_3(\sigma_1, \sigma_2, \sigma_3) = -2k_2 \int_{-\infty}^{\infty} h_1(\tau_4) h_1(\sigma_1 - \tau_4) h_2(\sigma_2 - \tau_4, \sigma_3 - \tau_4) d\tau_4 \quad (C.18)$$

$$- k_3 \int_{-\infty}^{\infty} h_1(\tau_4) h_1(\sigma_1 - \tau_4) h_1(\sigma_2 - \tau_4) h_1(\sigma_3 - \tau_4) d\tau_4.$$

The third order Volterra transfer function is obtained by taking the 3-dimensional Laplace transform of Equation (C.18) which yields

$$H_3(s_1, s_2, s_3) = -2k_2 H_1(s_1 + s_2 + s_3) H_1(s_1) H_2(s_2, s_3) \\ - k_3 H_1(s_1 + s_2 + s_3) H_1(s_1) H_1(s_2) H_1(s_3)$$

$$H_3(s_1, s_2, s_3) = H_1(s_1 + s_2 + s_3) H_1(s_1) [-2k_2 H_2(s_2, s_3) \\ - k_3 H_1(s_2) H_1(s_3)] \quad (C.19)$$

We can now substitute Equation (C.13) into (C.19) which yields

$$H_3(s_1, s_2, s_3) = H_1(s_1) H_1(s_2) H_1(s_3) H_1(s_1 + s_2 + s_3) \\ [2k_2^2 H_1(s_2 + s_3) - k_3] . \quad (C.20)$$

The third order transfer function thus depends only on the constants k_2 , k_3 and the linear transfer function.

C.6 FOURTH ORDER RESPONSE AND TRANSFER FUNCTION

We now consider the fourth order response. The driving sources of the linear network are the voltage controlled current sources $k_2 v^2 + k_3 v^3 + k_4 v^4$. The fourth order voltage $v_4(t)$ can only be due to the combinations of the voltages v_1 , v_2 and v_3 . The source driving the network is then

$$k_2 v^2 + k_3 v^3 + k_4 v^4 = k_2 (v_1 + v_2 + v_3)^2 + k_3 (v_1 + v_2 + v_3)^3 \\ + k_4 (v_1 + v_2 + v_3)^4 . \quad (C.21)$$

The terms that contribute to the fourth order response are shown in Figure C-7. From Figure C-7, we find that the fourth order response $v_4(t)$ is given by

$$v_4(t) = - \int_{-\infty}^{\infty} h_1(\tau) [2k_2 v_1(t-\tau) v_3(t-\tau) + k_2 v_2^2(t-\tau) + 3k_3 v_1^2(t-\tau) v_2(t-\tau) + k_4 v_1^4(t-\tau)] d\tau \quad (C.22)$$

Substituting Equations (C.3), (C.11), and (C.17) into (C.21) yields

$$\begin{aligned} v_4(t) = & -2k_2 \iiint h_1(\tau_5) h_1(\tau_1) h_3(\tau_2, \tau_3, \tau_4) \prod_{i=1}^4 i_a(t-\tau_5-\tau_i) d\tau_i d\tau_5 \\ & -2k_2 \iiint h_1(\tau_5) h_2(\tau_1, \tau_2) h_2(\tau_3, \tau_4) \prod_{i=1}^4 i_a(t-\tau_5-\tau_i) d\tau_i d\tau_5 \\ & -3k_3 \iiint h_1(\tau_5) h_1(\tau_1) h_1(\tau_2) h_2(\tau_3, \tau_4) \prod_{i=1}^4 i_a(t-\tau_5-\tau_i) d\tau_i d\tau_5 \\ & -k_4 \iiint h_1(\tau_5) h_1(\tau_1) h_1(\tau_2) h_1(\tau_3) h_1(\tau_4) \prod_{i=1}^4 i_a(t-\tau_5-\tau_i) d\tau_i d\tau_5. \end{aligned} \quad (C.23)$$

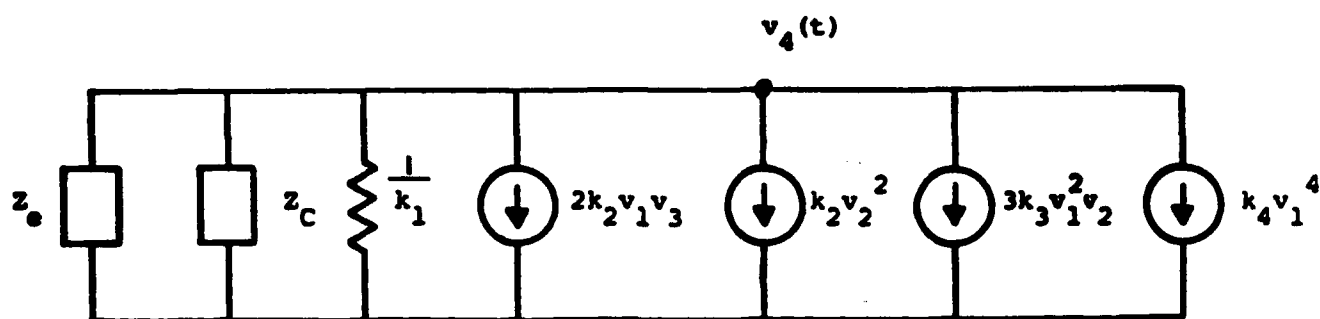


Figure C-7 Circuit Used in Determining the Fourth Order Response $v_4(t)$.

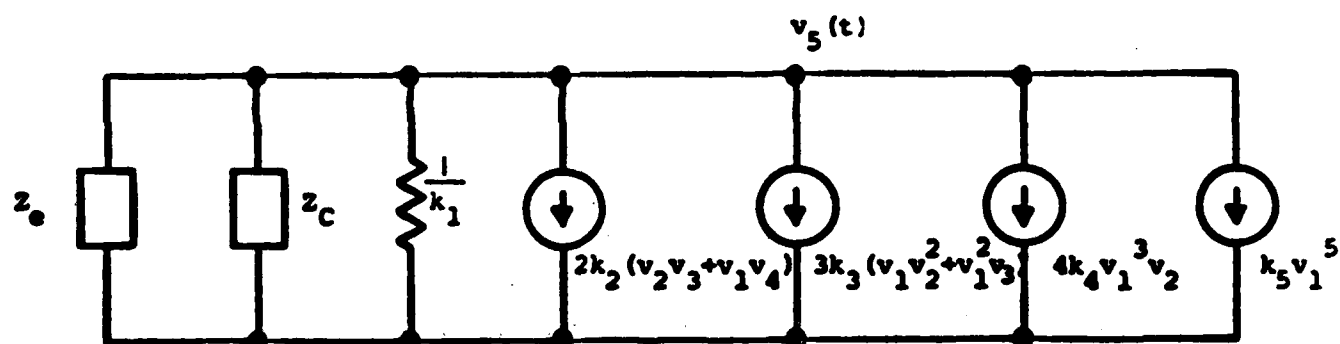


Figure C-8 Circuit Used in Determining the Fifth Order Response $v_5(t)$.

We now can make a change of variables $\sigma_i = \tau_5 + \tau_i$ ($i = 1$ to 4) and rearrange the above equation to yield

$$v_4(t) = \iiint h_4(\sigma_1, \sigma_2, \sigma_3, \sigma_4) \prod_{i=1}^4 i_a(t - \sigma_i) d\sigma_i \quad (C.24)$$

where

$$\begin{aligned} h_4(\sigma_1, \sigma_2, \sigma_3, \sigma_4) = & -k_2 \int_{-\infty}^{\infty} [2h_1(\tau_5)h_1(\sigma_1 - \tau_5)h_3(\sigma_2 - \tau_5, \sigma_3 - \tau_5, \sigma_4 - \tau_5) \\ & + h_1(\tau_5)h_2(\sigma_1 - \tau_5, \sigma_2 - \tau_5)h_2(\sigma_3 - \tau_5, \sigma_4 - \tau_5)] d\tau_5 \\ & - 3k_3 \int_{-\infty}^{\infty} h_1(\tau_5)h_1(\sigma_1 - \tau_5)h_1(\sigma_2 - \tau_5)h_2(\sigma_3 - \tau_5, \sigma_4 - \tau_5) d\tau_5 \\ & - k_4 \int_{-\infty}^{\infty} h_1(\tau_5) \prod_{i=1}^4 h_1(\sigma_i - \tau_5) d\tau_5 . \end{aligned} \quad (C.25)$$

The fourth order Volterra transfer function can now be obtained by taking the 4-dimensional Laplace transform of the above equation which yields

$$\begin{aligned}
 H_4(s_1, s_2, s_3, s_4) = & -k_2 H_1(s_1 + s_2 + s_3 + s_4) [H_2(s_1, s_2) H_2(s_3, s_4) \\
 & + 2H_1(s_1) H_3(s_2, s_3, s_4)] \\
 & -k_3 H_1(s_1 + s_2 + s_3 + s_4) H_1(s_1) H_1(s_2) H_2(s_3, s_4) \\
 & -k_4 H_1(s_1 + s_2 + s_3 + s_4) H_1(s_1) H_1(s_2) H_1(s_3) H_1(s_4)
 \end{aligned}
 \tag{C.26}$$

The second order and third order transfer function depends only on constants and the linear transfer function. Therefore the fourth order Volterra transfer function will only depend on the constants k_2 , k_3 , k_4 and the linear transfer function.

C.7 FIFTH ORDER RESPONSE AND TRANSFER FUNCTION

We will now consider the fifth order Volterra transfer function for the simple rusty bolt equivalent circuit. The driving sources of the network for this case are the voltage controlled current sources $k_2 v^2 + k_3 v^3 + k_4 v^4 + k_5 v^5$. The fifth order voltage $v_5(t)$ can only be due to the combinations of the voltages v_1 , v_2 , v_3 and v_4 . Thus the driving source becomes

$$\begin{aligned}
k_2 v^2 + k_3 v^3 + k_4 v^4 + k_5 v^5 &= k_2 (v_1 + v_2 + v_3 + v_4)^2 \\
&+ k_3 (v_1 + v_2 + v_3 + v_4)^3 \\
&+ k_4 (v_1 + v_2 + v_3 + v_4)^4 \\
&+ k_5 (v_1 + v_2 + v_3 + v_4)^5 . \quad (C.27)
\end{aligned}$$

The terms that contribute to the fifth order response are shown in Figure C-8. Following a procedure similar to the previous section we get that

$$v_5(t) = \iiiii h_5(\sigma_1, \sigma_2, \sigma_3, \sigma_4, \sigma_5) \prod_{i=1}^5 i_a(t - \sigma_i) d\sigma_i \quad (C.28)$$

where

$$\begin{aligned}
h_5(\sigma_1, \sigma_2, \sigma_3, \sigma_4, \sigma_5) = & -2k_2 \int_{-\infty}^{\infty} h_1(\tau_6) h_2(\sigma_1 - \tau_6) h_2(\sigma_1 - \tau_6, \sigma_2 - \tau_6) \\
& h_3(\sigma_3 - \tau_6, \sigma_4 - \tau_6, \sigma_5 - \tau_6) d\tau_6 \\
& -2k_2 \int_{-\infty}^{\infty} h_1(\tau_6) h_1(\sigma_1 - \tau_6) h_4(\sigma_2 - \tau_6, \sigma_3 - \tau_6, \sigma_4 - \tau_6, \sigma_5 - \tau_6) d\tau_6 \\
& -3k_3 \int_{-\infty}^{\infty} h_1(\tau_6) h_1(\sigma_1 - \tau_6) h_2(\sigma_2 - \tau_6, \sigma_3 - \tau_6) h_2(\sigma_4 - \tau_6, \sigma_5 - \tau_6) d\tau_6 \\
& -3k_3 \int_{-\infty}^{\infty} h_1(\tau_6) h_1(\sigma_1 - \tau_6) h_3(\sigma_3 - \tau_6, \sigma_4 - \tau_6, \sigma_5 - \tau_6) d\tau_6 \\
& -4k_4 \int_{-\infty}^{\infty} h_1(\tau_6) h_1(\sigma_1 - \tau_6) h_1(\sigma_2 - \tau_6) h_1(\sigma_3 - \tau_6) h_2(\sigma_4 - \tau_6, \sigma_5 - \tau_6) d\tau_6 \\
& -k_5 \int_{-\infty}^{\infty} h_1(\tau_6) \prod_{i=1}^5 h_1(\sigma_i - \tau_6) d\tau_6 .
\end{aligned} \tag{C.29}$$

The fifth order Volterra transfer function is then given by

$$\begin{aligned}
 H_5(s_1, s_2, s_3, s_4, s_5) = & H_1(s_1 + s_2 + s_3 + s_4 + s_5) \{ -2k_2 H_2(s_1, s_2) H_3(s_3, s_4, s_5) \\
 & -2k_2 H_1(s_1) H_4(s_2, s_3, s_4, s_5) \\
 & -3k_3 [H_1(s_1) H_2(s_2, s_3) H_2(s_4, s_5) \\
 & + H_1(s_1) H_1(s_2) H_3(s_3, s_4, s_5)] \\
 & -4k_4 H_1(s_1) H_1(s_2) H_1(s_3) H_2(s_4, s_5) \\
 & -k_5 \prod_{i=1}^5 H_1(s_i) \} \quad (C.30)
 \end{aligned}$$

The fifth order Volterra transfer function will only depend on the constants k_2 , k_3 , k_4 , k_5 and the linear transfer function because all the low order transfer functions only depend on constants and $H_1(s)$.

C.8 VOLTAGE TO VOLTAGE "RUSTY BOLT" VOLTERRA TRANSFER FUNCTION

In the previous subsections, we derived the transfer functions by considering the output to be a voltage and the input a current. In this section, we derive voltage to voltage nonlinear Volterra transfer functions. We consider as input the antenna voltage and as output the voltage generated across the parallel

combination of the capacitor and the nonlinear resistor shown in Figure C-2. The linear voltage to voltage transfer function was derived in Section 3 and is given by Equation (C.7).

In order to find the higher order voltage to voltage responses, we can again use the circuits shown in Figures C-5 through C-8. The only change compared to the derivation of the output voltage to the input current response occurs in the expression for $v(t)$. The second order response is given by

$$v_2(t) = k_2 \int_{-\infty}^{\infty} h_1(\tau) v_1^2(t-T) dT \quad (C.31)$$

where $h_1(t)$ is the linear impulse response when the input is a current and the linear output voltage is given by

$$v_1(t) = \int_{-\infty}^{\infty} h_{v1}(\tau) v_1(t-\tau) d\tau. \quad (C.32)$$

The impulse response due to the input antenna voltage $v_a(t)$ is denoted by $\tilde{h}_{v1}(t)$. We can now substitute Equation (C.32) in (C.31) and obtain the result

$$v_2(t) = -k_2 \iiint h_1(\tau_3) \prod_{i=1}^2 h_{v1}(\tau_i) v_a(t-\tau_3-\tau_i) d\tau_i d\tau_3 \quad (C.33)$$

and the limits of integration are understood to be from $-\infty$ to ∞ . Now, if we let $\sigma_1 = \tau_1 + \tau_3$ and $\sigma_2 = \tau_2 + \tau_3$, then we can write the above equation as

$$v_2(t) = \iint h_{v2}(\sigma_1, \sigma_2) v_a(t-\sigma_1) v_1(t-\sigma_2) d\sigma_1 d\sigma_2 \quad (C.34)$$

where

$$h_{v2}(\sigma_1, \sigma_2) = -k_2 \iint h_1(\tau) h_{v1}(\sigma_1 - \tau) h_{v1}(\sigma_2 - \tau) d\tau . \quad (C.35)$$

The second order voltage to voltage Volterra transfer function is obtained by taking the two-dimensional Laplace transform of Equation (C.35) which yields

$$\begin{aligned} H_{v2}(s_1, s_2) &= -k_2 H_{v1}(s_1) H_{v1}(s_2) H_1(s_1 + s_2) \\ &= -k_2 H_{v1}(s_1) H_{v1}(s_2) H_{v1}(s_1 + s_2) Z_e(s_1 + s_2) \end{aligned} \quad (C.36)$$

where we have made use of the fact that $H_1(s) = H_{v1}(s) Z_e(s)$ (Equation (C.7)). Similarly, we can use Figure C-6 to determine the third order response. The third order response $v_3(t)$ from Figure C-6 is given by

$$v_3(t) = - \int_{-\infty}^{\infty} h_1(\tau) [2k_2 v_1(t-\tau) v_2(t-\tau) + k_3 v_1^3(t-\tau)] d\tau . \quad (C.37)$$

Substituting Equations (C.32) and (C.34) into the above equation and making a change of variables $\sigma_i = \tau_4 + \tau_i$; , $i=1,3$ we have

$$v_3(t) \iiint h_{v3}(\sigma_1, \sigma_2, \sigma_3) \prod_{i=1}^3 v_a(t - \sigma_i) d\sigma_i \quad (C.38)$$

where

$$\begin{aligned} h_{v3}(\sigma_1, \sigma_2, \sigma_3) = & -2k_2 \int_{-\infty}^{\infty} h_1(\tau) h_{v1}(\sigma_1 - \tau) h_{v2}(\sigma_2 - \tau, \sigma_3 - \tau) d\tau \\ & - k_3 \int_{-\infty}^{\infty} h_1(\tau) \prod_{i=1}^3 h_{v1}(\sigma_i - \tau) d\tau. \end{aligned} \quad (C.39)$$

The third order voltage to voltage Volterra transfer function for the lumped parameter "rusty bolt" circuit is obtained by taking the three-dimensional Laplace transformation of the above equation which yields

$$\begin{aligned} H_{v3}(s_1, s_2, s_3) = & [-2k_2 H_{v2}(s_2, s_3) - k_3 H_{v1}(s_2) H_{v1}(s_3)] \\ & H_{v1}(s_1) H_{v1}(s_1 + s_2 + s_3) Z_e(s_1 + s_2 + s_3) \end{aligned} \quad (C.40)$$

From the second and third order transfer functions, we see that the voltage to voltage nonlinear transfer functions take the same form as the expressions for the output voltage to input current transfer functions. The only difference is the impedance factor that appears and which multiplies all terms. The impedance factor is evaluated at the sum frequency. All the Volterra functions derived in this Appendix can be put into their symmetrical form.

C.9 CONCLUSION

We have seen that all the nonlinear transfer functions for a single nonlinearity and a simple rusty bolt equivalent circuit depend only on constants and the linear transfer function, and, in the case of the voltage to voltage transfer function also on the equivalent antenna impedance. The linear transfer function plays a crucial role in the identification of the nonlinear parts of the system. It is also clear from the analysis that the formal complexity of Volterra kernels rapidly increases with their order.

APPENDIX C
REFERENCES

- Bond Clarence P., Charles S. Guenzer and Carmine A. Carosella, "Intermodulation generation by Electronic Tunneling through Aluminum-Oxide Films", Proc. IEEE Vol. 67, No. 12, pp. 1643-1652, December 1979.
- Bör-Long, T.W.U. and Schwartz, S.E., (1974), "Mechanism and Properties of Point-Contact Metal-Insulator-Metal diode detectors at 10.6 μ ", Appl. Phys. LETT., Vol. 25, No. 10, November 1974.
- Bussgang, J.J., Ehrman, L. and Graham, J.W., (1974), "Analysis of Nonlinear Systems with Multiple Inputs", Proc. IEEE, Vol. 62, pp. 1088-1119, August 1974.
- Flies, M., Lamnabhi M. and Lagarrigue F (1980), "An Algebraic Approach to Nonlinear Functional Expansions", IEEE Trnas. Circuits Syst., Vol. 30, No. 8, pp. 554-570, August 1983.
- Simmons, John G., "Generalized formula for the electric tunnel effect between similar electrodes separated by a thin insulating film", Journal Appl. Physics, Vol. 34, No. 6, June 1963.
- Uslenghi P., editor, "Nonlinear Electromagnetics", Academic Press, pp. 303-341, New York, 1980.

MISSION **of** **Rome Air Development Center**

RADC plans and executes research, development, test and selected acquisition programs in support of Command, Control Communications and Intelligence (C³I) activities. Technical and engineering support within areas of technical competence is provided to ESD Program Officers (POs) and other ESD elements. The principal technical mission areas are communications, electromagnetic guidance and control, surveillance of ground and aerospace objects, intelligence data collection and handling, information system technology, ionospheric propagation, solid state sciences, microwave physics and electronic reliability, maintainability and compatibility.